CHARACTERIZATION OF THE EFFECTS OF A HIGH FAT-HIGH SUCROSE DIET IN WILD-TYPE AND ROCK2 HETEROZYGOUS MICE

by

Yanzhi Jia

B.Sc. (Hons), The University of Saskatchewan, 2017

A THESIS SUBMITTED IN PARTIAL FULFILLMENT OF

THE REQUIREMENTS FOR THE DEGREE OF

MASTER OF SCIENCE

in

THE FACULTY OF GRADUATE AND POSTDOCTORAL STUDIES

(PHARMACEUTICAL SCIENCES)

THE UNIVERSITY OF BRITISH COLUMBIA

(Vancouver)

December 2019

The following individuals certify that they have read, and recommend to the Faculty of Graduate and Postdoctoral Studies for acceptance, a thesis entitled:

CHARACTERIZATION OF THE EFFECTS OF A HIGH FAT-HIGH SUCROSE DIET IN WILD-TYPE AND ROCK2 HETEROZYGOUS MICE

submitted by Yanzhi Jia in partial fulfillment of the requirements for

the degree of Master of Science

in Pharmaceutical Sciences

Examining Committee:

Dr. Kathleen MacLeod
Supervisor

Dr. Brian Rodrigues
Supervisory Committee Member

Dr. Colin Ross
Supervisory Committee Member

Dr. Ismail Laher
Additional Examiner

Additional Supervisory Committee Members:

Dr. Harvey Wong
Supervisory Committee Member

Dr. Judy Wong
Supervisory Committee Member

Abstract

Obesity is associated with systemic insulin resistance, impaired insulin signaling, and increased inflammation, as well as with the development of cardiomyopathy. Heterozygous deletion of ROCK2 has been demonstrated to protect CD-1 mice from cardiac contractile dysfunction and insulin resistance induced by a high fat diet. A high fat-high sucrose diet (HFHS) more closely resembles the human "Western diet" than a high fat diet, but it is unclear whether ROCK2 contributes to the obesity-related complications caused by this diet. The purpose of the work described here was to characterize the effects of a HFHS diet on cardiac function and insulin tolerance in wild-type (WT) and ROCK2+/- CD-1 mice.

In Chapter 2, the effect of a HFHS diet containing 45% kcal from fat and 17% kcal from sucrose on cardiac function and systemic insulin sensitivity of WT and ROCK2+/- CD-1 mice was assessed. Despite the development of severe obesity and systemic insulin intolerance, WT + HFHS animals did not develop cardiac contractile dysfunction, while no increase in ROCK2 expression and or impaired insulin signaling was detected in these hearts. Furthermore, HFHS diet-fed ROCK2+/- mice were not protected from systemic insulin intolerance.

In Chapter 3, the mechanisms underlying whole-body insulin intolerance at the level of insulin signaling in the liver and adipose tissue from WT and ROCK2+/- mice were evaluated. Although no over-expression of ROCK2 or activation of ROCK could be detected in the liver or adipose tissue of HFHS diet-fed mice, both WT and ROCK2+/- animals had significantly elevated levels of liver triglycerides and impaired insulin signaling in the liver and adipose tissue. In addition, elevated levels of inflammatory factors were found in adipose tissue from both WT + HFHS and ROCK2+/- + HFHS mice.

Overall, feeding CD-1 mice a HFHS diet failed to induce cardiac dysfunction, despite producing obesity and systemic insulin resistance that were resistant to heterozygous deletion of ROCK2. These data suggest that ROCK2 does not appear to contribute to the complications of obesity induced by a HFHS diet. However, the liver and adipose tissue may be potential tissue targets for improving disrupted insulin signaling and inflammation induced by this diet.

Lay Summary

Obesity has negative effects on the body, and can lead to complications such as heart failure, diabetes and liver disease. A signaling protein known as ROCK2 has been implicated in the development of obesity cardiomyopathy, a form of heart failure associated with obesity. Reducing the amount of ROCK2 is able to protect mice from heart dysfunction and also from the high blood sugar caused by a diet very high in fat. However, a diet containing a combination of high fat and high sugar, which also caused obesity and high blood sugar, failed to lead to heart dysfunction. Moreover, reducing ROCK2 levels was not sufficient to decrease blood sugar or reduce inflammation. My data demonstrated that ROCK2 may not contribute to the complications of obesity induced by the combination of high fat and sugar. However, the liver and adipose tissue are possible targets for reducing high blood sugar and inflammation.

Preface

All the work outlined in this thesis was carried out by Yanzhi Jia under the guidance and supervision of Dr. Kathleen MacLeod in the Faculty of Pharmaceutical Sciences, University of British Columbia. Dr. Kathleen MacLeod and Yanzhi Jia were responsible for designing the experiments. Dr. Kathleen MacLeod also provided revisions for the writing in this thesis. All research and experimental work was completed by Yanzhi Jia except for the sections specified below.

In Chapter 3, levels of hepatic triglycerides and cholesterols were measured by Dr. Vongai Nyamandi. Dr. Vongai Nyamandi also assisted with the data analysis of adipose tissue properties.

All animal experiments were approved by the University of British Columbia as follows:

1. For breeding the CD-1 mice – Animal Care Committee Certificate A17-0271
2. For studies on diabetic cardiomyopathy in CD-1 mice - Animal Care Committee Certificate A18-0005

Table of Contents

List of Tables

List of Figures

List of Abbreviations

°C	Degrees Celsius
ACC	Acetyl-CoA carboxylase
AET	Aortic ejection time
AMPK	5' adenosine monophosphate-activated protein kinase
ANOVA	Analysis of variance
AS160	Akt substrate 160
ATP	Adenosine triphosphate
AUC	Area under the curve
BMI	Body mass index
bpm	Beats per minute
CH	Chow
DNL	*de novo* lipogenesis
Drp1	Dynamin-related protein 1
E/A	Ratio of early (E) to late (A) ventricular filling velocities
Elovl3	Elongation of very long chain fatty acid protein 3
EMR1 (F4/80)	EGF-like module-containing mucin-like hormone receptor-like 1
ET	Ejection time
FAS	Fatty acid synthase
Fis1	Fission 1
GAPs	GTPase activating proteins
GEFs	Guanine nucleotide exchange factors
GLUT	Glucose transporter

GTP	Guanosine triphosphate
GTT	Glucose tolerance test
HF	High fat
HFHS	High fat-high sucrose
IGF-1	Insulin-like growth factor-1
IL-6	Interleukin-6
IRS-1	Insulin receptor substrate 1
ITT	Insulin tolerance test
IVCT	Isovolumic contraction time
IVRT	Isovolumic relaxation time
LFLS	Low fat-low sucrose
LIMK	LIM-Kinase
LV	Left ventricular
LVAW; d	Left ventricular anterior wall (diastole)
LVAW; s	Left ventricular anterior wall (systole)
LVID; d	Left ventricular internal diameter (diastole)
LVID; s	Left ventricular internal diameter (systole)
LVPW; d	Left ventricular posterior wall (diastole)
LVPW; s	Left ventricular posterior wall (systole)
LV Vol; d	Left ventricular volume (diastole)
LV Vol; s	Left ventricular volume (systole)
MCP-1	Monocyte chemotactic protein-1
Mfn1	Mitofusin 1

Mfn2	Mitofusin 2
MLC	Myosin light chain
MPI	Myocardial performance index
MV	Mitral valve
MYPT1	Myosin phosphatase target subunit 1
NAFLD	Non-alcoholic fatty liver disease
OPA1	Optic atrophy protein 1
PDK1	Phosphoinositide-dependent protein kinase-1
PKB/Akt	Protein kinase B
PIP3	Phosphatidylinositol (3,4,5)-trisphosphate
PI3K	Phosphoinositide 3-kinase
PPARγ	Peroxisome proliferator-activate receptor gamma
ROCK	Rho-associated coiled-coil-containing protein kinase
ROCK2+/-	ROCK2 heterozygous whole-body knockdown
ROS	Reactive oxygen species
RT-PCR	Real time-polymerase chain reaction
SDS-PAGE	Sodium dodecyl sulphate-polyacrylamide gel electrophoresis
SREBP1c	Sterol regulatory element-binding protein 1c
TG	Triglyceride
TNFα	Tumor necrosis factor alpha
VLDL	Very low-density lipoprotein
WT	Wild-type
μ	Micro

μM	Micromolar

Acknowledgements

First of all, I would like to thank my supervisor, Dr. Kathleen MacLeod, for providing me the opportunity to study and research here at the faculty; for her guidance, support, and patience throughout my entire MSc study. Her hard-working, positive attitude, and insistence toward science and life motivated me not only to be a better graduate student, but also a better person.

Secondly, I would like to thank the members of my MSc committee, Dr. Brian Rodrigues, Dr. Judy Wong, and Dr. Colin Ross, as well as my MSc committee chair, Dr. Harvey Wong, for their valuable time, precious advice, and constant support on helping me complete my research.

I would also like to thank my former lab members: Dr. Vongai Nyamandi and Dr. Marysol Garcia-Patino, for their dedicated training and tremendous help over the past two and half years.

I would like to thank the Faculty of Pharmaceutical Sciences for providing state-of-the-art facilities and financial support. Special thanks to Dr. Thomas Chang and Ms. Shirley Wong, for their care and assistance throughout my graduate school journey.

I would like to thank all my graduate student peers, as well as past and present PharGS members, who have added so much fun and laughter into my graduate life. In particular, the members of the Rodrigues lab: Bahira, Nathaniel, Fulong, Rui, and Jason – you guys are the best lab neighbors ever.

I would like to thank Ms. Sarah Hulme, Ms. Megan Herrington, and all other MBF staff for their dedicated work and immense help on our animal projects.

I would like to thank my family for their love and support: thanks to my dad, for your giant support, both mentally and financially; thanks to my mom, for your unconditional love and care; thanks to my grandparents, for your encouragement and always being proud of me.

I would like to thank all of my friends, for your company and always being ready to lend me a hand whenever I needed one. Without all of you, I would not have been able to achieve what I have achieved today.

Last but not least, Boris, thank you for always being here for me no matter what and no matter when. Your motivation, ethics towards work and life, and persistence inspire and encourage me to be better and achieve higher. I'm very lucky to have you being by my side and I'm grateful forever.

To my family and all of whom I love

Chapter 1: Introduction

1.1 Overview of obesity

1.1.1 Prevalence of obesity

The epidemic of obesity is rising dramatically over time worldwide. According to the World Health Organization, worldwide obesity has nearly tripled since 1975. In 2016, more than 1.9 billion adults aged 18 years and older were overweight, which account for 39% (39% of men and 40% of women) of the whole adult population. Over 650 million were obese, which account for 13% (11% of men and 15% of women) of the whole adult population. As for children and adolescents aged 5-19, over 18% were overweight, and 7% were obese in 2016, compared to 4% and 1% in 1975, respectively (World Health Organization, 2018). Nowadays, overweight and obesity contribute to more deaths worldwide than underweight, and more populations are overweight and obese than those who are underweight globally, except in sub-Saharan Africa and Asia. Although the overall prevalence of obesity is increasing significantly around the world, there are differences between countries and regions. For example, an accelerated increase in body mass index (BMI) was particularly reported in South Asia, Southeast Asia, the Caribbean, and Southern Latin America, while in Eastern Europe, almost no BMI increase was noted over the past 40 years (Abarca-Gómez *et al.*, 2017).

Overweight and obesity are defined as abnormal or excessive fat accumulation, and can be calculated based on the BMI, as weight (kg) divided by height^2 (m). Overweight is defined as a BMI from 25 – 29.9 kg/m^2, and obesity is defined as a BMI $\geqslant$ 30 kg/m^2 (Clinical guidelines on the identification, evaluation, and treatment of overweight and obesity in adults: executive summary. Expert Panel on the Identification, Evaluation, and Treatment of Overweight in Adults, 1998). In addition to BMI, waist circumference can also be used to evaluate the potential health

risks associated with overweight and/or obesity for individuals. Men and women with a waist circumference less than 94 cm and 80 cm, respectively, are considered to have normal fat distribution and a low risk of obesity-related comorbidities. When the waist circumference in men is between 94-101.9 cm, and in women is between 80-87.9 cm, individuals are considered to have moderate central fat accumulation and an increased risk of obesity-related comorbidities. Men who have a waist circumference exceeding 102 cm, and women who have a waist circumference exceeding 88 cm are categorized as having high central fat accumulation and a high risk of obesity-related comorbidities (Han and Lean, 2016).

1.1.2 Medical complications of obesity

Obesity affects most of our body systems negatively and is associated with many medical complications such as diabetes, lung disease, including asthma and pulmonary blood clots, non-alcoholic fatty liver disease, stroke, and heart disease, such as cardiomyopathy (Fig. 1.1) (Kinlen *et al.*, 2018). Although the exact underlying mechanisms and relationships between obesity and its medical complications have not been well defined yet, it is believed that obesity can significantly increase the risk of those morbidities and individuals who are overweight or obese tend to have a higher chance of developing the above diseases.

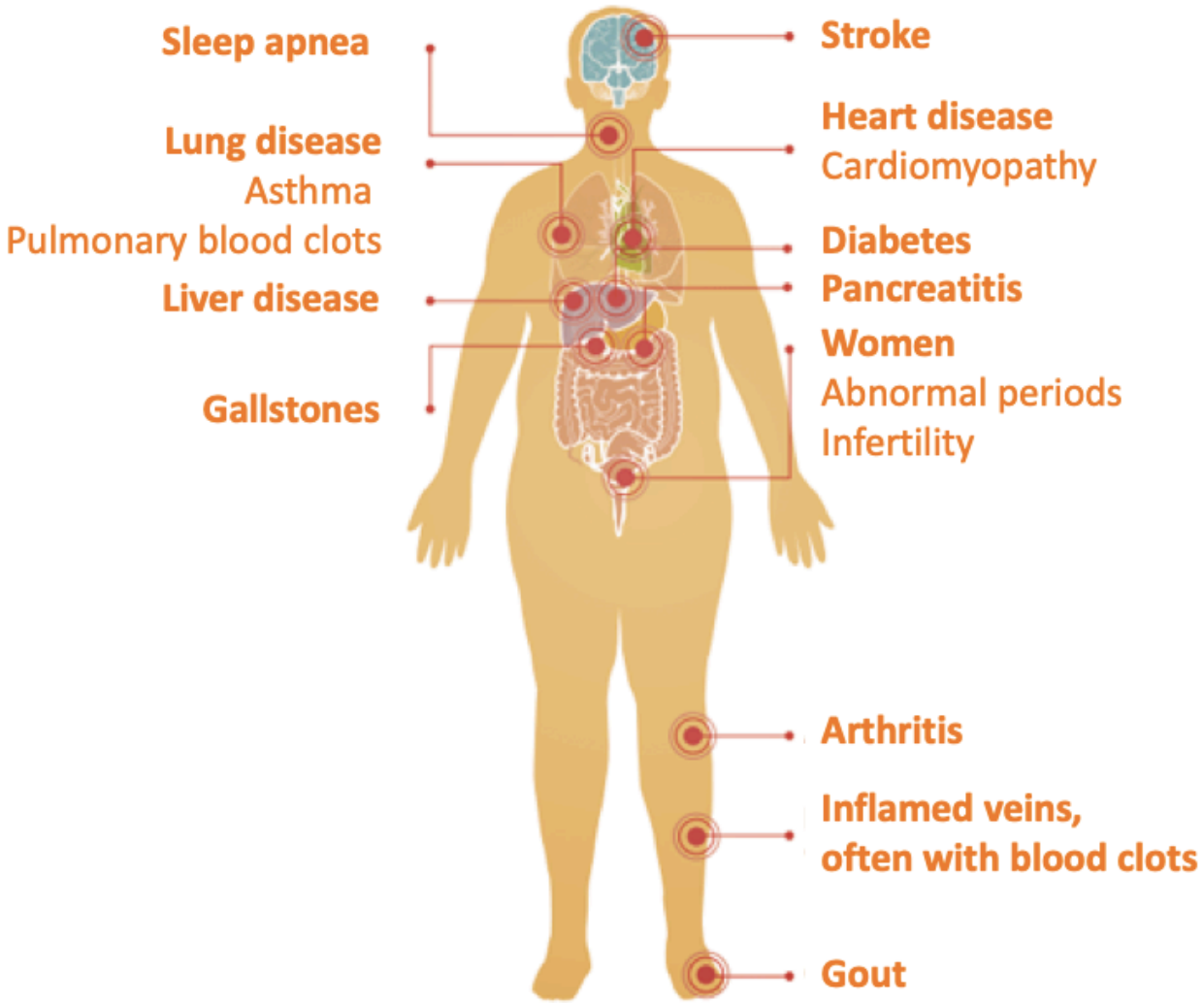

Figure 1.1 Medical complications of obesity

Obesity increases the risk of medical complications, including sleep apnea; lung disease, for example, asthma and pulmonary blood clots; liver disease; gallstones; stroke; heart disease, such as cardiomyopathy; diabetes; pancreatitis; abnormal periods and infertility in women; arthritis; inflamed veins, often with blood clots, as well as gout. Retrieved and modified from Centers for Disease Control and Prevention. Reproduce with permission under CC-BY https://creativecommons.org/licenses/by/4.0/.

The accumulation of excess fat accelerates insulin resistance, endothelial dysfunction and leads to the development of diabetes (Al-Goblan *et al.*, 2014). High blood pressure, high content of cholesterol, and high blood glucose associated with the progression of obesity can contribute to cardiovascular diseases and related comorbidities such as heart failure and stroke (Kinlen *et al.*, 2018). Extra weight on a joint increases the pressure and stress around the joint, and further increases the chance of arthritis especially in overweight and obese people (Magliano, 2008). In addition, there is a tight association between excess body weight and the risk of developing gout. Gout is a form of inflammatory arthritis and is caused by a high level of uric acid buildup around the joint. Overweight and obesity slow down the clearance of uric acid from the body and lead to gout attacks (Juraschek *et al.*, 2013). Obesity can also increase fat accumulation around certain parts of the body and in the blood circulation to cause sleep apnea, inflamed veins, and blood clots in veins (Romero-Corral *et al.*, 2010; Borch *et al.*, 2011). Moreover, obesity can affect regular hormonal signaling and contributes to abnormal periods and infertility in women (Dağ and Dilbaz, 2015).

Overall, obesity is closely associated with increased risks of various comorbidities, and weight loss remains the best way to tackle complications (Kinlen *et al.*, 2018). Although the cause of obesity is multifactorial and there are many factors involved in its development, including genetics, ethnicities, socio-economic status, and psychological factors (Lakerveld and Mackenbach, 2017; Stryjecki *et al.*, 2018), the fundamental cause of obesity is an energy imbalance between calories taken in and calories expended. There has been an increased intake of foods that are high in fat and carbohydrates, and a reduction in physical activity due to an increasingly sedentary lifestyle and increasing urbanization. Therefore, health recommendations

focus on promoting healthy eating habits and increasing physical activity (Franco *et al.*, 2013; Ortiz and Kwo, 2015; Camacho and Ruppel, 2017).

1.1.3 Mechanism of complications of obesity

1.1.3.1 Insulin signaling

Insulin was discovered in 1921 by a team of researchers, Frederick G Banting, Charles Best, James B. Collip, and their supervisor J.J.R. MacLeod at the University of Toronto (Brownsey *et al.*, 1997). Insulin is produced by beta cells of the pancreas as a peptide hormone to regulate the metabolism of carbohydrates, fats, and protein in the body (Wilcox, 2005).

Elevated concentrations of glucose in circulation trigger the release of insulin. Insulin then acts on cells of different tissues to stimulate uptake, utilization and storage of glucose, to decrease the concentration of glucose in the circulation. Insulin binds to the insulin receptor (IR), which is a tetrameric enzyme that is comprised of 2 extracellular α-subunits and 2 transmembrane β-subunits located on the cell membrane, to mediate its signaling (Ottensmeyer *et al.*, 2000). IR is a member of the tyrosine kinase family of cell surface receptors and is closely associated with the receptor for insulin-like growth factor-1 (IGF-1) (Nakae *et al.*, 2001). Upon insulin binding, IR is autophosphorylated, and thus has increased tyrosine kinase activity for other substrates, such as insulin receptor substrates (IRS) proteins. Tyrosine phosphorylation of insulin receptor substrate 1 (IRS-1) by IR introduces multiple binding sites for proteins that have SH2 homology domain, including phosphatidylinositol 3-kinases (PI3Ks). PI3K binds to tyrosine residues of IRS-1 to produce phosphatidylinositol 3,4,5-triphosphate (PIP3), which activates a series of downstream signaling proteins, including phosphoinositide-dependent protein kinase-1 (PDK1), protein kinase B (PKB/Akt) and Akt substrate 160 (AS160) to facilitate membrane glucose transport through

glucose transporters (GLUTs), such as GLUT4 (Fig. 1.2) (Thirone *et al.*, 2006; Muniyappa *et al.*, 2007; Thorn *et al.*, 2013).

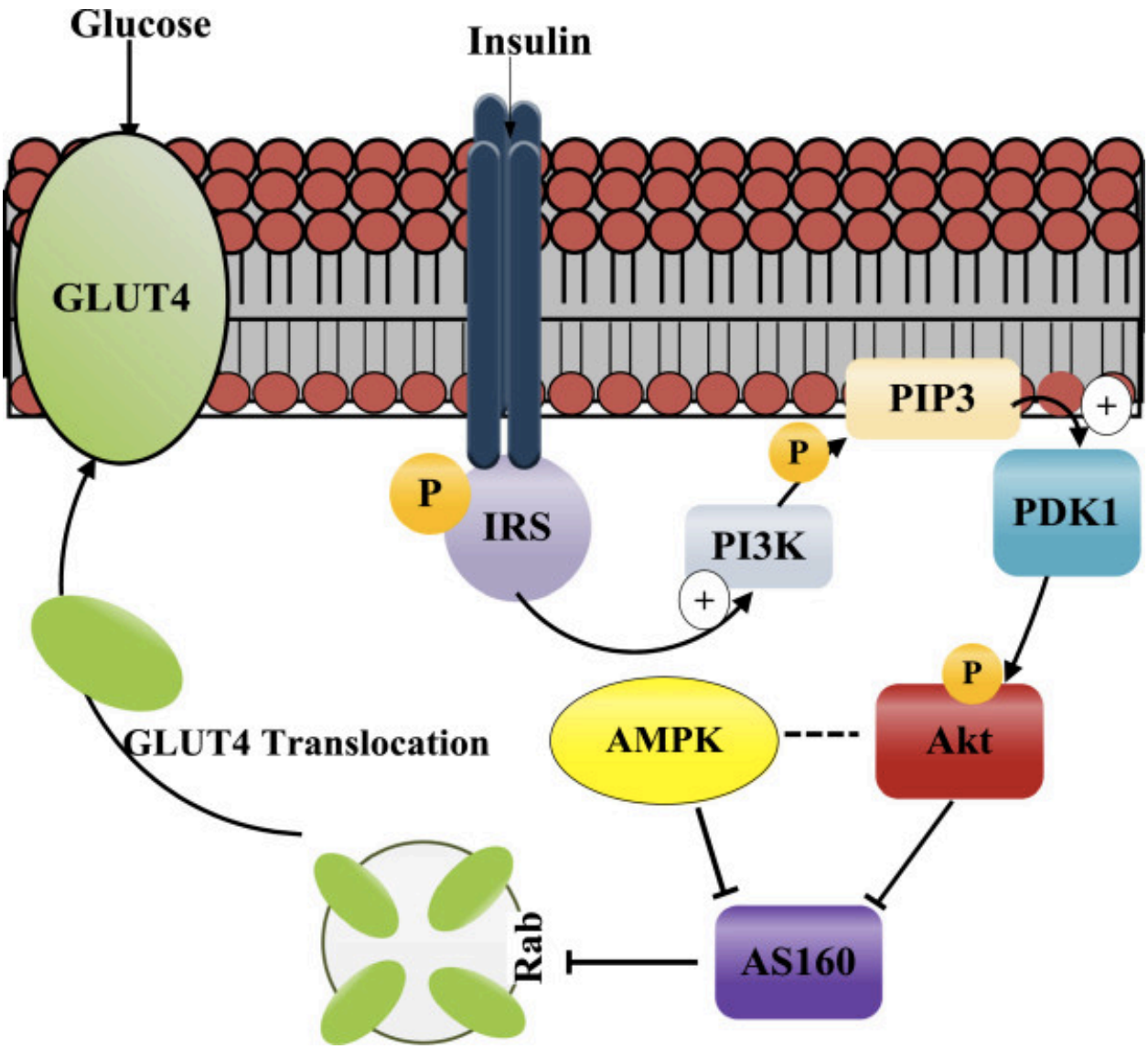

Figure 1.2 Insulin signaling pathway

Insulin binds to the IR, which is a transmembrane receptor. Upon insulin binding, IR is autophosphorylated, and thus has increased tyrosine kinase activity for other substrates, such as IRS proteins. Tyrosine phosphorylation of IRS-1 by IR introduces multiple binding sites for proteins that have SH2 homology domain, including PI3Ks. PI3K binds to tyrosine residues of IRS-1 to produce PIP3, which activates a series of downstream signaling proteins, including PDK1,

Akt and AS160 to facilitate membrane glucose transport through GLUTs, such as GLUT4 (Thorn *et al.*, 2013).

A number of GLUTs have been identified. GLUT 1 is present in all cell types, and is responsible for basal glucose uptake to sustain cellular respiration (Ciaraldi *et al.*, 2005). GLUT 2 is mainly located in the kidney, intestine, liver, and pancreas. In the liver, GLUT 2 facilitates glucose uptake for glycolysis and glycogenesis, and releases glucose during gluconeogenesis. In the beta cells of the pancreas, GLUT 2 plays a crucial role in ensuring the homeostasis of glucose levels in the intracellular environment (Thorens, 2015). GLUT 4, on the other hand, is the major transporter presents in insulin sensitive tissues, including skeletal muscle, heart, and adipose tissue. Upon stimulation with insulin, GLUT 4 translocates from the transport vesicles in the cytoplasm to the cell membrane to facilitate the entry of glucose (Abel, 2004). In the liver, insulin stimulates the storage of glucose in the form of glycogen by promoting glycogen synthesis. When the level of glycogen in the liver saturates and further glycogen synthesis is suppressed, insulin then stimulates the synthesis of fatty acids, which are exported as lipoproteins. Lipoproteins exported from the liver through the circulation can reach other tissues, such as adipose tissue, to be used for glycerol and further triglyceride synthesis. In addition, insulin can also stimulate the uptake of amino acids to contribute to its overall anabolic effect and cell growth (Bertrand *et al.*, 2008).

Skeletal muscle is the main tissue for insulin-stimulated glucose utilization, where around 60-70% of glucose uptake occurs under euglycemic conditions (Thiebaud *et al.*, 1982; Rask-Madsen and Kahn, 2012). Glucose can be either converted into glycogen for storage or enters the glycolytic pathway to be oxidized for energy production (Ijuin *et al.*, 2015). Although glucose uptake into the liver is not insulin-dependent, the liver is another major site (30%) of insulin-stimulated glucose disposal (Smith, 2002). Insulin stimulates glycogen synthesis and modulates protein synthesis and lipoprotein metabolism. At the same time, gluconeogenesis and ketone body production are inhibited (González-Sánchez and Serrano-Ríos, 2007). Adipocytes account for 10%

insulin-stimulated glucose uptake through GLUT4, and play a crucial role in regulating systemic insulin sensitivity in obesity (Frayn, 2001). Insulin promotes lipogenesis while suppressing lipolysis, and therefore, the release of free fatty acids into the bloodstream. Adipose tissue not only can store and release fatty acids, but adipocytes also function as endocrine glands, and release a variety of molecules including hormones to regulate energy balance and glucose homeostasis in other organs (Kershaw and Flier, 2004, Scherer, 2006).

1.1.3.2 Insulin resistance

One of the hallmarks of obesity is insulin resistance. The term "insulin resistance" refers to a decreased metabolic response/sensitivity of a target cell to insulin, which at the whole organism level, can be observed as a reduced ability to lower blood glucose by circulating or injected insulin (Czech, 2017). Glucose homeostasis is a balance between the production of glucose from the liver, and its metabolism in skeletal muscle and adipose tissue. The role of insulin is to inhibit glucose output from the liver, and to increase glucose uptake into skeletal muscle and adipose tissue during times of nutrient uptake. Obesity-associated insulin resistance is often manifested by impaired suppression of glucose output from the liver, as well as decreased insulin-stimulated glucose transport and metabolism in skeletal muscle and adipose tissue (Kahn and Flier, 2000). At the molecular level, impaired insulin signaling can contribute to the development of insulin resistance through increased serine phosphorylation of IRS-1 and inhibition of IRS-1 tyrosine phosphorylation, decreased activation of PI3K, and reduced phosphorylation and activation of Akt (Rask-Madsen and Kahn, 2012). In addition, reduced protein expression and translocation to the cell membrane of cytoplasmic glucose transporter 4 (GLUT 4) is associated with decreased glucose uptake and oxidation in obesity and diabetes (DeFronzo and Tripathy, 2009).

During the progression of insulin resistance, the normal lipoprotein metabolism is significantly altered, in that insulin-resistant adipocytes increase free fatty acids production, and reduce very low-density lipoprotein (VLDL) catabolism, which further results in increased triglyceride content and VLDL secretion in the liver (Wilcox, 2005). Moreover, resistance to insulin's metabolic effects results in increased hepatic glucose output via increased gluconeogenesis. Insulin resistance in adipose tissue is associated with impaired inhibition of lipolysis by insulin and leads to increased release of fatty acids and inflammatory cytokines such as interleukin-6 (IL-6) and tumor necrosis factor α (TNFα). Elevated levels of fatty acids further contribute to the accumulation of lipids, and worsen the development of insulin resistance in other tissues such as the liver, skeletal muscle, and the heart (Arner and Langin, 2014, Perry et al., 2015).

1.1.3.3 Inflammation

Accumulation of excess lipids in tissues, including adipose tissue and the liver, is often accompanied by chronic low-grade inflammation, which is evidenced by elevated levels of proinflammatory macrophages and inflammatory factors, including TNFα, monocyte chemoattractant protein-1 (MCP-1), and EGF-like module-containing mucin-like hormone receptor-like 1 (EMR1 or F4/80) (Weisberg *et al.*, 2003; Xu *et al.*, 2003; Shoelson *et al.*, 2007). Particularly, adipose tissue inflammation is closely associated with insulin resistance, and inflammatory molecules secreted by adipose tissue can affect insulin sensitivity in other tissues like skeletal muscle and the liver (Wu and Ballantyne, 2017). The relationship between obesity and inflammation was first established by Hotamisligil's team, which demonstrated that there was a positive correlation between adipose tissue mass and levels of TNFα in adipocytes. Hotamisligil et al proposed that TNFα, which is a cytokine secreted by immune cells and adipocytes, is involved in the development of insulin resistance in adipose tissue (Hotamisligil *et al.*, 1993). Several

studies have shown that mRNA and protein levels of TNFα in adipose tissue increased significantly in obese human subjects and mouse models compared to lean individuals and WT controls (Hotamisligil *et al.*, 1995; Schäfer *et al.*, 2001). Elevated levels of TNFα lead to insulin resistance by inhibiting the tyrosine phosphorylation of IRS-1 (Hotamisligil, 2003). In addition, a chemoattractive protein, MCP-1 recruits immune cells to sites of inflammation in response to obesity. For example, elevated expression of MCP-1 has been found in adipose tissue in mouse models of obesity and diabetes, and overexpression of MCP-1 increases macrophage recruitment and contributes to systemic insulin resistance (Kamei *et al.*, 2006; Kanda *et al.*, 2006). Furthermore, Weisberg et al have demonstrated that the expression of F4/80, which is a major macrophage marker, in adipose tissue is positively correlated with both adipocyte size and body mass. Specifically, the percentage of cells expressing F4/80 in adipose tissue was 3-fold more in obese mice in contrast to their lean littermates (Weisberg *et al.*, 2003).

On the other hand, peroxisome proliferator-activated receptors (PPARs) are ligand-activated transcription factors, which play an important role in regulating overall energy homeostasis, and are involved in lipid and glucose metabolism, as well as the inflammatory response (Stienstra *et al.*, 2007). In particular, peroxisome proliferator-activated receptor γ (PPARγ), which is considered as a master regulator of adipogenesis and lipogenesis, is mainly expressed in adipose tissue (Lazar, 2005). Diet-induced obesity contributes to increased expression of inflammatory genes in adipose tissue and leads to adipocyte hypertrophy and macrophage infiltration. Activation of PPARγ has been shown to be able to reverse macrophage infiltration, and down-regulate the expression of inflammatory genes in macrophages (Sugii *et al.*, 2009).

1.1.4 Obesity cardiomyopathy

As one of the growing worldwide health issues, obesity and obesity-associated complications contribute to the development of heart failure and cardiovascular diseases (Barouch *et al.*, 2006; Bhatheja *et al.*, 2016). Obesity itself is an independent risk factor for the development of left ventricular (LV) dysfunction as demonstrated in the Framingham Heart Study. In this study, among 6,000 people (mean age 55 years) without a history of heart failure, the risk of heart failure increased approximately 2-fold in obese individuals in contrast to non-obese subjects after 14 years (Kenchaiah *et al.*, 2002). Increased risk of heart failure is associated with several heart conditions, including increased incidences of hypertension, atherosclerosis, myocardial infarction, and obesity cardiomyopathy (Ebong *et al.*, 2014).

Obesity cardiomyopathy is defined as changes in the structure and function of the myocardium, contributing to mechanical consequences of structural remodeling of the heart and eventually leading to LV dysfunction (Dela Cruz and Matthay, 2009). The accumulation of fatty acids, the development of insulin resistance, cardiac steatosis, and overactivation of renin-angiotensin-aldosterone and sympathetic nervous system can contribute to ventricular remodeling and the development of ventricular hypertrophy (Kasper *et al.*, 1992; Kenchaiah *et al.*, 2002; Dela Cruz and Matthay, 2009). Obesity cardiomyopathy can develop without the presence of other risk factors such as coronary artery disease and hypertension, and can contribute to the development of LV failure and worsen myocardial infarction (Hubert *et al.*, 1983; Wong and Marwick, 2007; Boudina and Abel, 2010). In addition to cardiac structural and functional adaptations during the progression of obesity, the metabolism of the heart is often changed in obesity cardiomyopathy.

The heart has very high energy demands and has almost no energy reserves. In order to produce a large amount of adenosine triphosphate (ATP) for energy consumption, the heart

consumes a variety of substrates, including fatty acids (60-80%), glucose (40-20%), lactate, ketones, pyruvate, and amino acids (Lopaschuk *et al.*, 2010). Cardiac efficiency is defined as the ratio of the energy delivered by the heart to the energy supplied to it (Schipke, 1994). It is a measure of the efficiency of using energy to produce ATP and cardiac contraction. In fact, the cardiac efficiency of producing ATP varies significantly among different energy substrates, and most of the ATP production is accompanied by oxygen consumption for mitochondrial oxidative metabolism. For example, mitochondrial oxidation of fatty acids consumes more oxygen per molecule of ATP production than other energy substrates. In obesity, impaired glucose uptake and oxidation can lead to increased fatty acid utilization for ATP production, which causes decreased cardiac efficiency, and further leads to the accumulation of fatty acid oxidation byproducts and toxic fatty acid metabolites (Jaswal *et al.*, 2011). For example, the accumulation of intra-myocardial diacylglycerol found in C57BL/6J mice fed a HF (60% kcal from fat) diet has been implicated in cardiac insulin resistance (Lopaschuk, 2016).

Energy generation takes place mainly in mitochondria. There are around 7000 mitochondria present in an adult ventricular myocyte. The high amount of mitochondria, which take up 35% of the cell volume, meets the high-energy demands of cardiomyocytes by generating ATP (Dedkova and Blatter, 2012). Increased fatty acid utilization is associated with elevated mitochondrial reactive oxygen species (ROS) production because of elevated oxygen consumption per molecule of ATP production through a highly regulated and crucial process known as oxidative phosphorylation (Tseng *et al.*, 2010). Moreover, high ROS levels are associated with cell damage and mitochondrial dysfunction and further contributes to cardiac dysfunction (Fillmore *et al.*, 2014).

Insulin resistance also has profound adverse effects on cardiac function, and has a strong association with the progression of obesity cardiomyopathy (Aroor *et al.*, 2012). Cardiac insulin signaling plays an important role in the regulation of glucose uptake, since the heart requires the consistent utilization of glucose, fatty acids, and other metabolic substrates regardless of changes in insulin concentration (Abel, 2004). Insulin in the heart has been shown to be able to increase glucose transporter translocation, glycolytic flux, and rates of glucose oxidation through the IRS-PI3K-Akt signaling axis, as well as to suppress fatty acid utilization by the heart (Belke *et al.*, 2002). In insulin resistance, upregulation of the cluster differentiation protein 36 (CD36) increases uptake of free fatty acids into the heart and promotes fatty acid utilization. On the other hand, due to the inhibition of glucose utilization, a glycolytic intermediate accumulates in the heart and induces glucotoxicity (Taegtmeyer *et al.*, 2002). As insulin resistance progresses, the heart starts to lose its metabolic flexibility. Metabolic flexibility is the ability of the heart to adapt fuel oxidation to fuel availability (Galgani *et al.*, 2008). The inability to adapt fuel oxidation in response to changes in nutrient availability, including carbohydrates and fatty acids, lead to the accumulation of lipid. Lipid accumulation can further contribute to apoptosis, mitochondrial dysfunction, cardiac hypertrophy and cardiac contractile dysfunction (Unger and Orci, 2002; Goldberg *et al.*, 2012).

1.2 The RhoA-ROCK pathway

1.2.1 Overview

The RhoA-ROCK pathway is actively involved in a wide range of physiological functions, including smooth muscle contraction, and the regulation of cell migration, motility and adhesion (Kaibuchi *et al.*, 1999; Wang *et al.*, 2009). Ras homolog gene family, member A (RhoA) is a small

GTPase protein in the Rho family. GTPase proteins are regulatory proteins that are involved in signaling events. Guanine nucleotide exchange factors (GEFs) promote the activation of RhoA by facilitating the exchange of GDP for GTP. On the other hand, GTPase activating proteins (GAPs) deactivate RhoA through hydrolyzing GTP to GDP (Luo, 2000). Different stimuli, such as growth factors, hormones, cytokines, and integrins can promote the activation of RhoA. RhoA is mainly associated with cytoskeleton regulation such as stress fiber formation and actomyosin contractility (Fig. 1.3) (Spiering and Hodgson, 2011; Hartmann *et al.*, 2015).

Rho-associated protein kinase (ROCK), a serine/threonine kinase, is a downstream target of RhoA. There are two isoforms of ROCK, ROCK1 and ROCK2. ROCK1 and ROCK2 have an overall 65% homology in their amino acid sequence, and 92% homology in their kinase domain, which is important for phosphorylation (Wang *et al.*, 2009). Despite the similarities of ROCK1 and ROCK2, differences exist in their activation, intracellular location and interaction with target proteins (Amano *et al.*, 2010; Julian and Olson, 2014). ROCK1 is ubiquitously expressed except in the brain and muscle, while ROCK2 is mostly expressed in the brain, muscle, heart, lung, and placenta (Hartmann *et al.*, 2015). In addition, ROCK1 is specifically cleaved by caspase-3, while ROCK2 is cleaved by granzyme B. Caspase-3 and granzyme B cleave the carboxyl terminus of ROCK1 and ROCK2 respectively, and uncovering the kinase domain to promote persistent activation independent of RhoA (Coleman *et al.*, 2001; Sebbagh *et al.*, 2001, 2005). Furthermore, ROCK1 is mostly involved in the formation of stress fibers, whereas ROCK2 plays a more important role in phagocytosis and cell contraction (Yoneda *et al.*, 2005; Wang *et al.*, 2009).

ROCK can phosphorylate many downstream substrates such as LIM-Kinase (LIMK), ezrin-radixin-moesin (ERM), myosin light chain (MLC) and myosin phosphatase target subunit 1 (MYPT1) (Fig. 1.3) (Riento and Ridley, 2003; Loirand *et al.*, 2006; Hartmann *et al.*, 2015).

MYPT1 is the best-characterized ROCK substrate and can be directly bound and phosphorylated by ROCK2 to stimulate smooth muscle contraction (Amano *et al.*, 2010).

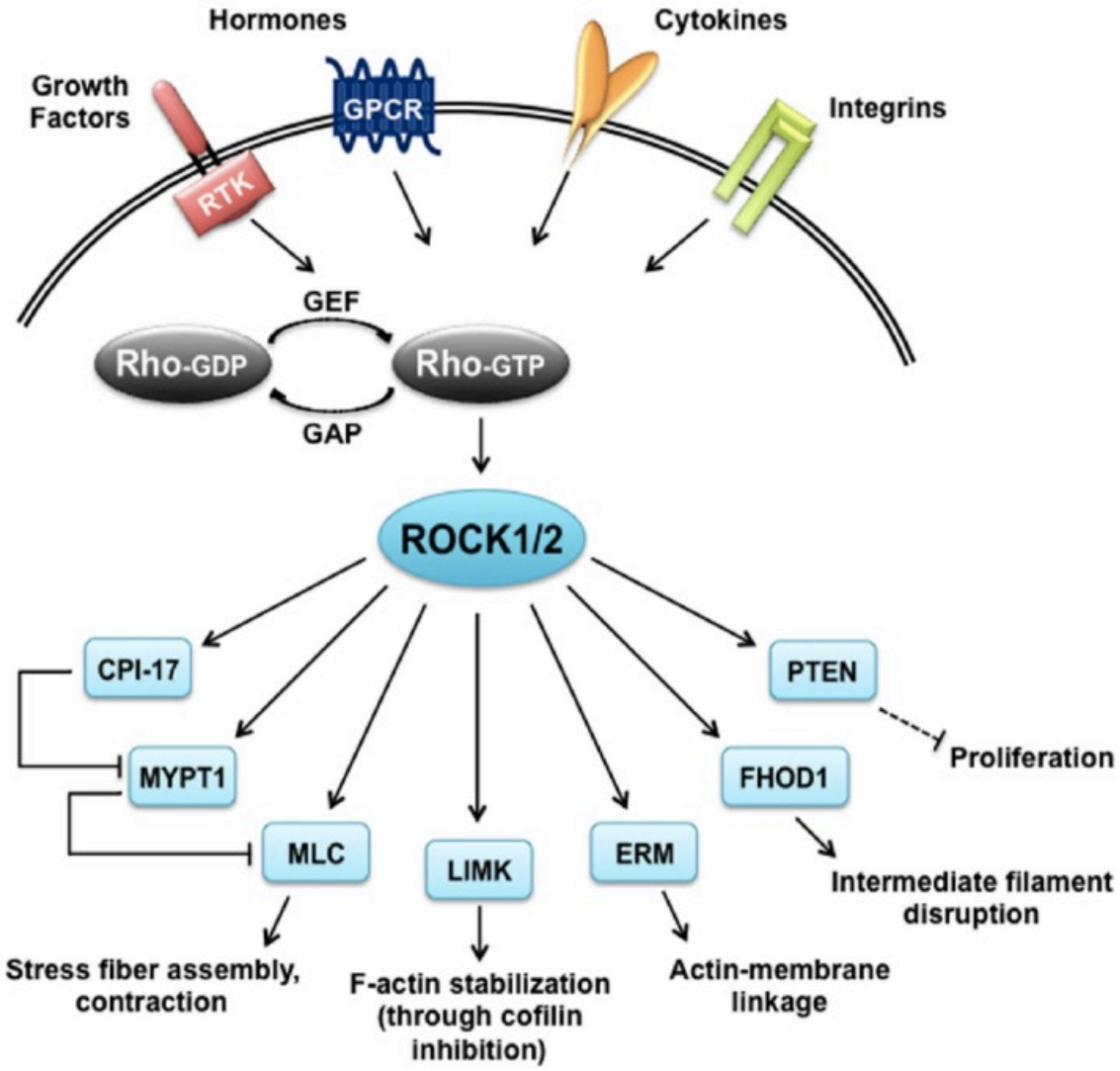

Figure 1.3 RhoA/ROCK signaling pathway

Different stimuli such as growth factors, hormones, cytokines and integrins, can stimulate the activation of the GTPase proteins, for example, RhoA, which is a small GTPase protein in the Rho family. RhoA is activated when GTP is bound to it. ROCK is a downstream target of RhoA, which has two isoforms, ROCK1 and ROCK2. Both ROCK1 and ROCK2 have multiple targets including MYPT1, MLC, LIMK, ERM, and PTEN, and are involved in stress fiber assembly and F-actin stabilization, for example (Hartmann *et al.*, 2015). Reproduce with permission under CC-BY https://creativecommons.org/licenses/by/4.0/.

1.2.2 The role of RhoA-ROCK pathway in cardiovascular diseases

Increased ROCK activity has been implicated in cardiovascular diseases and associated conditions, such as diabetic cardiomyopathy, hypertension, pulmonary hypertension, stable angina pectoris, vasospastic angina, heart failure, and stroke (Masumoto *et al.*, 2001, 2002; Shimokawa *et al.*, 2002; Kishi *et al.*, 2005; Shibuya *et al.*, 2005; Vicari *et al.*, 2005; Ishikura *et al.*, 2006). For example, our lab has previously demonstrated that the RhoA-ROCK pathway contributes to the development of diabetic cardiomyopathy and a non-specific ROCK inhibitor improved the cardiac function in a rat model of streptozotocin-induced type 1 diabetes (Lin *et al.*, 2007). In addition, in experimental hypertension models and hypertensive human patients, elevated activity of the RhoA-ROCK pathway was observed, and treatment with the non-isoform selective ROCK inhibitor, fasudil, was able to decrease the peripheral vascular resistance (Masumoto *et al.*, 2001). Moreover, increased ROCK expression is found in rat models with pulmonary hypertension, while long-term treatment with fasudil improved pulmonary hypertension and ventricular hypertrophy, as well as increased survival rate in these rats (Abe *et al.*, 2004). Overall, above studies suggest that the RhoA-ROCK pathway is a potential therapeutic target for a number of cardiovascular diseases.

Commonly used ROCK inhibitors such as fasudil lack specificity and act on both ROCK isoforms, and may also block other serine-threonine kinases, including protein kinase C-related kinase 1 and protein kinase C-related kinase 2, cAMP-activated protein kinase, and AMP-activated protein kinase (Bain *et al.*, 2007). Therefore, mouse models with ROCK specific isoform deletions have been developed to elucidate the functions of ROCK1 and ROCK2 separately *in vivo.*

ROCK1 heterozygous knockout (ROCK1+/-) mice exhibit reduced perivascular and interstitial fibrosis in myocardia, which is closely associated with decreased expression of

extracellular matrix proteins and fibrogenic cytokines compared to control mice in response to pressure overload on the heart (Zhang *et al.*, 2006). Moreover, increased suppression of cardiomyocyte apoptosis and reduced cardiac hypertrophy were observed in ROCK1 deletion (ROCK1-/-) mice in contrast to their WT littermates, indicated the beneficial effects of ROCK1 deficiency in hypertrophic decompensation and limiting heart failure progression in pressure overload (Shi *et al.*, 2010).

Mice with a cardiomyocyte-specific deletion of ROCK2 display normal cardiac anatomy, function, and hemodynamic parameters, and are protected from cardiac hypertrophy, intraventricular fibrosis, cardiac apoptosis, and oxidative stress induced by angiotensin II infusion compared to control mice (Okamoto *et al.*, 2013). Furthermore, fibroblast-specific deletion of ROCK2 protected mice from angiotensin II-induced increases in left ventricular wall thickness and fibrosis, and improved cardiac diastolic function compared to WT mice (Shimizu *et al.*, 2017).

In addition, in contrast to WT mice in which transverse aortic constriction induces cardiac diastolic dysfunction, mice with cardiac-specific deletion of ROCK2 (cROCK2-/-) showed improved cardiac diastolic function, as demonstrated by a decreased E/A ratio and reduced deceleration of the mitral E wave. This indicates the ability of ROCK2 deficiency to attenuate diastolic dysfunction in response to pressure overload (Sunamura *et al.*, 2018).

To conclude, the overactivation of ROCK is involved in the development of cardiovascular diseases. ROCK inhibitors and ROCK specific isoform deletions are able to help to lessen symptoms associated with those conditions.

1.2.3 The role of RhoA-ROCK pathway in the development of obesity cardiomyopathy and obesity-induced insulin resistance

Previous studies from our lab have demonstrated that detrimental effects of over-activation of the RhoA-ROCK pathway found in diabetic rats and HF diet-induced obese WT CD-1 mice contributes to the development of diabetic and obesity cardiomyopathy. Increased expression and activity of ROCK2 plays a crucial role in the progression of cardiomyopathy and is closely associated with mechanisms such as mitochondrial dysfunction and insulin resistance (Soliman *et al.*, 2012, 2015; Lin *et al.*, 2014). We found that in WT CD-1 mice fed a HF diet, elevated ROCK2 activity, mild cardiac contractile dysfunction, and systemic insulin resistance were observed. However, those were prevented in animals with heterozygous deletion of ROCK2 (ROCK2+/-), and ROCK2+/- mice showed improved cardiac contractile function and insulin sensitivity (Soliman *et al.*, 2015).

In addition, the study of the role of heterozygous deletion of ROCK2 in adipose tissue of HF diet-induced obese CD-1 mice revealed that over-activation of ROCK2 leads to whole-body insulin resistance, which appeared to be due in part to reduced expression of PPARγ, expanded adipocyte hypertrophy, and increased inflammatory factor production (Soliman *et al.*, 2016). Furthermore, our preliminary data also suggested that heterozygous deletion of ROCK2 was able to protect HF diet-induced obese CD-1 mice from abnormal mitochondrial morphology and imbalanced mitochondrial mediators of fission found in the left ventricular tissue of WT CD-1 mice.

Overall, over-activation of the RhoA-ROCK pathway mediated through the increased activity of ROCK2 contributes to cardiac contractile dysfunction and systemic insulin resistance

observed in HF diet-induced obesity in WT CD-1 mice. Heterozygous deletion of ROCK2 helps protect mice from HF diet-induced complications associated with obesity.

1.3 Animal models

1.3.1 Diet-induced obesity in mice

Mice are one of the most commonly used animal models to study obesity-induced human heart diseases, because of the similar cardiac developmental sequences between humans and mice, and because there is a large availability of genetically modified models (Krishnan *et al.*, 2014; Camacho *et al.*, 2016). Since the cause of obesity is multifactorial and there are many risk factors associated with it, mouse models of obesity have been categorized into different groups. There are two major categories, with one category describing animals that have one or a few genes being mutated or manipulated, and another one being the dietary-induced models. Dietary-induced obesity models mimic the main obesity trend in humans (Wang and Liao, 2012).

Dietary fat and carbohydrates such as a high-fat (HF) diet or a high fat-high sucrose (HFHS) diet, have been used to trigger diet-induced obesity and diabetes in mice (Lutz and Woods, 2012). A HF diet, generally including 45%-60% kcal from fat but low in sugars, can be used to induce obesity and insulin resistance in mouse models (Gao *et al.*, 2015; Ternacle *et al.*, 2017; Speakman, 2019). A HFHS diet, on the other hand, containing a slightly lower amount of fat but a relatively higher amount of sucrose, is thought to more closely resemble the human "Western diet", which has dramatically increased obesity levels over the past few decades (Ishimoto *et al.*, 2013; King and Austin, 2017; Burchfield *et al.*, 2018). A "Western diet" is defined as a diet containing high fat, salt, and sugars. It is generally characterized by high intakes of highly refined and saturated fats, red meat, animal protein, and over-refined sugars (Statovci *et al.*, 2017). A

typical "Western diet" consists of about 2,200 calories per day, with 35% of calories from fat, 50% of calories from carbohydrate, and 15% of calories from protein (Last and Wilson, 2006).

Many studies have shown that mice fed either a HF or a HFHS diet exhibit obesity and obesity-associated symptoms, including cardiac dysfunction and insulin resistance. For example, CD-1 mice gained a significant amount of body weight and chronic inflammation in adipose tissue was triggered after being fed a HF (60% kcal from fat) diet for 12 weeks (Gao *et al.*, 2015). C57BL/6J mice placed on a HF (60% kcal from fat) diet demonstrated myocardial dysfunction, myocardial fibrosis, and increased apoptosis after 20 weeks of feeding, in contrast to mice fed a normal diet (13% kcal from fat) (Ternacle *et al.*, 2017). Moreover, studies have reported that CD-1 mice fed a HFHS (42% kcal from fat and 30% kcal from sucrose) diet develop cardiac systolic and diastolic dysfunction after 8 weeks of feeding (Carbone *et al.*, 2015, 2017; Chen *et al.*, 2017; Zhang *et al.*, 2017). In addition, prolonged exposure (24 weeks) to a HFHS (47% kcal from fat and 32% kcal from carbohydrate) diet leads to a series of metabolic disturbances including obesity, fasting hyperglycemia, glucose intolerance and insulin resistance in the C57BL/6 male mice model (Burchfield *et al.*, 2018).

In our previous study in C57BL/6 male mice, a HF diet (60% kcal from fat and 7% kcal from sucrose) was used to mimic human obesity and insulin resistance, and a HFHS (45% kcal from fat and 17% kcal from sucrose) diet was used because its composition is closer to a human "Western diet". Although there are no specific compositions of fat and sucrose in a HF or a HFHS diet, a HFHS diet containing 45% kcal from fat and 17% kcal from sucrose was chosen in the present study because of the induction of cardiac dysfunction in C57BL/6 mice fed this HFHS diet (Pulinilkunnil *et al.*, 2014). We found that both HF and HFHS diet-fed mice exhibited glucose and insulin intolerance, and were considered pre-diabetic, which is consistent with the above studies.

However, animals fed the HFHS diet developed more severe systolic and diastolic dysfunction after 18 weeks of feeding compared to the HF group, which might be due to the higher level of fibrosis found in HFHS group according to our preliminary data.

Overall, despite similarities of HF and HFHS diets in terms of triggering obesity-associated symptoms, the underlying severity of cardiac dysfunction in mouse models of obesity may not always be the same between various regimens used and different mouse strains may also respond differently.

1.3.2 ROCK2 heterozygous (ROCK2+/-) mouse

ROCK2 plays a pivotal role in normal embryonic development and is important for cytoskeleton regulation and smooth muscle contraction. Complete ROCK2 knockout (ROCK2-/-) mice were first generated in 2003, but more than 90% of ROCK2-/- embryos died due to severe thrombus formation, placental dysfunction, and consequent intrauterine growth retardation (Thumkeo *et al.*, 2003). Therefore, ROCK2 heterozygous whole-body knockdown mouse models have been used to study the effect of ROCK2 heterozygous deletion *in vivo*.

1.4 Study aim

Previous studies from our lab have demonstrated that diet-induced obesity in mouse models is closely associated with the development of obesity cardiomyopathy (Soliman *et al.*, 2015, 2016). WT CD-1 animals fed a HF diet demonstrated significantly elevated ROCK2 activity, mild global cardiac contractile dysfunction, whole-body insulin resistance, disrupted insulin signaling in the heart and adipose tissue, and increased levels of inflammatory factor in adipocytes. However, CD-1 mice with heterozygous deletion of ROCK2 were protected from HF diet-induced obesity and associated symptoms. Moreover, in preliminary studies, heterozygous deletion of ROCK2 also

prevented HF diet-induced disrupted mitochondrial morphology and increased activity of mitochondrial mediators of fission. In addition, according to our preliminary data, a HFHS diet more closely resembling the human "Western diet", with a high content of fat and sugar, was shown to have a more detrimental effect on cardiac structure and function than a HF diet alone in WT C57BL/6J mice.

The purpose of the research in this thesis was to characterize the effect of heterozygous deletion of ROCK2 on cardiac contractile function and insulin tolerance of HFHS diet-induced obese CD-1 mice, in comparison to the HF diet-induced obese mice. Specifically, as described in Chapter 2, I investigated if a HFHS diet induced cardiac contractile dysfunction and insulin resistance in WT CD-1 animals, and if so, whether these were prevented by heterozygous deletion of ROCK2. Unexpectedly, the results of the characterization of the effects of a HFHS diet on systemic insulin sensitivity and cardiac function were not as predicted. First of all, I found that, unlike C57BL/6J mice in our previous studies, despite the development of severe obesity and systemic insulin resistance, HFHS diet-fed WT CD-1 animals were resistant to the development of cardiac contractile dysfunction. Secondly, ROCK2+/- mice were not protected against the development of systemic insulin resistance when fed a HFHS diet, as they had been when fed a HF diet in our previous studies.

In Chapter 3 I focused on investigating the insulin signaling pathway in both the liver and adipose tissue. Since we observed suppressed PPARγ expression and elevated levels of inflammatory factor production in adipose tissue of HF diet-fed WT CD-1 mice, I also investigated the same parameters in adipose tissue of HFHS diet-fed animals. I found that the expression of the RhoA-ROCK pathway in the liver and adipose tissue was very consistent with what I observed in the heart. Moreover, both ROCK2+/- mice and their WT littermates had disrupted insulin signaling

in the liver and adipose tissue when fed a HFHS diet. In addition, unlike what we found in HF diet-fed ROCK2+/- mice, HFHS diet-fed ROCK2+/- mice had elevated levels of inflammatory factor production in adipocytes, which was comparable to WT + HFHS animals. Although the exact mechanism of the loss of protection of heterozygous deletion of ROCK2 on insulin resistance is yet to be explained, the systemic insulin intolerance found in ROCK2+/- mice may be explained, at least in part, by the insulin resistance and increased levels of inflammatory factor production in tissues such as the liver and adipose tissue.

Chapter 2: Characterization of the effects of a HFHS diet on cardiac function and insulin sensitivity in WT and ROCK2+/- CD-1 mice

2.1 Introduction

Obesity is one of the major risk factors of heart failure and myocardial diseases and is associated with various medical conditions, including stroke, lung disease, and non-alcoholic fatty liver disease (Csige *et al.*, 2018). Obesity cardiomyopathy is characterized by left ventricular dysfunction with impaired ventricular filling and ejection, known as diastolic and systolic dysfunction, respectively (Carbone *et al.*, 2015). It is well-known that obesity is multifactorial, and that both genetic factors and a sedentary lifestyle contribute to the rising prevalence of obesity. A diet that is composed of a high content of fat and sugar, which is known as the Western diet, is considered to be the main cause of obesity nowadays (Bhadoria *et al.*, 2015). However, the effects of a HFHS diet on cardiac function and insulin sensitivity in mouse models of diet-induced obesity and whether they are different from the cardiac dysfunction and insulin resistance provoked by a HF diet are yet to be fully determined. Moreover, previous studies from our lab showed that heterozygous deletion of ROCK2 is able to protect mice from cardiac contractile dysfunction and insulin resistance induced by a HF diet. Therefore, in the current study, I was interested in investigating the effect of heterozygous deletion of ROCK2 on mice with a HFHS diet-induced obesity.

Our lab has previously demonstrated that WT CD-1 mice fed a HF diet (60% kcal from fat and 7% kcal from sucrose) for 17 weeks developed mild global cardiac contractile dysfunction, indicated by an elevation of the myocardial performance index (MPI). In addition, speckle-tracking-based strain echocardiography also showed regional wall motion impairment in the left

ventricle of hearts from WT + HF animals (Soliman *et al.*, 2015). Moreover, our preliminary studies have implied that there is an association between mitochondrial dysfunction and the progression of cardiac dysfunction, indicated by decreased phosphorylation of serine 637 in the mitochondrial mediator of fission, dynamin-related protein 1 (Drp1), in WT + HF mice. A reduction of serine 637 phosphorylation of Drp1 activates mitochondrial fission, which leads to a disruption of mitochondrial morphology and contributes to mitochondrial dysfunction. Consistent with the decrease in the level of ^{Ser637}pDrp1 in hearts from WT + HF mice, we also found that the mitochondria in left ventricular tissue of these mice were quite abnormal, as shown by the disruption of mitochondrial cristae, and the appearance of more and smaller mitochondria using transmission electron microscopy in our preliminary studies. However, ROCK2+/- + HF mice demonstrated more regular mitochondrial morphology and organization than WT + HF mice. Thus, ROCK2 heterozygous deletion may be able to reduce mitochondrial fission and prevent the development of abnormal mitochondrial dynamics and cardiac function.

A diet composed of a high content of fat and sucrose more closely resembles the human daily diet than a diet that is only rich in fat. This “Western-style” diet has been reported to contribute to the current epidemic of obesity and associated metabolic disorders (Yang *et al.*, 2012). Moreover, we observed more detrimental effects on cardiac contractile dysfunction in WT C57BL/6J mice fed a HFHS diet (45% kcal from fat and 17% kcal from sucrose) than mice fed a HF diet alone after 18 weeks of diet feeding in our preliminary studies. However, it is not clear whether a HFHS diet would induce greater cardiac contractile dysfunction than a HF diet in WT CD-1 mice, and how long a feeding period would be needed. Therefore, the purpose of the current study was to investigate the effect of a HFHS diet containing 45% kcal from fat and 17% kcal from sucrose on cardiac contractile function and insulin resistance in WT CD-1 mice, and to

determine whether heterozygous deletion of ROCK2 was able to protect animals from resulting obesity-induced morbidities.

I found that despite a significant gain in body weight, and the development of systemic glucose and insulin intolerance, HFHS diet-fed WT CD-1 mice were resistant to the development of cardiac dysfunction, which differs from what we observed in both HF diet-fed WT CD-1 animals and in HFHS diet-fed WT C57BL/6J animals. In addition, heterozygous deletion of ROCK2 did not protect these mice from systemic glucose and insulin intolerance induced by a HFHS diet.

2.2 Materials and methods

2.2.1 Animals

CD-1 WT and ROCK2+/- male animals were used in this study. Male CD-1 ROCK2+/- mice were generated as previously described and were bred with female WT (ROCK2+/+) mice (Zhou *et al.*, 2009). Genotyping of offspring using polymerase chain reaction was performed to confirm their genotypes. Since complete ROCK2 knockout (ROCK2-/-) is embryonically lethal, ROCK2 mice (ROCK2+/-) were used. The CD-1 strain was chosen for the present study because of the minimal detrimental effects of ROCK2 heterozygous deletion on embryonic development in this genetic background compared to other strains (Thumkeo *et al*., 2003).

Three sets of animals were used. In first 2 sets of animals (set 1 and set 2), at the age of 6 weeks, WT male mice and their ROCK2+/- male littermates were divided into two groups each and fed either a low fat-low sucrose (LFLS) diet (Cat #:D12450J, Research Diets, New Brunswick, NJ, USA), containing 10% kcal from fat and 7% kcal from sucrose, or a high fat-high sucrose (HFHS) diet (Cat #:D12451, Research Diets, New Brunswick, NJ, USA), containing 45% kcal

from fat and 17% kcal from sucrose. In the 3rd set of mice (set 3), at the age of 6 weeks, WT male mice and their ROCK2+/- male littermates were divided into groups and were maintained on either a chow (CH) diet (Cat #:5053, LabDiet, St. Louis, MO), containing 13% kcal from fat or a high-fat (HF) diet (Cat #:D12492, Research Diets, New Brunswick, NJ, USA), containing 60% kcal from fat and 7% kcal from sucrose. The composition of the diets is described in Appendix. All animals were housed under identical conditions and given free access to food and water. Body weight was monitored weekly.

In the 1st set of mice (set 1), cardiac function was assessed using echocardiography in all animals after 16 to 18 weeks of feeding. Glucose tolerance tests (GTT) and insulin tolerance tests (ITT) were performed 1 and 2 weeks after echocardiography, respectively, to investigate glucose and insulin tolerance. Food and fluid intake were monitored for 5 consecutive days in a subgroup of animals (n=4-7 in each group). In the 2nd set of mice (set 2), GTT was performed in all mice after 21 weeks of feeding, and cardiac function was assessed in all animals using echocardiography at week 24. In the 3rd set of mice (set 3), cardiac function was assessed in all animals using echocardiography at week 16. Glucose tolerance tests (GTT) and insulin tolerance tests (ITT) were performed 1 and 2 weeks after echocardiography, respectively to investigate glucose and insulin tolerance.

On the day of termination (at week 19-20 for set 1, at week 26 for set 2, and at week 23 for set 3), all mice were fasted for 5-6 h and then injected with human insulin (Humulin R, Eli Lilly, ON, Canada; 10 U/kg ip); 5 min later, they were deeply anesthetized with 4% isoflurane. After 5 min, the mice were euthanized. Hearts and other organs, e.g. liver, epididymal adipose tissue and gastrocnemius muscle, were removed, and the apex of the heart and a small portion of adipose tissue were fixed in 10% formalin. The remaining tissues were frozen in liquid nitrogen and stored

at -80°C for later biochemical analysis. All animal studies were performed in accordance with the Canadian Council for Animal Care's Guide for the Care and Use of Experimental Animals and were approved by the Animal Care Committee of The University of British Columbia.

2.2.2 Glucose tolerance test (GTT)

Mice were fasted for 6 hours. Animals were weighed and a basal (time 0) blood sample was taken via tail vein sampling. Blood glucose was measured using One Touch Ultra test strips and a One Touch Ultra 2 glucometer (LifeScan, Burnaby, BC, Canada). Glucose (2 g/kg body weight) as a 40% solution (wt/vol) was then injected intraperitoneally using a 27 G insulin syringe, and blood glucose was measured in each animal at 15, 30, 60, 90, and 120 min following the glucose injection.

2.2.3 Insulin tolerance test (ITT)

Mice were fasted for 6 hours. Animals were weighed and a basal (time 0) blood sample was taken via tail vein sampling. Blood glucose was measured using One Touch Ultra test strips and a One Touch Ultra 2 glucometer (LifeScan, Burnaby, BC, Canada). Insulin (0.75 units/kg body weight) (Humulin R, Eli Lilly, ON, Canada; 10 U/kg ip) was then injected intraperitoneally using a 27 G insulin syringe, and blood glucose was measured in each animal at 10, 20, 40, and 60 min following the insulin injection.

2.2.4 Echocardiography and speckle-tracking analysis

To assess cardiac dimensions and function, transthoracic echocardiography of the left ventricle was carried out in anesthetized mice using a VisualSonics Vevo 2100 ultrasound (Fujifilm VisualSonics, Toronto, ON, Canada) as previously described (Soliman et al., 2015). Body hair on the mouse chest area was removed using depilatory cream one day prior to the echocardiography. Anesthesia was induced with 4% isoflurane and maintained with 1-1.5%

isoflurane. Mice were placed on a heating pad, and body temperature was maintained at 37 ± 0.5°C. M-mode and two-dimensional parasternal short- and long-axis scans were made to assess changes in left ventricular dimensions, fractional shortening (FS), ejection fraction (EF), and cardiac output (CO). An apical four-chamber view of the left ventricle was obtained, and a pulsed-wave Doppler system was used to determine the ratio of early to late transmitral velocities, isovolumic contraction and relaxation times (IVCT and IVRT), and MPI. Tissue Doppler was used to measure the movement of the mitral valve to generate the ratio of early (E') to atrial (A') peak velocities. Endocardial radial, longitudinal, and circumferential forward and reverse velocities, displacement, strain, and strain rates were determined using speckle-tracking echocardiography with VevoStrain software to detect left ventricular wall motion abnormalities.

2.2.5 Western blot protein analysis

Tissues were homogenized in radioimmunoprecipitation assay (RIPA) buffer with 1X protease/phosphatase inhibitors (Cell Signaling Technology, Beverly, MA). 20–40 μg of protein was loaded. Proteins were separated by 6-12% SDS-PAGE, transferred to nitrocellulose membrane, and immunoblotted using primary antibodies (range from 1:500 to 1: 1,000) against ROCK1 (611136) (BD Biosciences, San Jose, CA); RhoA (sc-418), ROCK2 (sc-5561), OPA1 (sc-393296), Mfn1 (sc-166644), Mfn2 (sc-515647), Fis1 (sc-376447) (Santa Cruz Biotechnology, Inc., Dallas, TX); Akt (9272), Ser473-phosphorylated Akt (9271), Thr642-phosphorylated AS160 (8881), Drp1 (5391), Ser637-phosphorylated Drp1 (4867), IRS-1 (2382), Ser307-phosphorylated IRS-1 (2381) (Cell Signaling Technology, Beverly, MA); Tyr612-phosphorylated IRS-1 (44-816G) (Thermo Fisher Scientific, Waltham, MA) at 4°C overnight. They were subsequently incubated with secondary antibodies (range from 1:2,500 to 1:10,000) at room temperature for 1 hr. Protein expression was visualized using a Li-Cor Odyssey CLX imaging system (Li-Cor

Biosciences, Lincoln, NE). Protein band intensity was determined by densitometry and normalized to vinculin or alpha-tubulin, or the corresponding total protein in the same preparation.

2.2.6 Statistical analysis

All values are shown as mean ± SEM; n denotes the number of animals in each group. Results were analyzed using GraphPad Prism version 8.0 (GraphPad Software, San Diego, CA). The body weight, GTT, and ITT were analyzed by two-way repeated measures ANOVA followed by a Bonferroni's post-hoc test. All other data was analyzed by one-way ANOVA followed by Newman-Keul's test. Differences were considered statistically significant at $p < 0.05$.

2.3 Results

2.3.1 HFHS diet-fed mice

2.3.1.1 Mouse phenotype

In HFHS diet-fed mice in set 1, both WT + HFHS and ROCK2+/- + HFHS mice gained a significant amount of body weight ($p < 0.05$) over 16 weeks compared to ROCK2+/- + LFLS animals (Fig. 2.1B), despite the fact that all animals started with similar body weight at week 0 (Fig. 2.1A). In addition, ROCK2+/- + HFHS mice gained slightly more body weight than WT + HFHS animals overall, although the difference was not statistically significant (Fig. 2.1A). Moreover, at termination (week 19-20), hearts ($p < 0.05$) and livers ($p < 0.05$) of ROCK2+/- + HFHS mice weighed significantly more than all other three groups of animals (Table 2.1).

Table 2.1 Phenotypic characterization (set 1)

Parameter	WT		ROCK2+/-	
	LFLS	**HFHS**	**LFLS**	**HFHS**
Food intake (g per day)	3.07 ± 0.43	2.86 ± 0.12	3.33 ± 0.23	3.31 ± 0.29
Water intake (ml per day)	1.90 ± 0.46	2.30 ± 0.31	2.43 ± 0.21	2.39 ± 0.11
Heart weight (g)	0.234 ± 0.001	0.250 ± 0.010	0.247 ± 0.008	0.277 ± 0.009*
Liver weight (g)	1.74 ± 0.05	1.99 ± 0.10	1.70 ± 0.04	2.51± 0.21*
Epididymal fat weight (g)	2.52 ± 0.40	4.14 ± 0.65	2.57 ± 0.36	3.87 ± 0.35
Tibial length (g)	1.18 ± 0.03	1.10 ± 0.03	1.14 ± 0.03	1.07 ± 0.02
Heart weight (g)/ Body weight (g)	0.00476 ± 0.0003	0.00438 ± 0.0003	0.00514 ± 0.0002	0.00424 ± 0.0002$
Liver weight (g) / Body weight (g)	0.0352 ± 0.002	0.0346 ± 0.002	0.0352 ± 0.001	0.0373± 0.002
Epididymal fat weight (g) / Body weight (g)	0.0485 ± 0.006	0.0697 ± 0.008	0.0504 ± 0.005	0.0583 ± 0.005

Food and fluid intake were monitored for 5 consecutive days in a subgroup of animals (n=4-7 in each group) 1 week prior to euthanasia. Mice were euthanized, heart weight, liver weight, epididymal fat weight, and tibial length were measured at week 19-20. *$p < 0.05$ compared to all other groups. $$p < 0.05$ compared to ROCK2+/- + LFLS. Data shown as mean ± S.E.M., n= 8-14 in each group.

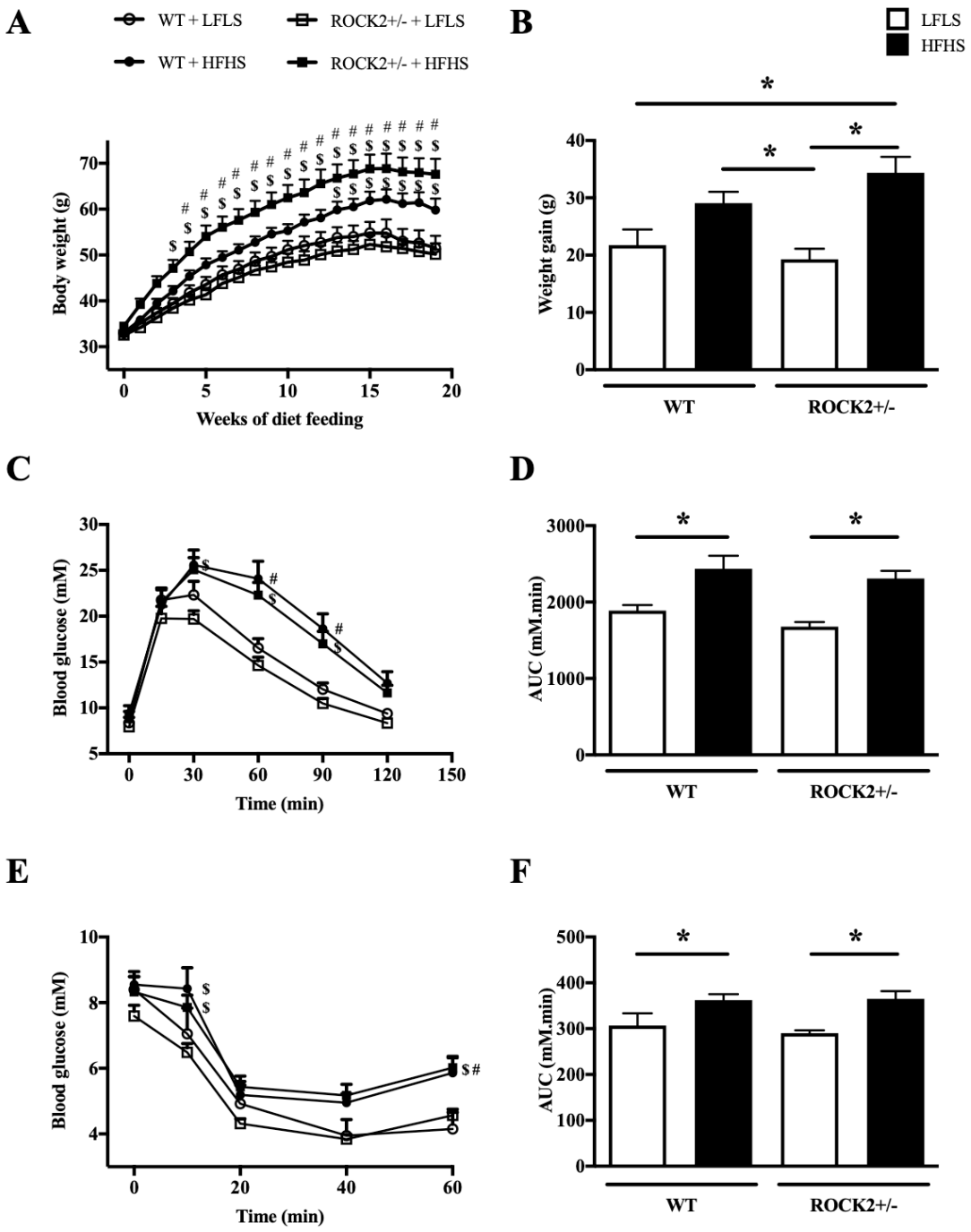

Figure 2.1 Effect of HFHS diet on body weight, and glucose and insulin tolerance (set 1)

(A) Body weight, (B) body weight gain over 16 weeks, (C) blood glucose levels measured by glucose tolerance tests (GTT), (D) area under GTT curves (AUC), (E) blood glucose levels measured by insulin tolerance tests (ITT), (F) area under ITT curves (AUC). *$p < 0.05$, #$p < 0.05$ compared to WT + LFLS, \$$p < 0.05$ compared to ROCK2+/- + LFLS. Data shown as mean ± S.E.M., n= 8-14 in each group.

In set 2 mice, both WT + HFHS and ROCK2+/- + HFHS mice gained a significant amount of body weight ($p < 0.05$) compared to their LFLS diet-fed littermates over 24 weeks of feeding (Fig. 2.2A-B). At termination (week 26), ROCK2+/- + HFHS mice had a slightly increased liver weight ($p < 0.05$) compared to all other animal groups as observed in set 1 (Table 2.2). In addition, both WT + HFHS and ROCK2+/- + HFHS mice gained significantly more epididymal fat weight ($p < 0.05$) than their LFLS diet-fed littermates (Table 2.2). However, unlike what I found in set 1, there was no difference in heart weight among animals in set 2 (Table 2.2).

Table 2.2 Phenotypic characterization (set 2)

Parameter	WT		ROCK2+/-	
	LFLS	HFHS	LFLS	HFHS
Heart weight (g)	0.195 ± 0.008	0.198 ± 0.007	0.185 ± 0.009	0.208 ± 0.005
Liver weight (g)	1.91 ± 0.05	2.14 ± 0.11	1.70 ± 0.08	2.48± 0.17*
Epididymal fat weight (g)	1.82 ± 0.14	3.50 ± 0.27*	2.05 ± 0.24	4.69 ± 0.37*
Tibial length (g)	1.17 ± 0.02	1.13 ± 0.03	1.16 ± 0.02	1.14 ± 0.02
Heart weight (g)/ Body weight (g)	0.00419 ± 0.0002	0.00338 ± 0.0001#$	0.00408 ± 0.0002	0.00309 ± 0.0001#$
Liver weight (g) / Body weight (g)	0.0411 ± 0.001	0.0364 ± 0.002	0.0373 ± 0.001	0.0369± 0.003
Epididymal fat weight (g) / Body weight (g)	0.0391 ± 0.003	0.0595 ± 0.004#$	0.0443 ± 0.004	0.0685 ± 0.003#$

Mice were euthanized, heart weight, liver weight, epididymal fat weight, and tibial length were measured at week 26. *$p < 0.05$ compared to all other groups. #$p < 0.05$ compared to WT + LFLS, $$p < 0.05$ compared to ROCK2+/- + LFLS. Data shown as mean ± S.E.M., n= 7-10 in each group.

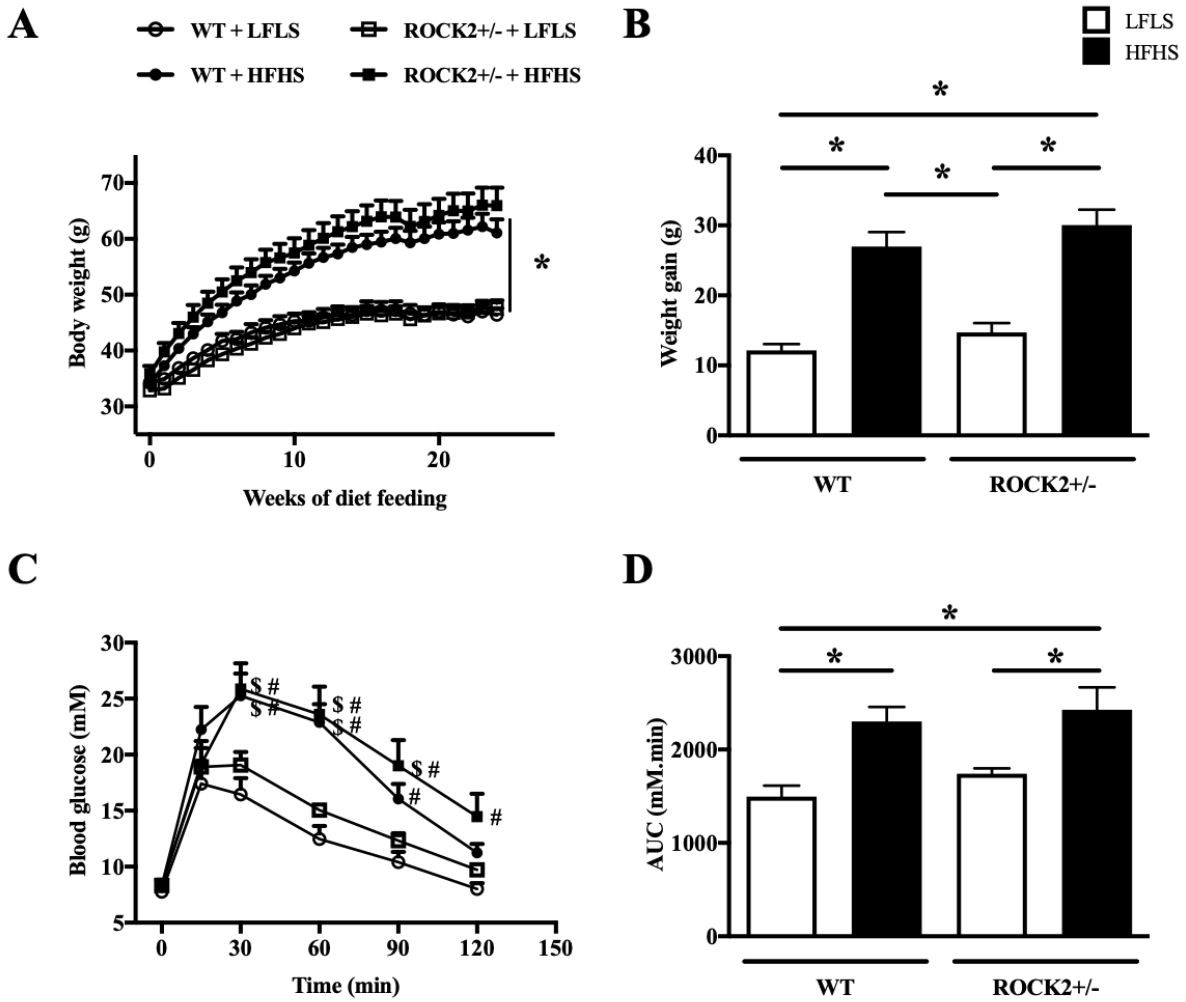

Figure 2.2 Effect of HFHS diet on body weight and glucose tolerance (set 2)

(A) Body weight, (B) body weight gain over 24 weeks, (C) blood glucose levels measured by glucose tolerance tests (GTT), (D) area under GTT curves (AUC), *$p < 0.05$, #$p < 0.05$ compared to WT + LFLS, \$$p < 0.05$ compared to ROCK2+/- + LFLS. Data shown as mean ± S.E.M., n= 7-10 in each group.

2.3.1.2 Glucose and insulin tolerance tests

The HFHS diet induced systemic glucose and insulin intolerance in both WT and ROCK2+/- animals. Fasted, basal blood glucose levels were not significantly different (Time 0) (Fig. 2.1C, E). WT + HFHS and ROCK2+/- + HFHS animals showed significantly higher levels of blood glucose ($p < 0.05$) compared to LFLS diet-fed WT and ROCK2+/- mice 30, 60, and 90 min after 2g/kg intraperitoneal glucose injection (Fig. 2.1C). Overall, HFHS diet-fed animals exhibited elevated blood glucose levels ($p < 0.05$) in contrast to their corresponding littermates, which was reflected in the area under the curve (AUC) for GTT (Fig. 2.1D).

Glucose levels of WT + HFHS and ROCK2+/- + HFHS animals remained above glucose levels of WT + LFLS and ROCK2+/- + LFLS animals from 10 min after 0.75U/kg intraperitoneal insulin injection (Fig. 2.1E). Elevated glucose levels in WT + HFHS and ROCK2+/- + HFHS animals were reflected in the AUC for ITT (Fig. 2.1F). Similar results in the GTT and AUC for GTT found in set 2 animals at week 21 further confirmed the glucose intolerance in HFHS diet-fed WT and ROCK2+/- animals (Fig. 2.2C-D).

2.3.1.3 Cardiac dimensions and function

Cardiac function and dimensional measurements were assessed by echocardiography at week 16-18 in set 1 animals. Only small variations of cardiac function and dimensions were observed among animal groups, and these differences were not statistically significant (Table 2.3-2.4). The increased left ventricular mass (LV mass) found in WT + HF mice was absent in WT + HFHS animals (Soliman *et al.*, 2015). However, WT + HFHS animals exhibited lower heart rate compared to WT + LFLS mice ($p < 0.05$) (Table 2.3). HFHS diet feeding had no significant effect on ejection fraction or fractional shortening, both of which are indices of systolic LV function, in hearts from WT or ROCK2+/- mice at week 16-18 (Fig. 2.3A-B). IVCT and IVRT, which are

measures of systolic and diastolic LV function, respectively, also did not show any significant differences among animals at week 16-18 (Fig. 2.3C-D). The MV E/A, E'/A', and MV E/E' are also measures of LV diastolic function. Although there were small differences among animal groups, these were not significant, except that WT + HFHS mice presented a decrease in E'/A' ratio compared to ROCK2+/- + HFHS animals ($p < 0.05$) (Fig. 2.3E-G). Furthermore, the relatively comparable results of LV MPI, which is a reflection of global left ventricular function, were also found in different groups of animals, (Fig. 2.3H).

Table 2.3 Effect of HFHS diet on cardiac function (set 1)

Parameter	**WT**		**ROCK2+/-**	
	LFLS	**HFHS**	**LFLS**	**HFHS**
Heart rate (BPM)	483.2 ± 12.97	433.8 ± 16.17$^{\#}$	461.1 ± 4.80	443.7 ± 3.39
CO (mL/min)	26.24 ± 2.61	24.64 ± 1.34	25.26 ± 1.86	24.65 ± 1.14
SV (μL)	54.06 ± 4.38	57.13 ± 3.47	54.78 ± 3.98	55.64 ± 3.87
AET (ms)	44.51 ± 1.92	47.54 ± 2.24	49.17 ± 1.62	51.63 ± 1.36
MV Decel (ms)	20.97 ± 2.14	23.43 ± 1.20	21.79 ± 0.43	24.40 ± 1.17
MV PHT (simplified) (ms)	6.08 ± 0.62	6.79 ± 0.35	6.32 ± 0.13	7.08 ± 0.34

Cardiac function was assessed by echocardiography, at week 16-18. **CO**, cardiac output; **SV**, stroke volume; **AET**, aortic ejection time; **MV Decel**, E wave deceleration time; **MV PHT**, mitral valve pressure half time. $^{\#}p < 0.05$ compared to WT + LFLS. Data shown as mean ± S.E.M., n= 4-7 in each group.

Table 2.4 Effect of HFHS diet on cardiac dimensional measurements (set 1)

Parameter	WT		ROCK2+/-	
	LFLS	**HFHS**	**LFLS**	**HFHS**
LV Mass (mg)	163.3 ± 2.69	143 ± 5.57	147.6 ± 9.51	158.5 ± 6.09
LV Vol;d (μL)	71.78 ± 6.23	83.57 ± 6.86	70.48 ± 4.28	69.58 ± 4.35
LV Vol;s (μL)	18.07 ± 3.29	24.62 ± 5.08	16.62 ± 2.08	13.94 ± 2.60
LVAW;d (mm)	1.12 ± 0.07	1.06 ± 0.03	1.17 ± 0.04	1.21 ± 0.04
LVAW;s (mm)	1.77 ± 0.16	1.73 ± 0.09	1.80 ± 0.05	1.99 ± 0.13
LVID;d (mm)	4.03 ± 0.15	4.29 ± 0.15	4.00 ± 0.99	3.98 ± 0.10
LVID;s (mm)	2.26 ± 0.19	2.52 ± 0.24	2.20 ± 0.11	2.03 ± 0.15
LVPW;d (mm)	1.18 ± 0.05	0.97 ± 0.04	1.06 ± 0.08	1.16 ± 0.06
LVPW;s (mm)	1.92 ± 0.06	1.54 ± 0.09	1.71 ± 0.16	1.91 ± 0.09

Cardiac dimensional measurements were assessed by echocardiography, at week 16-18. **LV Mass**, left ventricular mass; **LV Vol;d**, left ventricle volume systole; **LV Vol;s**, left ventricle volume diastole; **LVAW;d**, left ventricular anterior wall (diastole); **LVAW;s**, left ventricular anterior wall (systole); **LVID;d**, left ventricular internal wall (diastole); **LVID;s**, left ventricular internal wall (systole); **LVPW;d**, left ventricular posterior wall (diastole); **LVPW;s**, left ventricular posterior wall (systole). Data shown as mean ± S.E.M., n= 4-7 in each group.

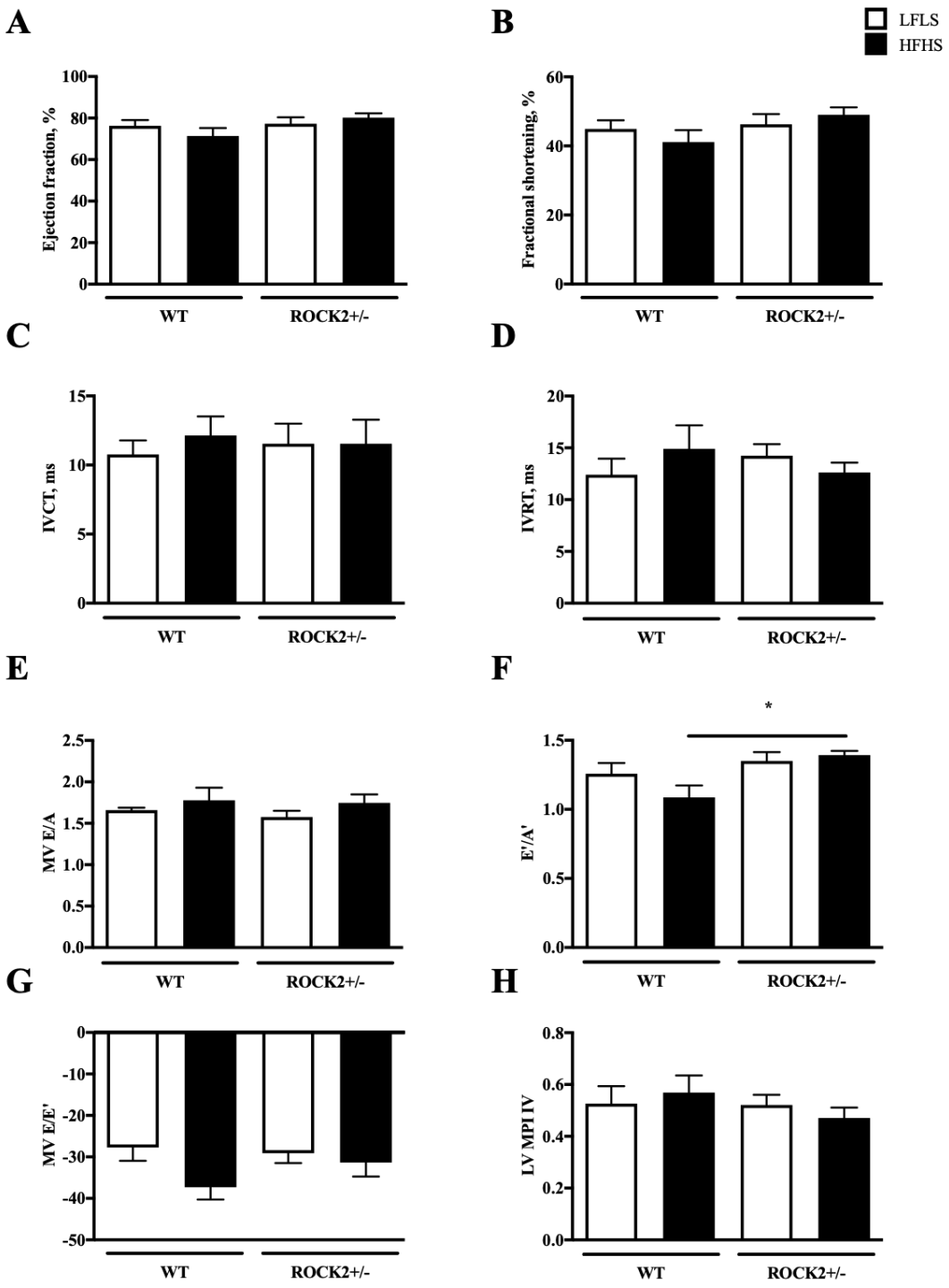

Figure 2.3 Echocardiographic measures of cardiac function at week 16-18 (set 1)

LV systolic function was assessed by measuring (A) ejection fraction, (B) fractional shortening, and (C) IVCT. LV diastolic function was assessed by determining (D) IVRT, (E) MV E/A, (F) E'/A', and (G) MV E/E'. (H) LV MPI IV reflects both LV systolic and diastolic function. *$p < 0.05$. Data shown as mean ± S.E.M., n= 4-7 in each group.

In order to assess whether there were any regional changes of wall motion in the left ventricles in mice at week 16-18, speckle-tracking-based strain echocardiography, which is a more sensitive measure of function than ejection fraction and fractional shortening (Stanton *et al.*, 2009; Kraigher-Krainer *et al.*, 2014), was used for early detection of myocardial dysfunction. However, there were only small variations in wall motion among the different animal groups with no significant differences between them (Fig. 2.4-2.6), except that WT + HFHS mice exhibited a significantly reduced endocardial radial forward displacement in contrast to ROCK2+/- + HFHS animals ($p < 0.05$) (Fig. 2.5C).

The cardiac function data obtained at week 16-18 suggested that cardiac dysfunction might be developing in WT + HFHS mice. Therefore, the second set of mice was followed for 24 weeks to determine whether more severe cardiac dysfunction could be detected with a longer period of HFHS diet feeding. In set 2 animals, cardiac function and dimensional measurements were assessed by echocardiography at week 24. Although ROCK2+/- + HFHS mice seemed to have enlarged left ventricles (LV) represented by slightly increased LV mass, and left ventricular volume during systole and diastole (LV Vol;d and LV Vol;s) (Table 2.6), these differences were not significant. The results of cardiac dimensions and function found in set 2 animals were similar to set 1 mice, in that despite the presence of small variations among animal groups, no statistically significant differences were observed (Table 2.5-2.6, Fig. 2.7). In addition, differences found between in set 1 animals, for example, in the heart rate and E'/A' ratio, were not observed in set 2 animals.

Table 2.5 Effect of HFHS diet on cardiac function (set 2)

Parameter	WT		ROCK2+/-	
	LFLS	**HFHS**	**LFLS**	**HFHS**
Heart rate (BPM)	464.1 ± 6.49	472.1 ± 10.03	445.7 ± 7.21	439.9 ± 15.16
CO (mL/min)	23.27 ± 1.46	24.32 ± 1.48	22.04 ± 1.13	23.90 ± 1.43
SV (μL)	50.35 ± 3.46	51.60 ± 3.07	49.46 ± 2.49	55.08 ± 4.44
AET (ms)	42.89 ± 1.58	43.75 ± 1.86	43.73 ± 1.04	45.00 ± 1.98
MV Decel (ms)	23.72 ± 0.78	22.00 ± 1.17	21.83 ± 1.32	22.26 ± 1.48
MV PHT (simplified) (ms)	6.88 ± 0.23	6.38 ± 0.34	6.33 ± 0.38	6.46 ± 0.43

Cardiac function was assessed by echocardiography, at week 24. **CO**, cardiac output; **SV**, stroke volume; **AET**, aortic ejection time; **MV Decel**, E wave deceleration time; **MV PHT**, mitral valve pressure half time. $^{\#}p < 0.05$ compared to WT + LFLS. Data shown as mean ± S.E.M., n= 7-10 in each group.

Table 2.6 Effect of HFHS diet on cardiac dimensional measurements (set 2)

Parameter	WT		ROCK2+/-	
	LFLS	**HFHS**	**LFLS**	**HFHS**
LV Mass (mg)	159.3 ± 15.6	156.6 ± 7.34	142.2 ± 9.59	176.3 ± 11.2
LV Vol;d (μL)	69.00 ± 5.06	66.79 ± 3.38	67.82 ± 5.48	78.92 ± 5.81
LV Vol;s (μL)	22.74 ± 2.27	17.22 ± 1.81	23.25 ± 4.94	27.11 ± 2.83
LVAW;d (mm)	1.15 ± 0.05	1.17 ± 0.05	1.09 ± 0.05	1.27 ± 0.05
LVAW;s (mm)	1.72 ± 0.07	1.83 ± 0.06	1.65 ± 0.09	1.85 ± 0.05
LVID;d (mm)	3.95 ± 0.12	3.91 ± 0.09	3.93 ± 0.14	4.19 ± 0.14
LVID;s (mm)	2.49 ± 0.10	2.23 ± 0.10	2.47 ± 0.21	2.67 ± 0.13
LVPW;d (mm)	1.16 ± 0.07	1.16 ± 0.05	1.12 ± 0.08	1.11 ± 0.05
LVPW;s (mm)	1.61 ± 0.08	1.73 ± 0.07	1.65 ± 0.13	1.59 ± 0.07

Cardiac dimensional measurements were assessed by echocardiography, at week 24. **LV Mass**, left ventricular mass; **LV Vol;d**, left ventricle volume systole; **LV Vol;s**, left ventricle volume diastole; **LVAW;d**, left ventricular anterior wall (diastole); **LVAW;s**, left ventricular anterior wall (systole); **LVID;d**, left ventricular internal wall (diastole); **LVID;s**, left ventricular internal wall (systole); **LVPW;d**, left ventricular posterior wall (diastole); **LVPW;s**, left ventricular posterior wall (systole). Data shown as mean ± S.E.M., n= 7-10 in each group.

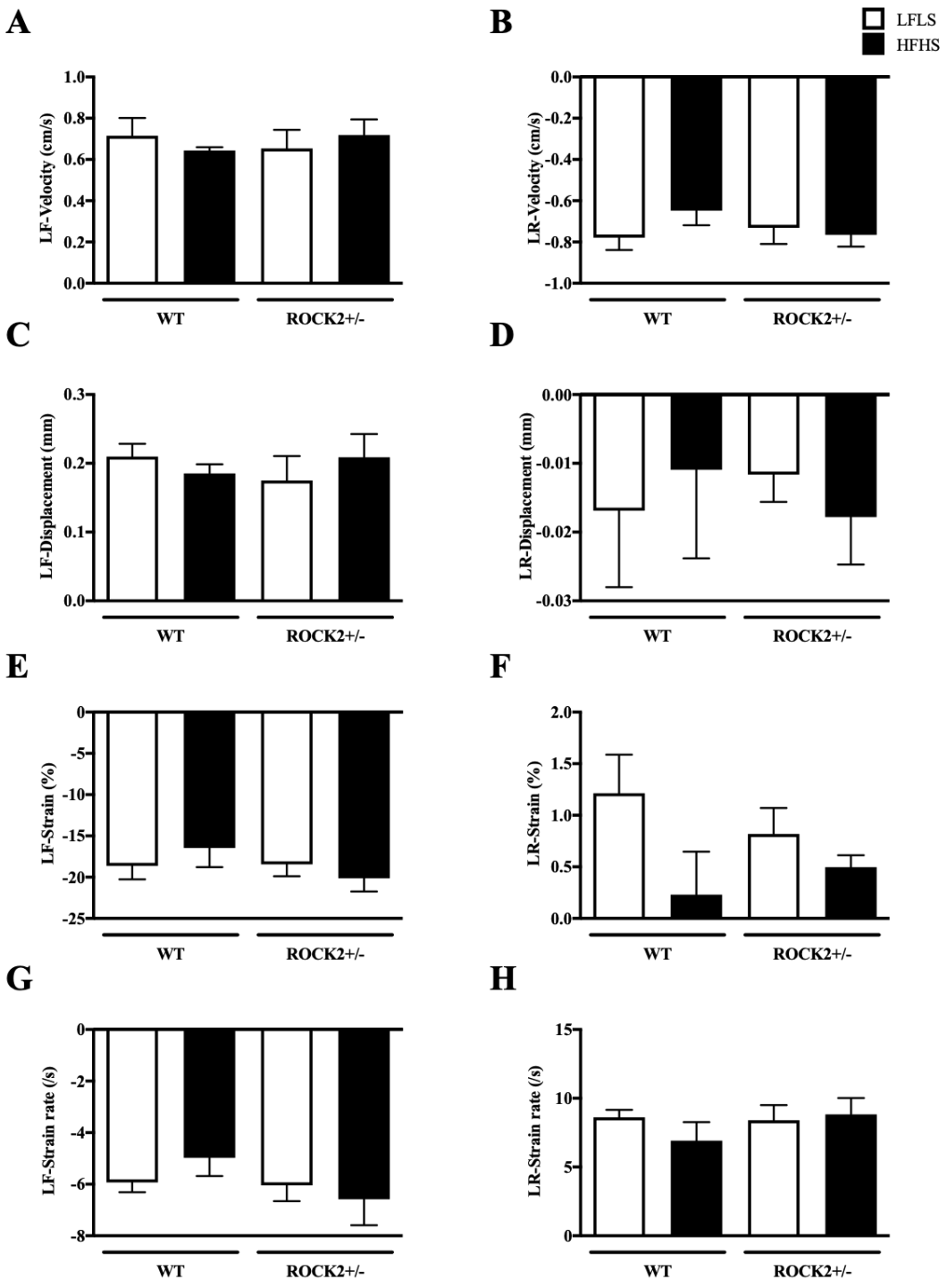

Figure 2.4 Speckle-tracking analysis of endocardial longitudinal wall motion along the long axis

Endocardial longitudinal forward (LF) and reverse (LR) velocity (A-B), displacement (C-D), strain (E-F), and strain rate (G-H) were assessed at week 16-18 in hearts from WT and ROCK2+/- mice fed LFLS and HFHS diets. Data shown as mean ± S.E.M., n= 4-7 in each group.

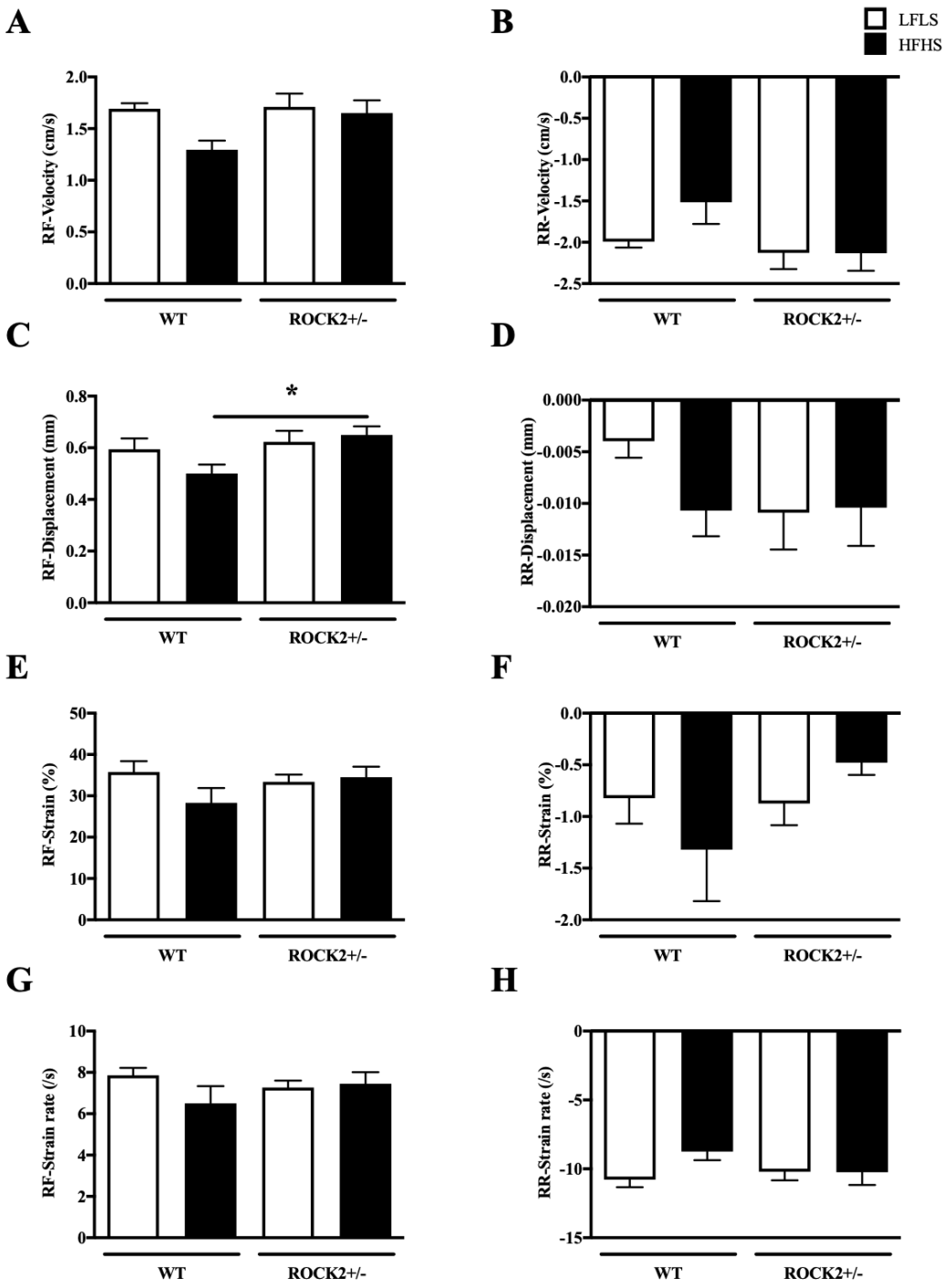

Figure 2.5 Speckle-tracking analysis of endocardial radial wall motion along the long axis

Endocardial radial forward (RF) and reverse (RR) velocity (A-B), displacement (C-D), strain (E-F), and strain rate (G-H) were assessed at week 16-18 in hearts from WT and ROCK2+/- mice fed LFLS and HFHS diets. *$p < 0.05$. Data shown as mean ± S.E.M., n= 4-7 in each group.

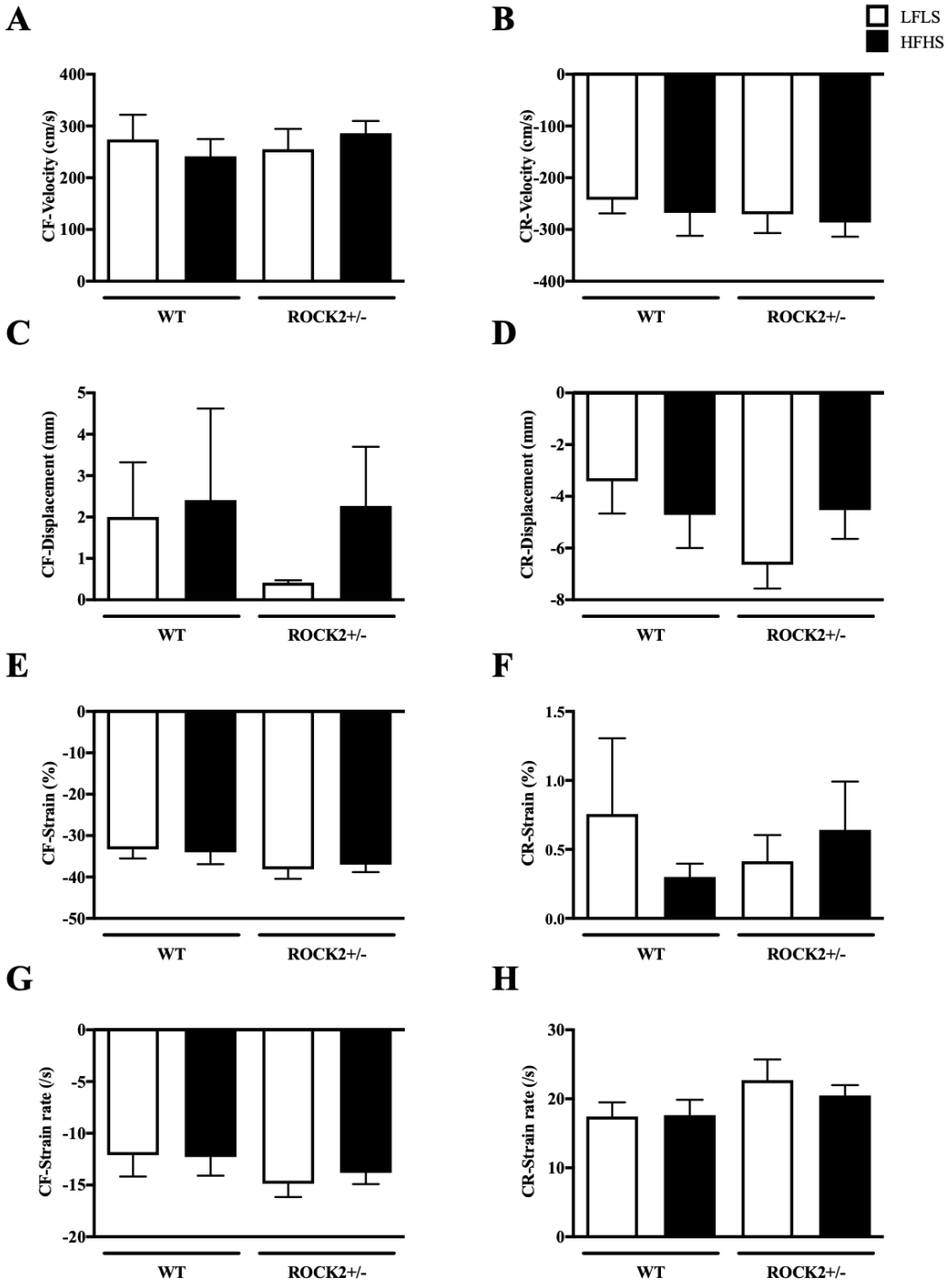

Figure 2.6 Speckle-tracking analysis of endocardial circumferential wall motion along the short axis

Endocardial circumferential forward (CF) and reverse (CR) velocity (A-B), displacement (C-D), strain (E-F), and strain rate (G-H) were assessed at week 16-18 in hearts from WT and ROCK2+/- mice fed LFLS and HFHS diets. Data shown as mean ± S.E.M., n= 4-7 in each group.

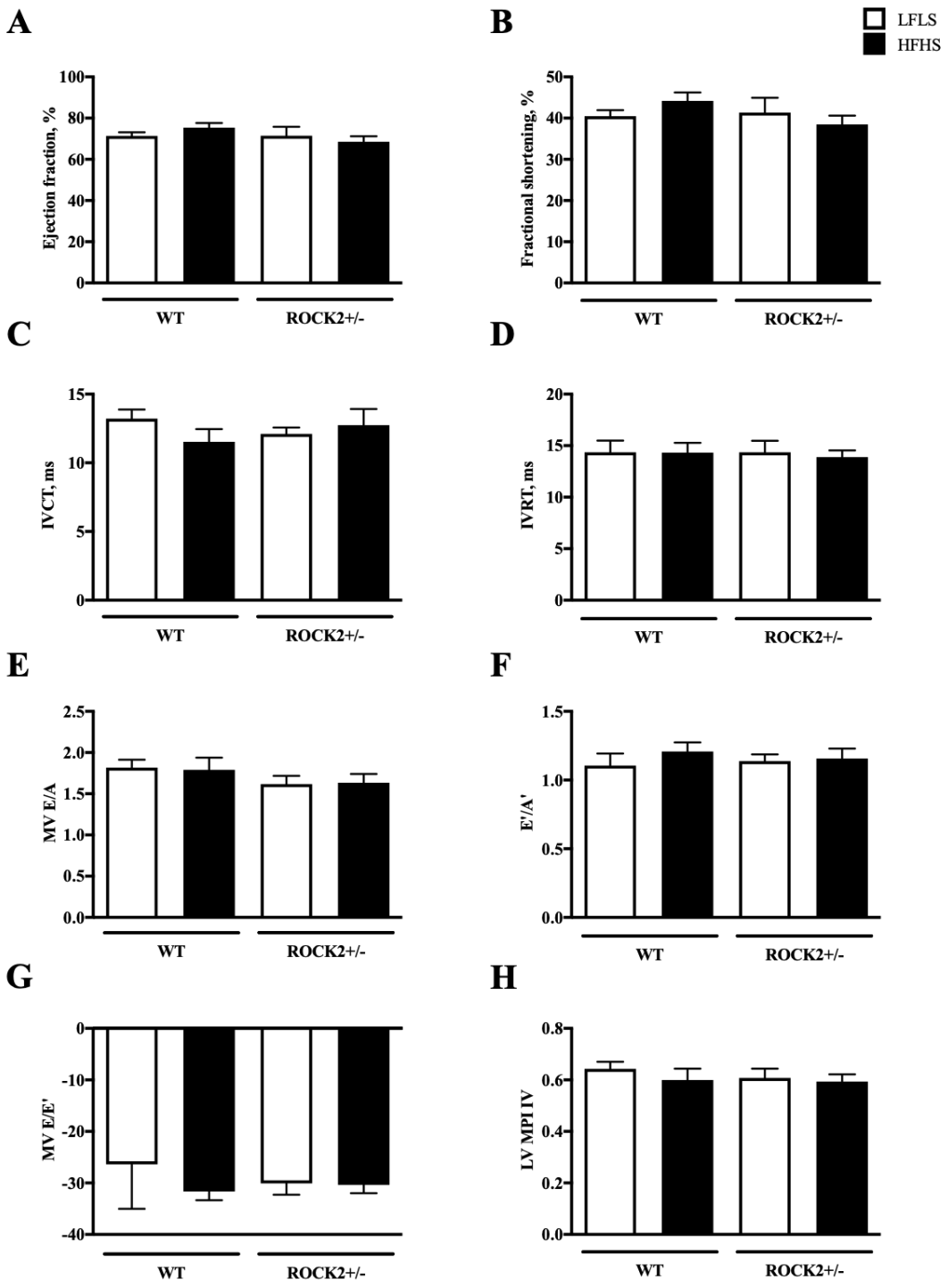

Figure 2.7 Echocardiographic measures of cardiac function at week 24 (set 2)

LV systolic function was assessed by measuring (A) ejection fraction, (B) fractional shortening, and (C) IVCT. LV diastolic function was assessed by determining (D) IVRT, (E) MV E/A, (F) E'/A', and (G) MV E/E'. (H) LV MPI IV reflects both LV systolic and diastolic function. *$p < 0.05$. Data shown as mean ± S.E.M., n= 7-10 in each group.

2.3.1.4 Effect of HFHS feeding on cardiac RhoA-ROCK signaling

There was no significant difference in terms of cardiac RhoA and ROCK1 expression among animals fed the different diets for 19-20 weeks (Fig. 2.8A-B). Cardiac expression of ROCK2 was about 50% lower ($p < 0.05$) in ROCK2+/- animals compared to their WT littermates, which confirmed the ROCK2 knockdown in ROCK2+/- animals (Fig. 2.8C). However, there was no over-expression of ROCK2 induced by a HFHS diet and the ROCK2 expression was comparable in WT + LFLS and WT + HFHS animals.

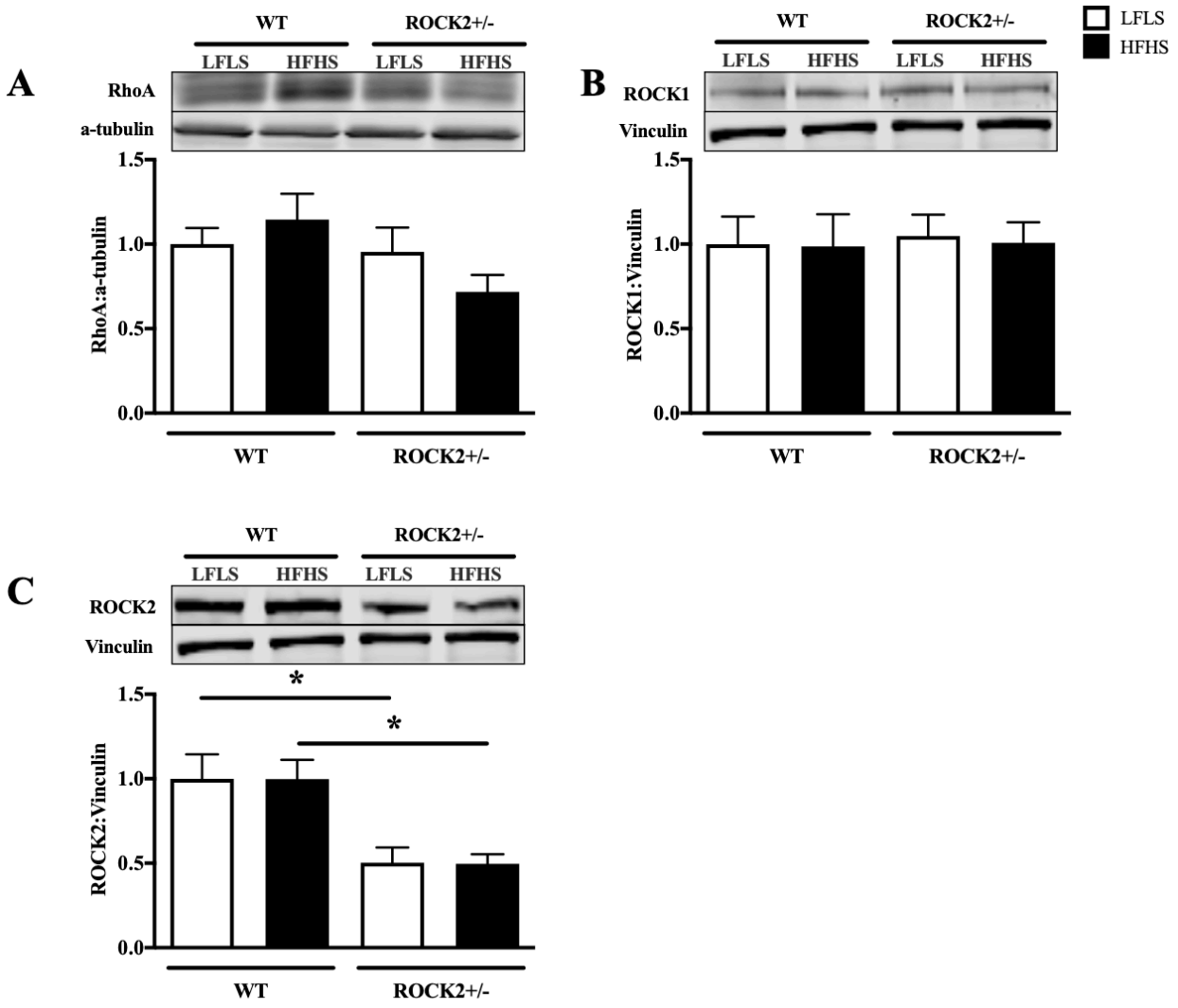

Figure 2.8 Effect of HFHS diet on cardiac RhoA-ROCK signaling in WT and ROCK2+/- mice

Representative Western blot images (top) and relative protein expression levels (bottom) of (A) RhoA, (B) ROCK1, and (C) ROCK2. *$p < 0.05$. Data shown as mean ± S.E.M., n= 8-14 in each group.

2.3.1.5 Effect of HFHS feeding on cardiac expression of mitochondrial mediators of fission and fusion

Disrupted mitochondrial structure in the left ventricular tissue of HF diet-fed WT CD-1 mice was observed in our preliminary data. Mitochondrial morphology is maintained by the balance of mitochondrial fission and fusion. A group of mediators are responsible for the process of fission and fusion. For example, Drp1 and fission 1 (Fis1) are primary mediators of fission, while mitofusins 1 and 2 (Mfn1 and Mfn2), along with optic atrophy protein 1 (OPA1) are crucial for the fusion of the membranes of mitochondria (Galloway and Yoon, 2015). A highly regulated cycle of mitochondrial fission and fusion is essential for cellular homeostasis. In our preliminary data, we found that the phosphorylation of Drp1 at serine 637 decreased significantly in WT + HF mice, while this was prevented in ROCK2+/- + HF mice. A decrease in phosphorylation of ^{Ser637}pDrp1 activates Drp1 and promotes mitochondrial fission. However, in the present study, the cardiac expression of mitochondrial mediators of fission and fusion was relatively consistent among animal groups with small variations. In particular, there was no change in phosphorylation of ^{Ser637}pDrp1 (Fig. 2.9). Overall, it is possible that no disrupted mitochondrial morphology was found in hearts from these HFHS diet-fed mice.

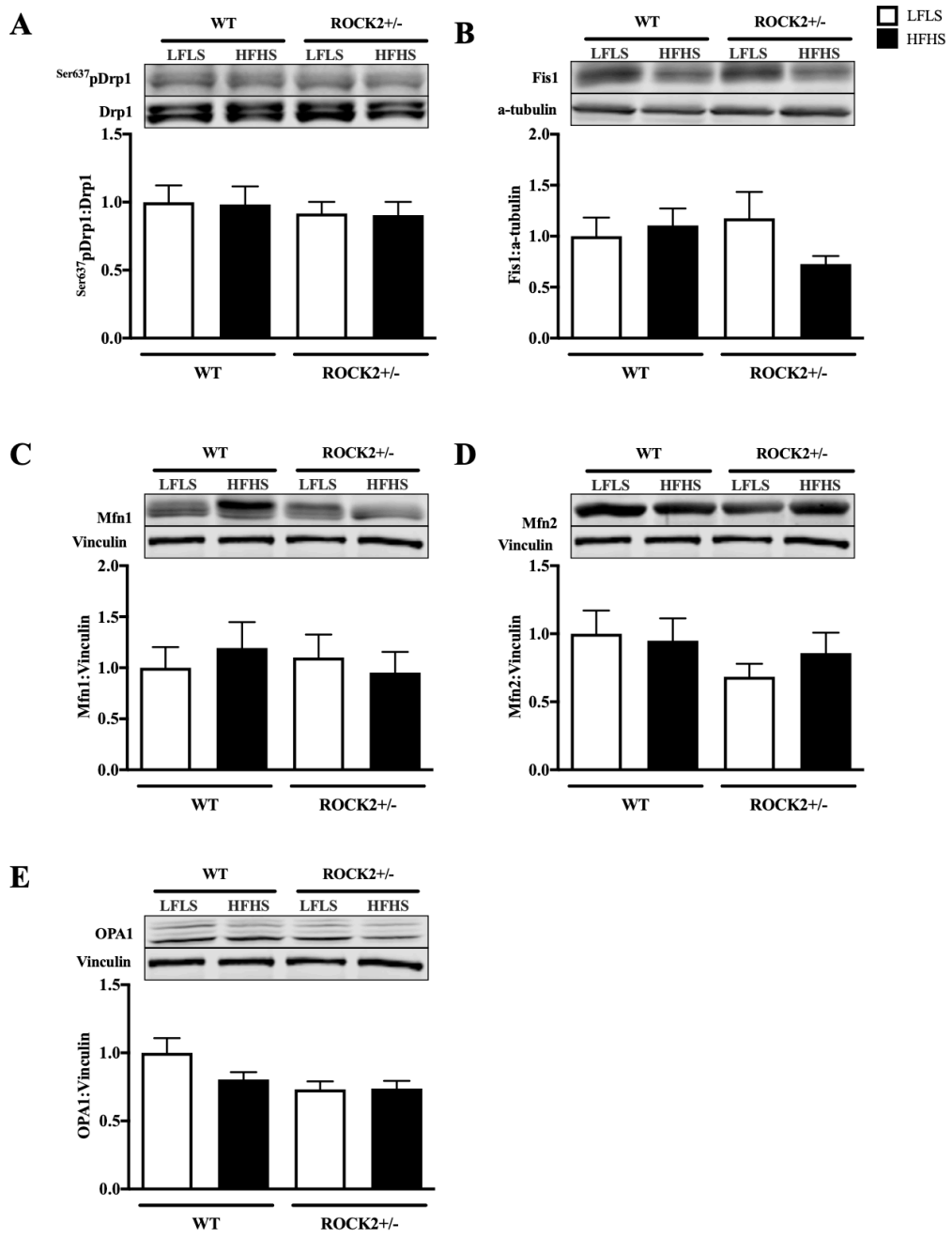

Figure 2.9 Effect of HFHS diet on the cardiac expression of mitochondrial mediators of fission and fusion in WT and ROCK2+/- mice

Representative Western blot images (top) and relative protein expression levels (bottom) of mitochondrial fission, which was determined by measuring (A) phosphorylation of Drp1 at Ser637 and (B) Fis1, and mitochondrial fusion, which was determined by measuring (C) Mfn1, (D) Mfn2, and (E) OPA1. Data shown as mean ± S.E.M., n= 8-14 in each group.

2.3.1.6 Effect of HFHS feeding on cardiac insulin signaling

The activity of IRS-1 is regulated by phosphorylation of serine and tyrosine residues. In particular, phosphorylation of IRS-1 at tyrosine 612 activates IRS-1, while phosphorylation of IRS-1 at serine 307 inhibits the activity of IRS-1. Hence, increased phosphorylation of ^{Ser307}pIRS-1 and decreased phosphorylation of ^{Tyr612}pIRS-1 are indicators of disrupted insulin signaling. In the present study, the expression of IRS-1 and the phosphorylation of IRS-1 at serine 307 and tyrosine 612 were very similar among different animal groups (Fig. 2.10A-C). Moreover, the levels of downstream targets of IRS-1 such as ^{Ser637}pAkt and ^{Thr642}pAS160 were also very comparable regardless of the diet and genotypes (Fig. 2.10D-F). Therefore, the hearts of HFHS diet-fed mice seem not to be susceptible to diet-induced resistance to insulin signaling.

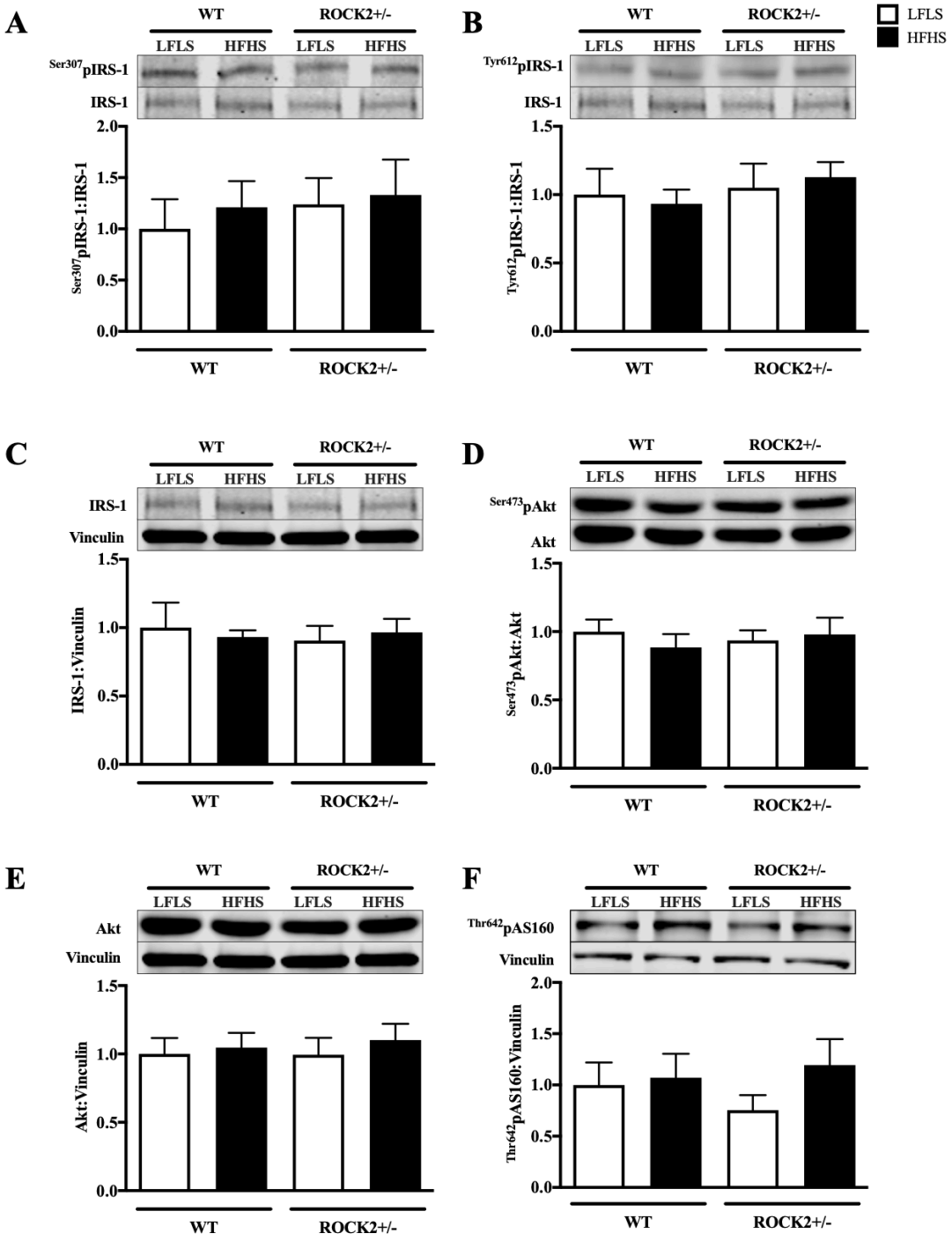

Figure 2.10 Effect of HFHS diet on the cardiac insulin signaling in WT and ROCK2+/- mice

Representative Western blot images (top) and relative protein expression levels (bottom) of (A) phosphorylation of IRS-1 at Ser307, (B) phosphorylation of IRS-1 at Tyr612, (C) IRS-1, (D) phosphorylation of Akt at Ser473, (E) Akt, and (F) phosphorylation of AS160 at Thr642. Data shown as mean ± S.E.M., n= 8-14 in each group.

2.3.2 HF diet-fed mice

2.3.2.1 Mouse phenotype

Another set of animals from the same generation of set 2 mice were placed on a HF diet and were followed for 18 weeks as described before to confirm that the results obtained previously were still evident (Soliman *et al.*, 2015). These are referred to as set 3. In set 3 animals, heart weight of WT + HF mice was significantly higher than WT + CHOW animals ($p < 0.05$), while there was no significant difference between ROCK2+/- + HF and WT + CHOW mice or ROCK2+/- + HF and WT + HF mice (Table 2.7). Moreover, the liver weights of both HF diet-fed animals were significantly larger than WT + CHOW animals ($p < 0.05$) (Table 2.7).

HF diet-fed animals gained slightly more body weight over the same period of feeding compared to HFHS diet-fed animals, although differences were not significant (Fig. 2.11A-B). Both HF diet and HFHS diet-fed animals had significantly increased body weight compared to their LFLS diet-fed littermates over 18 weeks of feeding.

Table 2.7 Phenotypic characterization (set 3)

Parameter	WT + CHOW	WT + HF	ROCK2+/- + HF
Heart weight (g)	0.196 ± 0.009	0.241 ± 0.014$^{\#}$	0.221 ± 0.012
Liver weight (g)	1.86 ± 0.14	2.81 ± 0.27$^{\#}$	2.94 ± 0.26$^{\#}$
Heart weight (g)/ Body weight (g)	0.00378 ± 0.0002	0.00319 ± 0.0001$^{\#}$	0.00299 ± 0.0001$^{\#}$
Liver weight (g) / Body weight (g)	0.0358 ± 0.002	0.0409 ± 0.004	0.0420 ± 0.004

Mice were euthanized, heart weight and liver weight were measured at week 23. $^{\#}p < 0.05$ compared to WT + CHOW. Data shown as mean ± S.E.M., n= 7-10 in each group.

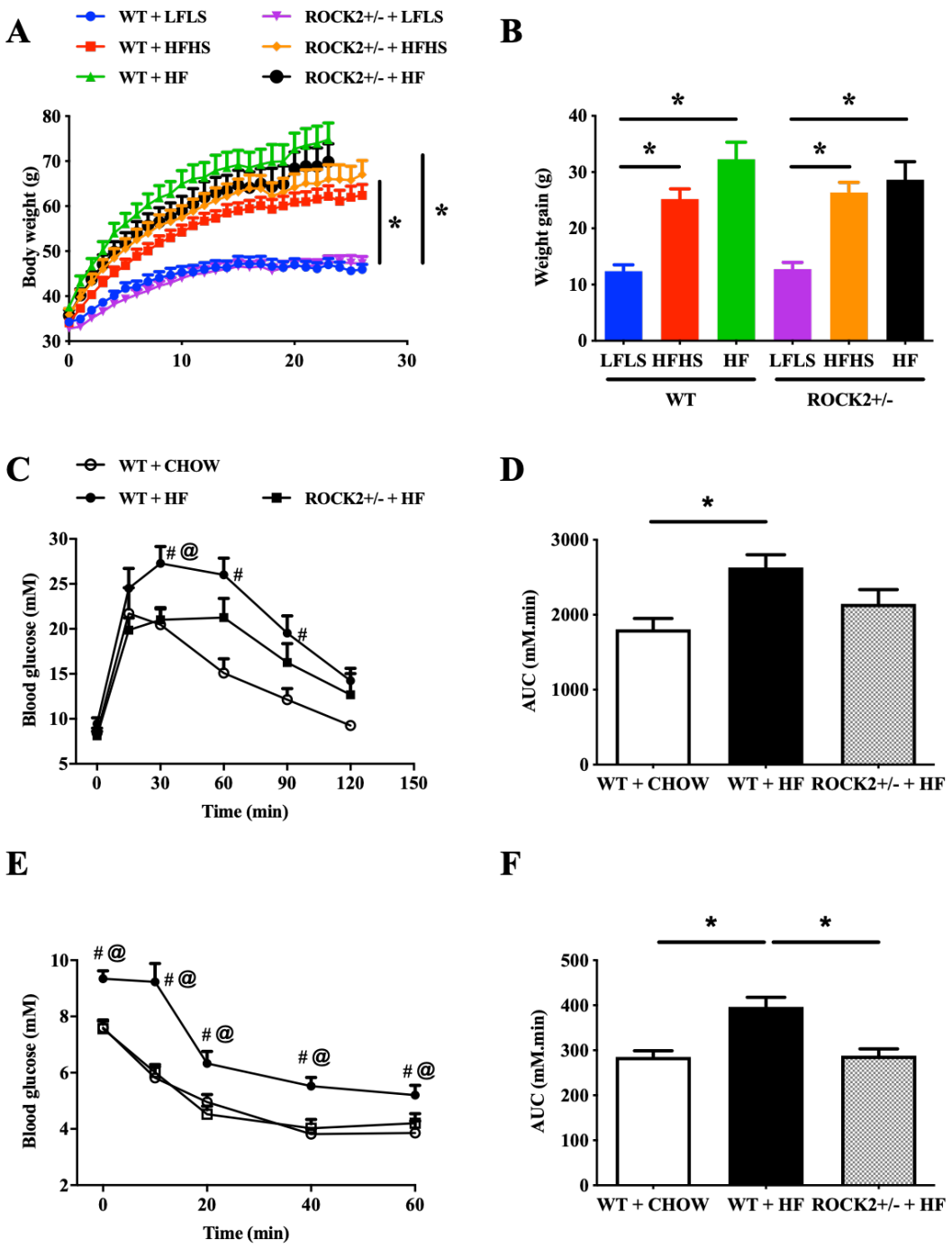

Figure 2.11 Effect of HF diet on body weight, and glucose and insulin tolerance (set 3)

(A) body weight, (B) body weight gain over 18 weeks, (C) blood glucose levels measured by glucose tolerance tests (GTT), (D) area under GTT curves (AUC), (E) blood glucose levels measured by insulin tolerance tests (ITT), (F) area under ITT curves (AUC). *$p < 0.05$, $^{\#}p < 0.05$ compared to WT + CHOW, $^{@}p < 0.05$ compared to ROCK2+/- + HF. Data shown as mean ± S.E.M., n= 7-10 in each group.

2.3.2.2 Glucose and insulin tolerance tests

In the 3rd set of animals, HF diet feeding provoked systemic glucose and insulin intolerance in WT animals. On the other hand, GTT showed improved glucose tolerance in ROCK2+/- + HF mice in contrast to WT + HF mice as blood glucose levels after glucose injection were not significantly different from those in WT + CHOW mice during the whole monitoring time. However, blood levels in WT + HF animals were significantly higher 30, 60, and 90 min after glucose administration than their littermates fed a chow diet (Fig. 2.11C). The improvement was also reflected in the AUC for GTT (Fig. 2.11D).

In addition, ROCK2+/- + HF mice demonstrated better insulin tolerance in contrast to WT + HF mice, in that blood glucose levels were not distinct from WT + CHOW animals, but were significantly lower compared to WT + HF animals after the insulin injection (Fig. 2.11E). This difference was reflected in the AUC for ITT, which was significantly greater in WT + HF than ROCK2+/- + HF mice (Fig. 2.11F). The results observed in the 3rd set of animals indicated that ROCK2+/- + HF mice have improved glucose and insulin tolerance, and are consistent with what we found in our previous studies (Soliman *et al.*, 2015, 2016).

2.3.2.3 Cardiac dimensions and function

Set 3 mice were placed on a HF diet for 16 weeks before cardiac function and dimensional measurements were determined by echocardiography. Both WT + HF and ROCK2+/- + HF mice exhibited a much lower heart rate than WT + CHOW mice (Table 2.8). WT + HF mice showed signs of left ventricle enlargement and dilation in comparison to WT + CHOW animals, as indicated by significantly increased LV Mass and left ventricular volume at both diastole and systole (LV Vol;d and LV Vol;s) ($p < 0.05$) (Table 2.9). The rest of the cardiac function and dimensional measurements were quite comparable among different animal groups (Table 2.8-2.9).

Although systolic dysfunction was not observed in either HF group, WT + HF mice had a tendency to a slightly decreased ejection fraction and fractional shortening compared to the other two groups (Fig. 2.12A-B). However, WT + HF animals exhibited overt diastolic dysfunction, as indicated by increased IVRT and LV MPI, and a decrease in E'/A' in contrast to WT + CHOW (Fig. 2.12D, F, H). These changes were not seen in hearts from ROCK2+/- + HF animals.

In summary, the results of cardiac functional and dimensional measurements indicated the development of cardiac contractile dysfunction in HF diet-induced obese WT CD-1 mice, whereas ROCK2+/- + HF mice were protected. These data are consistent with the results of our previous study (Soliman *et al.*, 2015), and confirm the adverse cardiac effects of a HF diet in WT CD-1 mice in contrast to the results I obtained with the HFHS diet.

Table 2.8 Effect of HFHS diet on cardiac function (set 3)

Parameter	**WT + CHOW**	**WT + HF**	**ROCK2+/- + HF**
Heart rate (BPM)	457.6 ± 18.7	401.6 ± 12.5$^{\#}$	409.4 ± 13.9$^{\#}$
CO (mL/min)	23.15 ± 1.46	24.26 ± 1.01	24.68 ± 1.79
SV (μL)	51.12 ± 3.94	60.41 ± 1.82	59.94 ± 3.09
AET (ms)	49.37 ± 0.94	41.90 ± 1.82	43.28 ± 0.96
MV Decel (ms)	25.75 ± 1.15	23.50 ± 0.67	22.75 ± 1.03
MV PHT (simplified) (ms)	7.47 ± 0.33	6.82 ± 0.19	6.60 ± 0.30

Cardiac function was assessed by echocardiography, at week 16. **CO**, cardiac output; **SV**, stroke volume; **AET**, aortic ejection time; **MV Decel**, E wave deceleration time; **MV PHT**, mitral valve pressure half time. $^{\#}p < 0.05$ compared to WT + CHOW, $^{\&}p < 0.05$ compared to WT + HF. Data shown as mean ± S.E.M., n= 7-10 in each group.

Table 2.9 Effect of HFHS diet on cardiac dimensional measurements (set 3)

Parameter	WT + CHOW	WT + HF	ROCK2+/- + HF
LV Mass (mg)	128.8 ± 9.38	158.6 ± 6.27[#]	149.3 ± 7.40
LV Vol;d (μL)	71.44 ± 5.70	90.39 ± 4.74[#]	80.17 ± 3.63
LV Vol;s (μL)	24.99 ± 2.91	39.02 ± 3.70[#]	30.72 ± 3.12
LVAW;d (mm)	1.06 ± 0.07	1.07 ± 0.05	1.10 ± 0.04
LVAW;s (mm)	1.62 ± 0.10	1.62 ± 0.04	1.63 ± 0.05
LVID;d (mm)	4.02 ± 0.13	4.45 ± 0.10	4.23 ± 0.08
LVID;s (mm)	2.60 ± 0.11	3.11 ± 0.12	2.82 ± 0.12
LVPW;d (mm)	0.98 ± 0.03	1.04 ± 0.05	1.04 ± 0.04
LVPW;s (mm)	1.39 ± 0.05	1.33 ± 0.04	1.47 ± 0.04

Cardiac dimensional measurements were assessed by echocardiography, at week 24. **LV Mass**, left ventricular mass; **LV Vol;d**, left ventricle volume systole; **LV Vol;s**, left ventricle volume diastole; **LVAW;d**, left ventricular anterior wall (diastole); **LVAW;s**, left ventricular anterior wall (systole); **LVID;d**, left ventricular internal wall (diastole); **LVID;s**, left ventricular internal wall (systole); **LVPW;d**, left ventricular posterior wall (diastole); **LVPW;s**, left ventricular posterior wall (systole). [#]$p < 0.05$ compared to WT + CHOW. Data shown as mean ± S.E.M., n= 7-10 in each group.

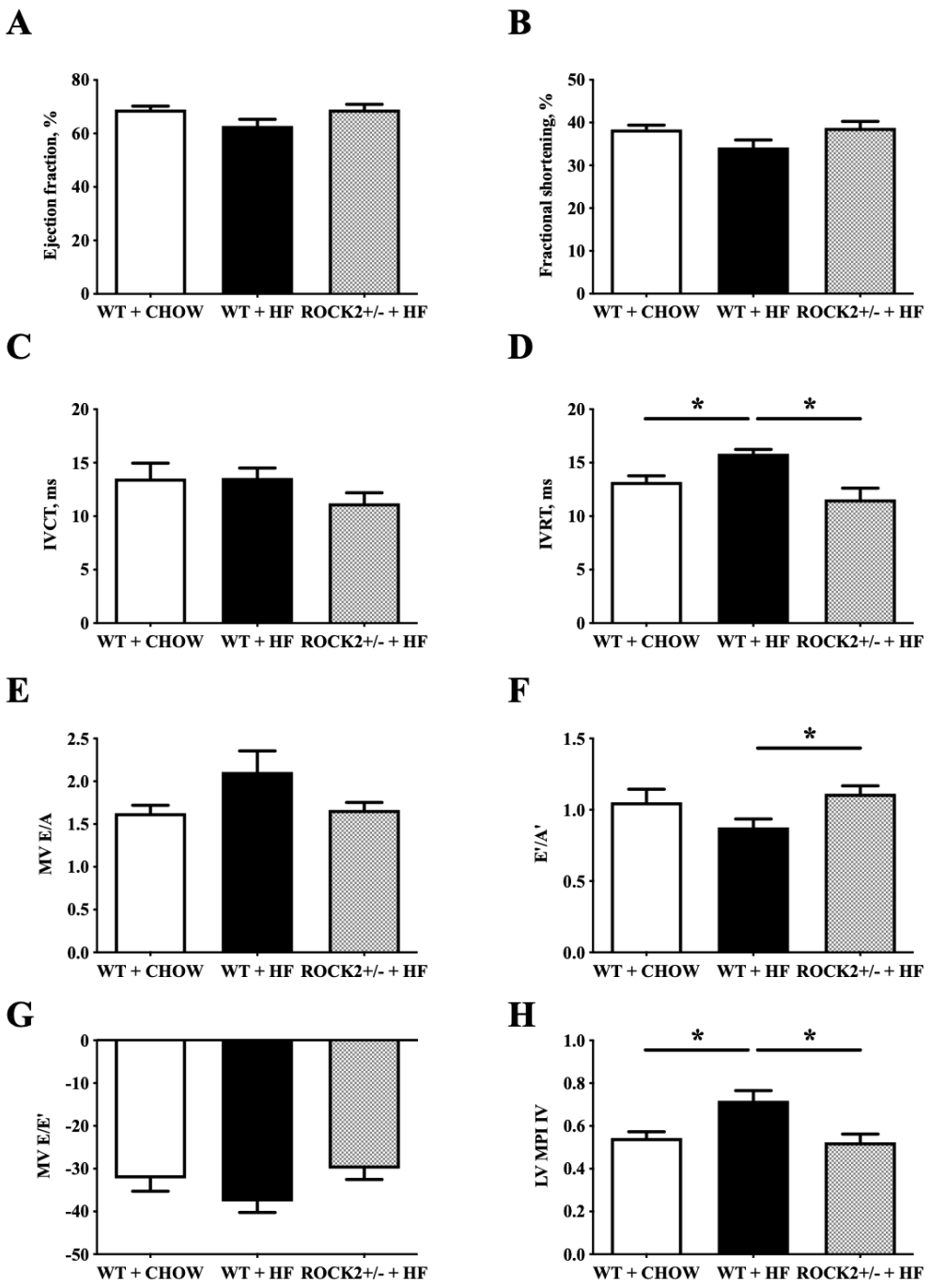

Figure 2.12 Echocardiographic measures of cardiac function at week 16 (set 3)

LV systolic function was assessed by measuring (A) ejection fraction, (B) fractional shortening, and (C) IVCT. LV diastolic function was assessed by determining (D) IVRT, (E) MV E/A, (F) E'/A', and (G) MV E/E'. (H) LV MPI IV reflects both LV systolic and diastolic function. *$p < 0.05$. Data shown as mean ± S.E.M., n= 7-10 in each group.

2.4 Discussion

The results of this study show that despite the development of severe obesity and systemic insulin resistance, HFHS diet-fed WT CD-1 animals were resistant to the development of cardiac contractile dysfunction. In addition, ROCK2+/- CD-1 mice were not protected against the development of systemic insulin intolerance when fed a HFHS diet, as they had been when fed a HF diet in our previous study (Soliman *et al.*, 2015). The set 3 animals confirmed the development of cardiac dysfunction and insulin resistance in WT + HF animals, and the protection by heterozygous deletion of ROCK2 against cardiac contractile dysfunction and glucose and insulin intolerance. The results in HF diet-fed mice confirmed the response to HF diet-induced obesity and associated complications in different generations of WT and ROCK2+/- CD-1 mice and eliminated the possibility of generational variations contributing to the findings observed in HFHS diet-fed mice.

In the current study, HFHS diet-fed mice gained significantly more body weight than LFLS diet-fed littermates, which is consistent with what we observed of weight gain in HF diet-fed animals in our previous study (Soliman *et al.*, 2015), as well as in other studies of HFHS diet-induced obesity conducted in CD-1 mice (Carbone *et al.*, 2015, 2017; Chen *et al.*, 2017; Zhang *et al.*, 2017). The higher body weight found in ROCK2+/- + HFHS mice compared to WT + HFHS mice may be explained at least in part by enlarged organ and tissue weight, including heart, liver, and epididymal fat tissue, since there exists a positive correlation between body weight and organ weight in rodents (Walter and Addis, 1939). Moreover, the fact that both WT + LFLS and ROCK2+/- + LFLS animals had similar body weights over the period of feeding, and there were no distinguishable differences between the food and water intake of the different animal groups

suggests that heterozygous deletion of ROCK2 did not have detrimental effects on the normal development of mice.

In obesity cardiomyopathy, in 54% of cases, diastolic dysfunction develops first and is followed by systolic dysfunction, while in 42% of cases the reverse is true (Boudina and Abel, 2010; Reuvekamp *et al.*, 2016). In the set 1 animals, WT + HFHS mice showed a significant decrease in E'/A', which could be an indicator of the development of diastolic dysfunction. Nevertheless, it is hard to conclude that diastolic dysfunction had developed in those animals, given that the E'/A' was the only parameter of diastolic function that was statistically significantly different between WT + HFHS and ROCK2+/- + HFHS mice. Furthermore, no cardiac dysfunction was detected in the 2nd set of animals, which were placed on the same diet for a longer period, 24 weeks. Therefore, in the current study, WT CD-1 mice fed a HFHS diet that contains 45% kcal from fat and 17% kcal from sucrose were resistant to the development of cardiac contractile dysfunction.

Several studies have shown that WT C57BL/6J mice exhibited cardiac dysfunction when placed on the same HFHS diet (45% kcal from fat and 17% kcal from sucrose) for periods ranging from 16 to 24 weeks (Fang *et al.*, 2008; Pulinilkunnil *et al.*, 2014; Cao *et al.*, 2016). Specifically, WT C57BL/6J mice fed a HFHS diet for 16 weeks developed moderate systolic dysfunction, as represented by reduced ejection fraction and fractional shortening using echocardiography (Pulinilkunnil *et al.*, 2014). Moreover, cardiac dysfunction, demonstrated through decreased fractional shortening, was also observed in WT C57BL/6J mice fed a HFHS diet for 20 weeks (Cao *et al.*, 2016). In addition, increased left ventricular mass and reduced fractional shortening were reported in WT C57BL/6J mice placed on a HFHS diet for 24 weeks (Fang *et al.*, 2008). Furthermore, in a previous study from our lab, a decline in systolic function was seen at 18 weeks

of feeding. At 24 weeks, not only was systolic dysfunction maintained and even slightly worsened, but diastolic dysfunction was detected at this point in WT C57BL/6J animals on a HFHS diet (Nyamandi *et al*., submitted). Therefore, these studies suggested that a HFHS diet, which has 45% kcal from fat and 17% kcal from sucrose contributes to a prolonged cardiac contractile dysfunction in WT C57BL/6J mice.

On the other hand, others have reported that feeding WT CD-1 mice a HFHS diet with a higher sucrose content (42% kcal from fat and 30% kcal from sucrose) results in the development of systolic and diastolic dysfunction as early as 8 weeks (Carbone *et al.*, 2015, 2017; Chen *et al.*, 2017; Zhang *et al.*, 2017). For instance, CD-1 mice fed this HFHS diet developed cardiac systolic dysfunction indicated by reduced ejection fraction and increased IVCT, and diastolic dysfunction represented by elevated IVRT and MPI after 8 weeks of feeding (Carbone *et al.*, 2015, 2017; Chen *et al.*, 2017; Zhang *et al.*, 2017). Therefore, it is possible that a HFHS diet containing a higher amount of calories from sucrose is required to induce cardiac dysfunction in WT CD-1 animals for the periods that I monitored.

In our previous study, WT CD-1 mice fed a HF diet (60% kcal from fat and 7% kcal from sucrose) for 17 weeks demonstrated cardiac contractile dysfunction, as indicated by elevated MPI and regional wall motion impairment in the left ventricle, determined using echocardiography (Soliman *et al.*, 2015). Moreover, in the current study, HF diet-fed WT CD-1 mice gained a bit more body weight than HFHS diet-fed mice over 18 weeks of feeding, 32 g and 25 g, respectively. The slightly increased body weight gain in HF diet-fed animals in contrast to HFHS diet-fed mice may be explained by the higher energy density of HF diet. The HF diet has an energy density of 5.21kcal/g, while a HFHS diet contains a slightly lower energy density of 4.7kcal/g. Therefore, the failure to develop cardiac contractile dysfunction in WT CD-1 animals fed the HFHS diet used

here may be explained in part by overall lower body weight and a lower energy density in the HFHS diet than in the HF diet.

Although there is no direct evidence comparing left ventricular function in diet-induced obesity in CD-1 and C57BL/6J mice, studies have shown that different mouse strains can result in model-associated variations because of their genetic backgrounds (Fengler *et al.*, 2016; Kohut *et al.*, 2016). For example, CD-1 mice are less prone to hepatic inflammation caused by diet-induced obesity in contrast to C57BL/6J mice, since CD-1 animals exhibit much lower levels of inflammatory factors such as IL-6, TNFα and monocyte chemoattractant protein-1 (MCP-1) after high fat diet feeding (Fengler *et al.*, 2016). A study reported that CD-1 mice fed a high fat (72% fat from corn oil and lard) diet did not develop any features of diabetes after 9 months of feeding when C57BL/6J mice started to show symptoms as early as 12 weeks (Burcelin *et al.*, 2002). Moreover, the fact that dimensions of the right heart are quite distinct in CD-1 mice compared to C57BL/6J mice (Kohut *et al.*, 2016) makes it possible that the left ventricle of these two strains is different from each other. Taken together, all this evidence suggests that the differences of the susceptibility of CD-1 and C57BL/6J mice to HFHS diet-induced cardiac dysfunction may be due at least in part to the variations in genetic determinants in the two strains. A higher content of sucrose, a diet with a higher energy density, and/or a longer feeding period might be needed before the detection of cardiac dysfunction in CD-1 than C57BL/6J animals.

The detection of decreased LV cardiac function is one of the key signs of the development of cardiac contractile dysfunction in both human and mouse models of obesity. However, a number of studies were unable to detect dysfunction in obese human subjects and diet-induced obese mouse models (Pascual *et al.*, 2003; Movahed and Saito, 2009; Yan *et al.*, 2009; Sung *et al.*, 2011; Böhm *et al.*, 2013; Brainard *et al.*, 2013). It is possible that when cardiac function is assessed under

baseline resting conditions, subtle functional differences may be masked and difficult to detect. A pharmacological stress simulator, dobutamine, which is a β-adrenergic agonist with a high affinity for β1-receptors expressed in the heart, can be administered systemically to increase cardiac demand and produce cardiac stress (Zaugg *et al.*, 2002), and under these circumstances, diet-induced cardiac dysfunction may be unmasked. For instance, under resting conditions, no differences were found in systolic strain rates or torsion, and only a slight reduction in longitudinal strain was observed in C57BL/6J mice after 42 weeks of a HF (60% kcal from fat and 7% kcal from sucrose) diet. Nevertheless, under dobutamine stress conditions, cardiac dysfunction was detected in these mice as early as 22 weeks on diet, indicated by reductions in longitudinal strain and circumferential and radial strain rates (Haggerty *et al.*, 2015). Moreover, the administration of dobutamine revealed impaired cardiac contractile and relaxation response in HF (60% kcal from fat and 7% kcal from sucrose) diet-induced obese C57BL/6J mice. However, cardiac dysfunction was masked in these mice, which exhibited normal cardiac function under basal conditions (Calligaris *et al.*, 2013). It is possible that had dobutamine been administered, the resulting stress might have assisted in unmasking underlying cardiac dysfunction and allowing its detection in mice fed a HFHS diet in the present study.

At the molecular level, the lack of development of cardiac contractile dysfunction in WT + HFHS mice may be explained at least partially by the fact that there was no over-expression of ROCK2 in these animals. Both LFLS and HFHS diet-fed WT animals had very comparable levels of cardiac ROCK2 expression, indicating that HFHS diet did not induce ROCK2 over-expression in the hearts of CD-1 mice. Previously, the cardiac contractile dysfunction observed in WT + HF mice was associated with the overexpression of ROCK2 in the hearts of these animals, and both were prevented in mice with heterozygous deletion of ROCK2 (Soliman *et al.*, 2015). In addition,

there were no differences in terms of the expression of mitochondrial mediators of fission and fusion, as well as no evidence of disrupted cardiac insulin signaling in the hearts of WT + HF mice.

Ultrastructural changes of cardiac muscle cells such as degradative changes of the myofilament apparatus and abnormal structural changes of mitochondria have been implicated in the development of cardiomyopathy (Rudge and Duncan, 1988). The proper function of mitochondria is essential in tissues and organs that have a high energy demand, such as the heart (Chistiakov *et al.*, 2018). Regular mitochondrial morphology plays an important role in regulating mitochondrial dynamics, and in maintaining normal cardiac function. Mitochondrial morphology is maintained by the balance of mitochondrial fission and fusion, and a group of mediators are responsible for these processes. For example, Drp1 and Fis1 are primary mediators of fission, while Mfn1 and Mfn2, along with OPA1 are crucial for the fusion of the membranes of mitochondria. A highly regulated cycle of mitochondrial fission and fusion is essential for cellular homeostasis, as mitochondria are closely involved in a series of cellular processes, including apoptosis, metabolism, and cell signaling (Galloway and Yoon, 2015). However, the homeostasis of mitochondria often changes in pathological situations such as obesity and associated cardiovascular diseases. Several studies have reported a relationship between mitochondrial dysfunction and heart diseases, and that reduced mitochondrial oxidative capacity contributes to cardiac dysfunction in rodent and human obesity (Christoffersen *et al.*, 2003; Szczepaniak *et al.*, 2003; Ballinger, 2005; Siasos *et al.*, 2018). Mitochondrial dysfunction has also been implicated in the development of insulin resistance, which is closely associated with the progression of obesity and cardiovascular diseases (Montgomery and Turner, 2015; Ormazabal *et al.*, 2018). For example, free fatty acids accumulation contributes to apoptosis and mitochondrial dysfunction by elevating levels of ROS production through fatty acid oxidation. Increased levels of ROS

production, in turn, leads to insulin resistance through activating the serine phosphorylation and inhibiting the tyrosine phosphorylation of IRS-1 (Unger and Orci, 2002; Morino *et al.*, 2005; Goldberg *et al.*, 2012). Moreover, the defect in myocardial energy production impairs cardiac systolic and diastolic contractile function and further leads to cardiomyopathy and heart failure (Feuvray *et al.*, 1979; Lewis and Steiner, 1996; Fricovsky *et al.*, 2012). Preliminary studies from our lab demonstrated that WT + HF mice had disrupted mitochondrial morphology via increased activity of mitochondrial mediators of fission, Drp1, disruption of mitochondrial cristae, and the appearance of more and smaller mitochondria. In addition, decreased insulin signaling mediated through IRS-1 and downstream targets including Akt and AS160 was also found in WT + HF mice. However, ROCK2+/- + HF mice showed improvements in terms of mitochondrial morphology in left ventricular tissue, and insulin signaling (Soliman *et al.*, 2015). In the current study, both cardiac expression of mitochondrial mediators of fission and fusion, and insulin signaling regulators were relatively comparable amongst all 4 groups of animals. Hence, the lack of cardiac contractile dysfunction in WT + HFHS mice could be explained in part by the lack of ROCK2 over-expression and the absence of disrupted mitochondrial structure and insulin signaling in the heart.

To conclude, my study demonstrated that a HFHS diet containing 45% kcal from fat and 17% kcal from sucrose was not able to induce cardiac contractile dysfunction in WT CD-1 mice over a period of 24 weeks of feeding. Furthermore, heterozygous deletion of ROCK2 failed to protect CD-1 mice from the development of systemic glucose and insulin resistance as it did when fed a HF diet. The lack of cardiac contractile dysfunction detected in WT + HFHS mice may be explained in part by the lack of ROCK2 over-expression, cardiac mitochondrial dysfunction and disrupted cardiac insulin signaling in these animals. A slightly lower fat content in the current

HFHS diet in comparison to the HF diet that we used in our previous studies, a relatively low sucrose content compared to other studies that provoked cardiac dysfunction in CD-1 mice, a lower energy density of the HFHS diet, and genetic variations between C57BL/6J and CD-1 mouse strains are possible reasons for the failure of a HFHF diet to induce cardiac contractile dysfunction in WT CD-1 mice. Nonetheless, it is not clear why heterozygous deletion of ROCK2 failed to protect systemic glucose and insulin tolerance in HFHS diet-fed animals. This is explored further in the next chapter.

Chapter 3: The effect of ROCK2 heterozygous deletion on insulin signaling and inflammation in mouse models of diet-induced obesity

3.1 Introduction

As a progressive chronic disease, obesity is characterized by expanded adipose tissue and an elevated degree of chronic inflammation. Obesity has severe impacts on the body systems of overweight and obese individuals. It is one of the leading causes of other health problems and morbidities, including diabetes, heart disease, stroke, high blood pressure, arthritis, and cancer. (Qureshi and Abrams, 2007).

Obesity is associated with an increased risk of non-alcoholic fatty liver disease (NAFLD), which is characterized as excessive fat build-up in the liver with insulin resistance due to causes other than alcohol use (Huang *et al.*, 2018). NAFLD occurs when the rate of hepatic fatty acid uptake and synthesis exceeds the rate of fatty acid oxidation and export. There are two types of NAFLD, non-alcoholic fatty liver and non-alcoholic steatohepatitis. Inflammation or liver damage usually does not present in non-alcoholic fatty liver. However, as fat continues to accumulate, it can lead to non-alcoholic steatohepatitis and eventually cirrhosis and liver failure (Rinella and Sanyal, 2016; Chalasani *et al.*, 2018).

Obesity is the direct consequence of an imbalance between energy intake and energy expenditure (Jernås *et al.*, 2006). As individuals become obese, their adipocytes enlarge, and adipose tissue undergoes molecular and cellular alterations affecting systemic metabolism. Increased release of free fatty acids and glycerol from adipocytes promotes insulin resistance in tissues such as skeletal muscle and liver (Shulman, 2000). Moreover, as obesity progresses,

elevated production of inflammatory factors, including TNFα, MCP-1, and IL-6 are also found in the adipose tissue (Chan and Hsieh, 2017).

Liver and adipose tissue both play important roles in metabolic regulation. As the adipose tissue becomes insulin resistant and accumulates inflammatory factors, increased amounts of free fatty acids are delivered to the liver instead of being stored in the adipose tissue, leading to the progression of fatty liver disease (Parker, 2018). An excessive amount of hepatic free fatty acids represents an imbalance of body metabolism (Fabbrini *et al.*, 2010). The existence of adipose-liver crosstalk contributes to the development of obesity-associated complications. The two most important mechanisms underlying the complications of obesity are insulin resistance and inflammation (Kinlen *et al.*, 2018). In obesity, impaired insulin signaling and an increased degree of inflammation lead to fatty liver and adipocyte hypertrophy, and further contribute to the development of a cluster of metabolic syndromes and increase the risk of heart diseases, NAFLD, and diabetes (Yang *et al.*, 2012).

Although both HFHS diet and HF diet can lead to obesity and insulin resistance, a HFHS diet differs from a HF diet mainly because of its increased sucrose content (Soliman *et al.*, 2015, 2016). Sucrose is a disaccharide that is composed of glucose and fructose. One molecule of sucrose can be broken down into one molecule of glucose and one molecule of fructose by a digestive enzyme called sucrase. After being absorbed, glucose and fructose require further metabolism to be converted into forms that can be used for energy production (Tappy and Lê, 2010). The metabolism of glucose is distinct from fructose. Glucose is metabolized primarily by glucokinase or hexokinase to yield pyruvates and ATP through a process called glycolysis. On the other hand, extra steps are needed before fructose enters the glycolysis pathway. Fructokinase in the liver plays an important role in fructose metabolism, since most fructose is metabolized in the liver. In

particular, one of the isoforms of fructokinase, fructokinase C, metabolizes fructose to fructose-1-phosphate very rapidly, with large ATP consumption (Froesch, 1976). Increased fructose metabolism through fructokinase C leads to fat accumulation in the liver and further contributes to fatty liver disease (Jensen *et al.*, 2018). In addition, fructose induces an increased rate of hepatic *de novo* lipogenesis through serving as a substrate for fatty acid synthesis and stimulating the expression of enzymes involved in lipogenesis via activation of the lipogenic transcription factors, such as *srebp1c*, and decreased fat oxidation in comparison to glucose (Zakim, 1972; Samuel, 2011; Janevski *et al.*, 2012; Kim *et al.*, 2016; Softic *et al.*, 2017). For example, human subjects have demonstrated decreased post-prandial fat oxidation and resting energy expenditure after consuming fructose-sweetened beverages in comparison to those who consuming calorically equivalent glucose-sweetened drinks (Cox *et al.*, 2012). Therefore, the progression of obesity-associated liver disease has been shown to be related to an increased intake of fructose.

Ishimoto et al showed that, WT C57BL/6J mice fed a HFHS (36% kcal from fat and 30% kcal from sucrose) diet and mice fed a HF (36% kcal from fat) diet both gained a significant amount of body weight over a period of 15 weeks. However, hepatic steatosis, indicated by the development of inflammation and fibrosis, was found in mice fed a HFHS diet, but not in mice fed a HF diet. Furthermore, these symptoms were improved in fructokinase knockout mice fed the same HFHS diet. Their results indicated that the sucrose content in the HFHS diet contributes to the greater inflammation and hepatic fibrosis through fructose metabolism in the liver (Ishimoto *et al.*, 2013). Furthermore, according to Sato et al, WT C57BL/6J mice also responded differently to a HFHS (42% kcal from fat and 30% kcal from sucrose) diet and a HF diet (60% kcal from fat and 7% kcal from sucrose) after a period of 20 weeks of feeding. Although both HFHS and HF mice developed a similar extent of obesity, hyperglycemia, hyperinsulinemia and hepatic steatosis

were more severe in the HFHS animals compared to the HF group, and this was associated with increased hepatic mRNA expression of lipogenic enzymes (Sato *et al.*, 2010). These studies suggest that there may be differences in the underlying mechanisms contributing to obesity and insulin resistance resulting from a HF and a HFHS diet, related to adverse effects of fructose on the liver.

Adipocyte hypertrophy is also closely associated with the development of obesity as an adaptive response to protect other tissues from lipotoxicity (Muir *et al.*, 2016). Increasing evidence from studies of dietary-induced mouse models of obesity has suggested a relationship between obesity, insulin resistance, and chronic inflammation of adipose tissue (Bastard *et al.*, 2006). In our previous study, in HF diet-fed WT CD-1 mice, the activation of ROCK2 in adipose tissue was associated with the development of systemic insulin intolerance and reduced insulin signaling. This was attributed to the suppression of PPARγ expression, which regulates fatty acid storage and glucose metabolism, leading to adipocyte hypertrophy and increased inflammatory cytokine production. However, HF diet-fed ROCK2+/- mice showed improved insulin sensitivity and reduced adipose tissue inflammation (Soliman *et al.*, 2016).

In Chapter 2, HFHS diet-fed animals were shown to develop significant whole-body glucose and insulin intolerance, although the hearts of these animals did not appear to be insulin resistant at the level of insulin signaling. Unlike what we observed in ROCK2+/- + HF animals, ROCK2+/- + HFHS animals were as insulin resistant as WT + HFHS animals. Furthermore, the liver weight of ROCK2+/- + HFHS mice was greater than that of WT + HFHS mice. The purpose of the present study was to investigate the effect of HFHS diet feeding on insulin signaling in the liver and adipose tissue, and inflammatory status in the adipose tissue. I found that the liver triglyceride levels increased significantly in both WT + HFHS and ROCK2+/- + HFHS mice in

comparison to their LFLS diet-fed littermates. Moreover, WT + HFHS mice demonstrated impaired insulin signaling mediated through IRS-1 in both liver and adipose tissue, and had a significant amount of inflammatory factor production in the adipose tissue, which was consistent with what we had previously found in WT + HF mice (Soliman *et al.*, 2016). However, distinct from HF diet-fed ROCK2+/- animals, no activation of PPARγ was observed in adipose tissue from ROCK2+/- + HFHS animals, and these mice had disrupted insulin signaling mediated through IRS-1 and its downstream target in the liver and adipose as observed in their WT littermates. Moreover, levels of inflammatory factor production in adipose tissue from ROCK2+/- + HFHS animals were as high as those in WT + HFHS animals. No over-expression or over-activation of ROCK2 was observed in adipose tissue of these mice, and this was believed to be the factor that leads to adipocyte hypertrophy, insulin resistance and increased inflammation in WT + HF mice (Soliman *et al.*, 2016). Therefore, the increased sucrose content in the HFHS diet may affect the mechanisms of insulin resistance and adipose tissue inflammation differently than a HF diet.

3.2 Materials and methods

3.2.1 Animals

CD-1 WT and ROCK2+/- male animals were used in this study. Male CD-1 ROCK2+/- mice were generated as previously described and were bred with female WT (ROCK2+/+) mice (Zhou *et al.*, 2009). Genotyping of offspring using polymerase chain reaction was performed to confirm their genotypes. Since complete ROCK2 knockout (ROCK2-/-) is embryonically lethal, heterozygous ROCK2 mice (ROCK2+/-) were used. The CD-1 strain was chosen for the present study because of the minimal detrimental effects of ROCK2 heterozygous deletion on embryonic development in this genetic background compared to other strains (Thumkeo *et al*., 2003).

These studies were conducted in tissues from animals in set 1, described in Chapter 2. At the age of 6 weeks, WT male mice and their ROCK2+/- male littermates were divided into two groups each and fed either a low fat-low sucrose (LFLS) diet (Cat #:D12450J, Research Diets, New Brunswick, NJ, USA), containing 10% kcal from fat and 7% kcal from sucrose, or a high fat-high sucrose (HFHS) diet (Cat #:D12451, Research Diets, New Brunswick, NJ, USA), containing 45% kcal from fat and 17% kcal from sucrose. The composition of the diets is described in Appendix. All animals were housed under identical conditions and given free access to food and water. Body weight was monitored weekly.

On the day of termination, at week 19-20, all mice were fasted for 5-6h and then injected with human insulin (Humulin R, Eli Lilly, ON, Canada; 10 U/kg ip); 5 min later, they were deeply anesthetized with 4% isoflurane. After 5 min, the mice were euthanized. Hearts and other organs, e.g. liver, epididymal adipose tissue and gastrocnemius muscle, were removed, and the apex of the heart and a small portion of adipose tissue were fixed in 10% formalin. The remaining tissues were frozen in liquid nitrogen and stored at -80°C for later biochemical analysis. All animal studies were performed in accordance with the Canadian Council for Animal Care's Guide for the Care and Use of Experimental Animals and were approved by the Animal Care Committee of The University of British Columbia.

3.2.2 Western blot protein analysis

Tissues were homogenized in radioimmunoprecipitation assay (RIPA) buffer with 1X protease/phosphatase inhibitors (Cell Signaling Technology, Beverly, MA). 20–40 µg of protein was loaded. Proteins were separated by 6-12% SDS-PAGE, transferred to nitrocellulose membrane, and immunoblotted using primary antibodies (range from 1:500 to 1: 1,000) against ROCK1 (611136) (BD Biosciences, San Jose, CA); RhoA (sc-418), ROCK2 (sc-5561) (Santa Cruz

Biotechnology, Inc., Dallas, TX); ACC (3662), Ser79-phosphorylated ACC (3661), AMPK (2532), Thr172-phosphorylated AMPK (2531), Akt (9272), Ser473-phosphorylated Akt (9271), MYPT1 (2634), Thr853-phosphorylated MYPT1 (4563), IRS-1 (2382), Ser307-phosphorylated IRS-1 (2381) (Cell Signaling Technology, Beverly, MA); Tyr612-phosphorylated IRS-1 (44-816G) (Thermo Fisher Scientific, Waltham, MA) at 4°C overnight. They were subsequently incubated with secondary antibodies (range from 1:2,500 to 10,000) at room temperature for 1 hr. Protein expression was visualized using a Li-Cor Odyssey CLX imaging system (Li-Cor Biosciences, Lincoln, NE). Protein band intensity was determined by densitometry and normalized to vinculin or alpha-tubulin, or the corresponding total protein in the same preparation.

3.2.3 Hepatic triglycerides and cholesterols

Hepatic triglycerides and cholesterol were measured by enzymatic analysis using commercially available kits (Pointe Scientific. Inc., Canton, MI). Liver triglyceride (TG) levels were determined using glycerol phosphate oxidase (GPO) reagent (catalog #: T7532) (Pointe Scientific. Inc., Canton, MI) according to the protocol of Palmer *et al.* (2009). Briefly, approximately 70-80 mg of liver tissue was homogenized in the KOH-EtOH solution. Samples were heated at 70°C for 1 hour and subsequently incubated at room temperature overnight. The next day, the volume in each sample was brought up to 1000µL using 2M Tris-HCL and samples were then diluted 1:5 with Tris-HCL for colometric quantification of TG using GPO reagent at 500nm. Liver cholesterol levels were measured using cholesterol reagent (catalog #: C7510) (Pointe Scientific. Inc., Canton, MI). One ml of the reagent in each tube was pre-warmed at 37°C for at least 5 min, then 10µl of each sample was added to respective tubes, mixed and heated at 37°C for another 5 min. After that, absorbances of all test tubes were read and recorded at 500nm.

Absorbance to concentration calculation was performed to determine the cholesterol levels in each sample.

3.2.4 Quantitative real-time PCR

RNA was extracted from tissue samples using TRIzol reagent (Invitrogen, Burlington, ON, Canada). Reverse transcription was carried out using a SuperScript VILO cDNA synthesis kit (Invitrogen, Carlsbad, CA) with 1 μg of total RNA. Quantitative RT-PCR was performed on an Applied Biosystems StepOnePlus PCR system using SYBR Select Master Mix (Applied Biosystems, Foster City, CA). Relative mRNA expression was calculated by the comparative threshold ($2^{\Delta\Delta CT}$) method and normalized to the 36b4 endogenous control, which is an acidic ribosomal phosphoprotein.

3.2.5 Adipocyte area and number

The size and number of adipocytes per mm^2 of tissue were determined according to the protocol described previously (Parlee *et al.*, 2014). Briefly, formalin-fixed, paraffin-embedded epididymal fat tissue was sectioned with a thickness of 5 μm, and stained with hematoxylin and eosin. Five representative digital images were taken under a 10X objective from 2 different sections per animal using a Zeiss microscope (North York, ON, Canada; LSM700). The area and number of adipocytes were measured using ImageJ v1.45 s (NIH, Bethesda, MD, USA).

3.2.6 Statistical analysis

All values are shown as mean ± SEM; n denotes the number of animals in each group. Results were analyzed using GraphPad Prism version 8.0 (GraphPad Software, San Diego, CA). The adipose tissue properties were analyzed by two-way repeated measures ANOVA followed by a Bonferroni's post-hoc test. All other data was analyzed by one-way ANOVA followed by Newman-Keul's test. Differences were considered statistically significant at $p < 0.05$.

3.3 Results

3.3.1 Liver

3.3.1.1 Effect of HFHS feeding on hepatic triglyceride and cholesterol levels

At termination, both HFHS diet-fed mouse groups had significantly ($p < 0.05$) increased levels of liver triglycerides, which were about 2-fold higher than their LFLS diet-fed counterparts (Fig. 3.1A). However, although both ROCK2+/- + HFHS and WT + HFHS animals had elevated levels of liver cholesterol, the differences were not statistically significant in comparison to LFLS diet-fed animals (Fig. 3.1B).

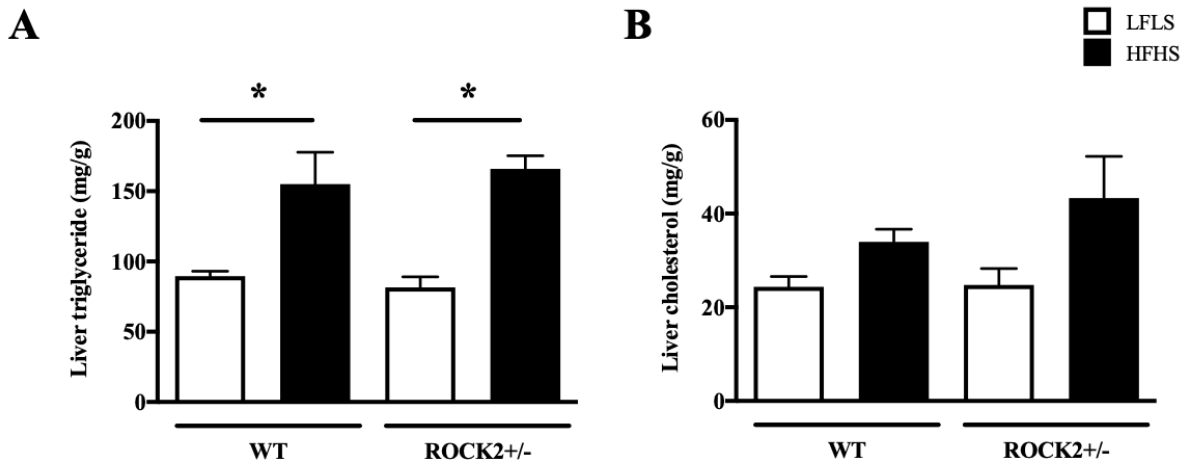

Figure 3.1 Effect of HFHS diet on hepatic triglyceride and cholesterol level in WT and ROCK2+/- mice

Levels of (A) liver triglyceride and (B) liver cholesterol were assessed. *$p < 0.05$. Data shown as mean ± S.E.M., n= 8 in each group.

3.3.1.2 Effect of HFHS feeding on hepatic RhoA-ROCK signaling

Similar to what I found in the heart of these animals (Chapter 2), there was no significant difference in hepatic ROCK1 expression among the different groups of animals (Fig. 3.2A). Liver expression of ROCK2 was about 50% lower ($p < 0.05$) in both ROCK2+/- + LFLS and ROCK2+/- + HFHS animals compared to their WT littermates, which confirmed the ROCK2 knockdown in ROCK2+/- animals (Fig. 3.2B). Also consistent with what I observed in the heart, there was no over-expression of hepatic ROCK2 in WT + HFHS mice compared to WT + LFLS mice. This indicated that HFHS diet feeding failed to induce ROCK2 over-expression in WT mice. In addition, the phosphorylation level of MYPT1 at Thr853, an index of total ROCK activity, was very comparable among animals fed the different diets (Fig. 3.2C).

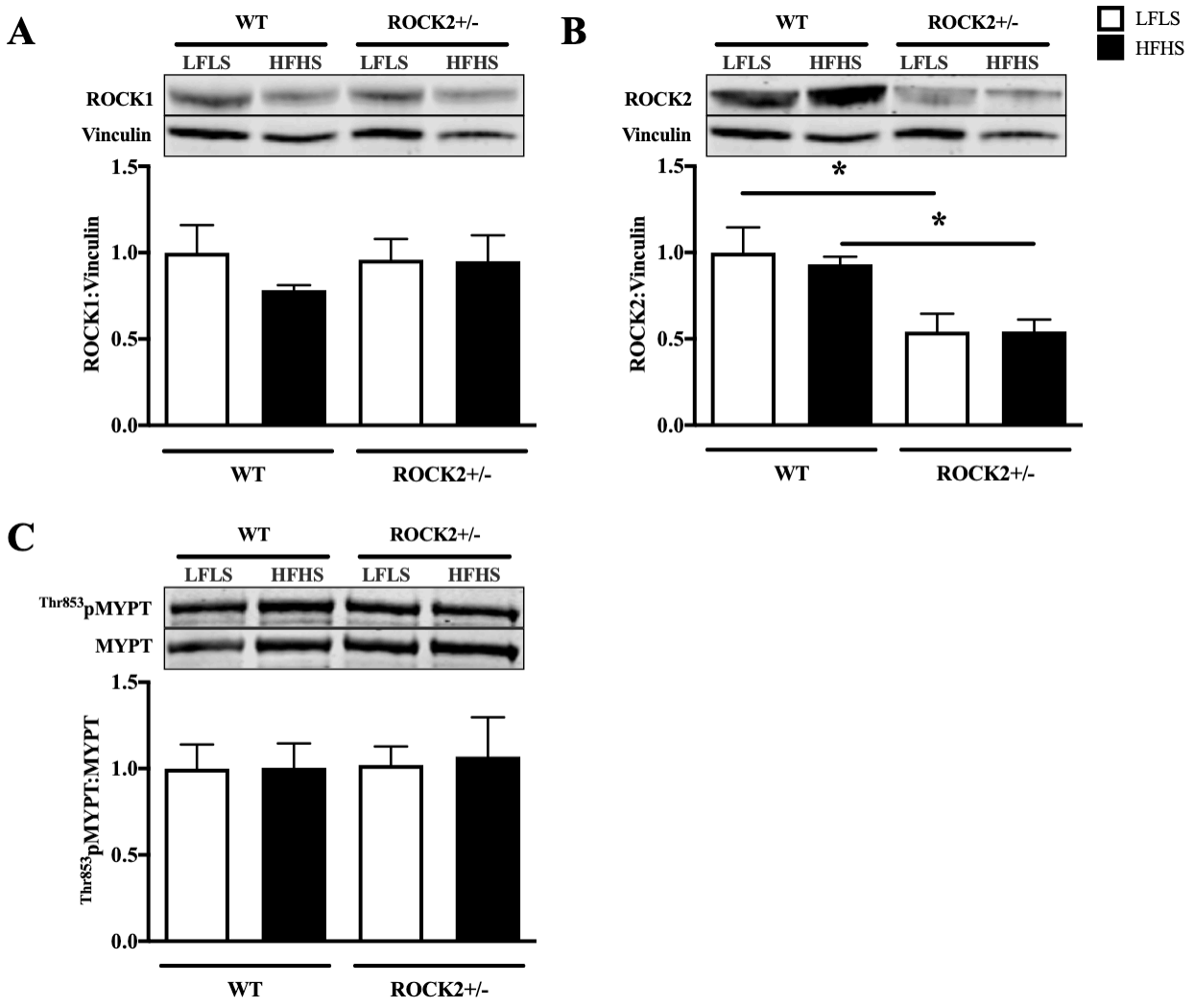

Figure 3.2 Effect of HFHS diet on hepatic RhoA-ROCK signaling in WT and ROCK2+/- mice

Representative Western blot images (top) and relative protein expression levels (bottom) of (A) ROCK1, (B) ROCK2, and (C) phosphorylation of MYPT1 at Thr853. *$p < 0.05$. Data shown as mean ± S.E.M., n= 8 in each group.

3.3.1.3 Effect of HFHS feeding on hepatic insulin signaling

As reported in Chapter 2, I observed systemic glucose and insulin intolerance in HFHS diet-fed animals, but hearts of these animals did not exhibit impaired insulin signaling. Since I found significantly enlarged liver weight in HFHS diet-fed animals and the liver plays an important role in metabolizing fructose, I was interested in investigating insulin signaling in the liver. I found that the expression level of IRS-1 and the phosphorylation of IRS-1 at Ser307 decreased ($p < 0.05$) more than 80% in both HFHS diet-fed animals in contrast to their LFLS diet-fed littermates (Fig. 3.3A, C). The massive decreased expression level of IRS-1 and reduced level of ^{Ser307}pIRS-1 indicate severely disrupted insulin signaling in the liver mediated through IRS-1. However, no difference was found in the phosphorylation of IRS-1 at Tyr612 (Fig. 3.3B). In addition, the phosphorylation of Akt at Ser473, which is a downstream target of IRS-1, was significantly ($p < 0.05$) reduced in both WT + HFHS and ROCK2+/- + HFHS mice compared to WT + LFLS and ROCK2+/- + LFLS mice (Fig. 3.3D-E), further indicating impaired insulin signaling in the liver. Overall, WT + HFHS and ROCK2+/- + HFHS mice had very comparable levels of disrupted IRS-1 mediated insulin signaling, indicating that heterozygous deletion of ROCK2 did not protect CD-1 mice from HFHS diet-induced impaired insulin signaling in the liver.

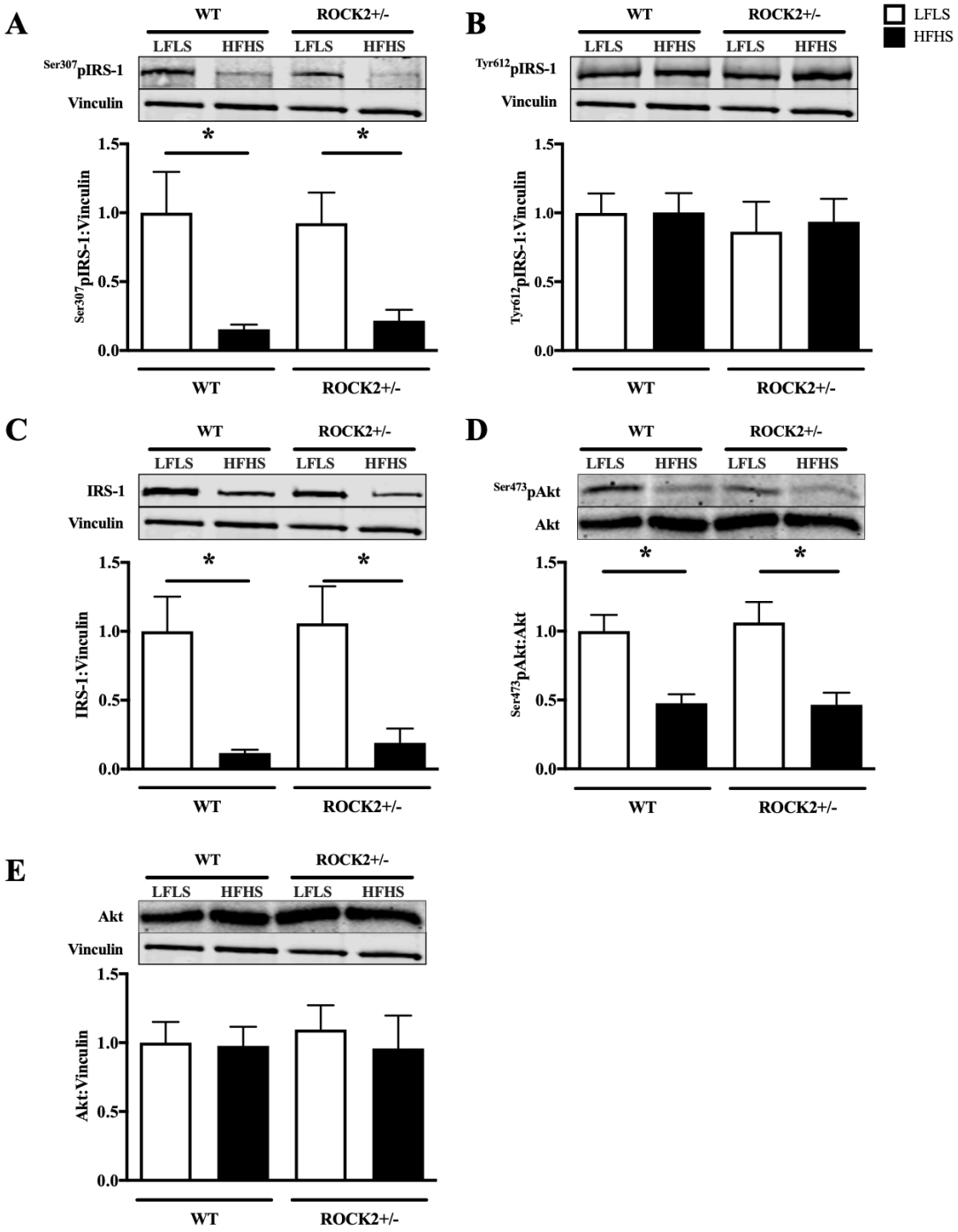

Figure 3.3 Effect of HFHS diet on the hepatic insulin signaling in WT and ROCK2+/- mice

Representative Western blot images (top) and relative protein expression levels (bottom) of (A) phosphorylation of IRS-1 at Ser307, (B) phosphorylation of IRS-1 at Tyr612, (C) IRS-1, (D) phosphorylation of Akt at Ser473, and (E) Akt. *$p < 0.05$. Data shown as mean ± S.E.M., n= 8 in each group.

3.3.1.4 Effect of HFHS feeding on the hepatic expression of ^{Thr172}pAMPK and ^{Ser79}pACC

According to a study by Huang et al, inactivation of ROCK1 signaling was able to protect mice from obesity-associated insulin resistance, and hepatic lipid accumulation induced by a diet containing 58% kcal from fat and 13% kcal from sucrose (Huang *et al.*, 2018). Liver-specific ROCK1 deletion prevented the development of hepatic steatosis and decreased hyperglycemia in obese mice through the activation of AMPK signaling (Huang *et al.*, 2018). In the present study, HFHS diet-fed animals seemed to have reduced phosphorylation of AMPK at Thr172 in the liver, which indicates a decreased activation of AMPK (Willows *et al.*, 2017), although the difference was not statistically significant (Fig. 3.4A-B). A downstream target of AMPK, acetyl-CoA carboxylase (ACC), is also involved in the process of fatty acid synthesis and the activation of ACC can promote *de novo* lipogenesis. I found that both the expression level of ACC and the phosphorylation of ACC at Ser79 were dramatically decreased ($p < 0.05$) in both WT and ROCK2+/- mice fed a HFHS diet (Fig. 3.4C-D).

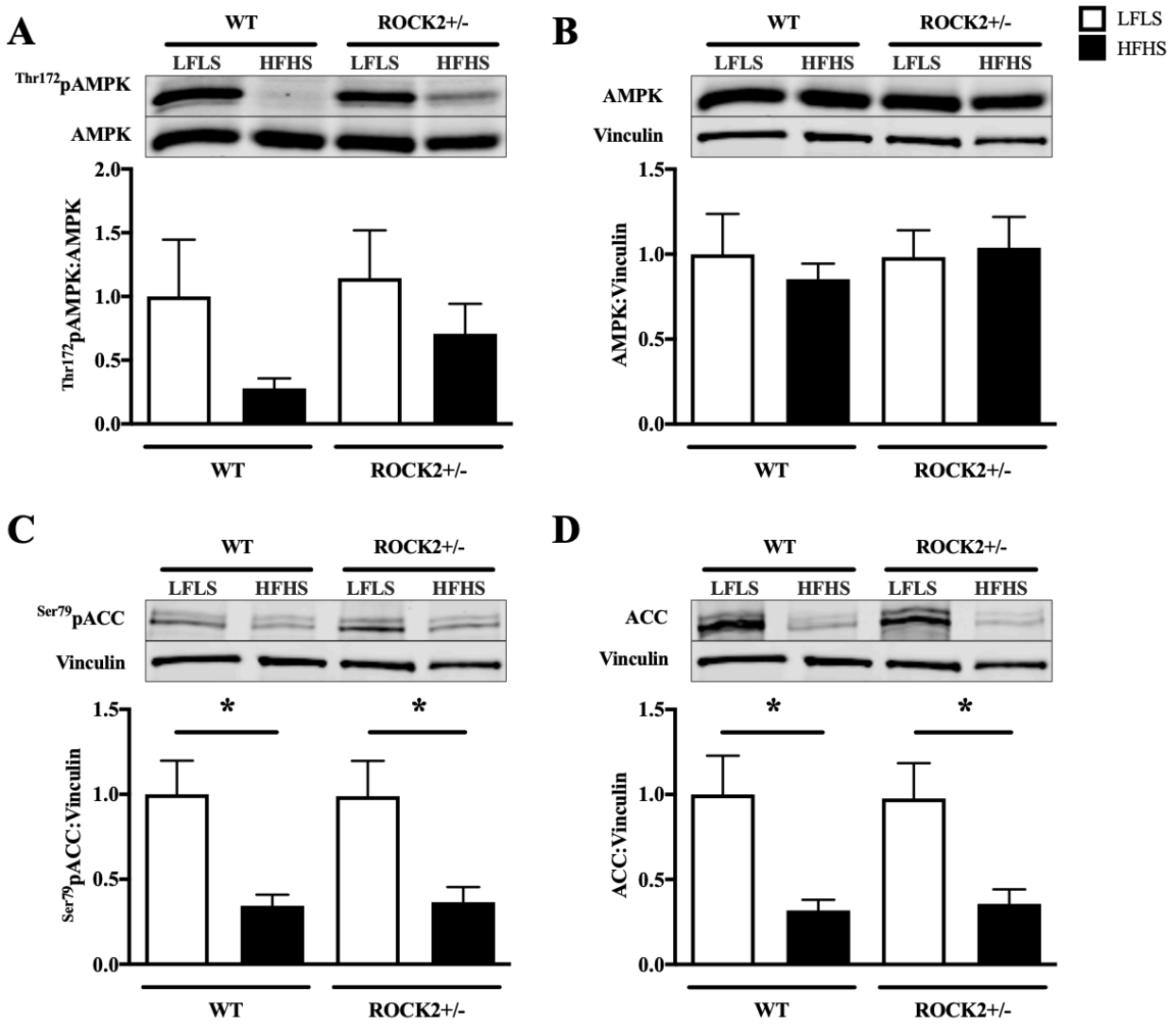

Figure 3.4 Effect of HFHS diet on the hepatic expression of Thr172pAMPK and Ser79pACC in WT and ROCK2+/- mice

Representative Western blot images (top) and relative protein expression levels (bottom) of (A) phosphorylation of AMPK at Thr172, (B) AMPK, (C) phosphorylation of ACC at Ser79, and (D) ACC. *$p < 0.05$. Data shown as mean ± S.E.M., n= 8 in each group.

3.3.1.5 Effect of HFHS feeding on hepatic mRNA expression of lipogenic enzymes

The mRNA expression of several hepatic lipogenic enzymes that are regulated by AMPK, such as fatty acid synthase (*fas*), elongation of very long-chain fatty acid protein 3 (*elovl3*), and sterol regulatory element-binding protein 1c (*srebp1c*) was also investigated. In general, I found that there was no significant difference in hepatic mRNA expression among animals fed different diets (Fig. 3.5). Although HFHS diet-fed mice had a slight decrease in FAS mRNA expression compared to their LFLS diet-fed littermates, differences were not statistically significant (Fig. 3.5A). In addition, ROCK2+/- + LFLS mice showed a drop ($p < 0.05$) in Elovl3 mRNA expression compared to WT + LFLS mice (Fig. 3.5B).

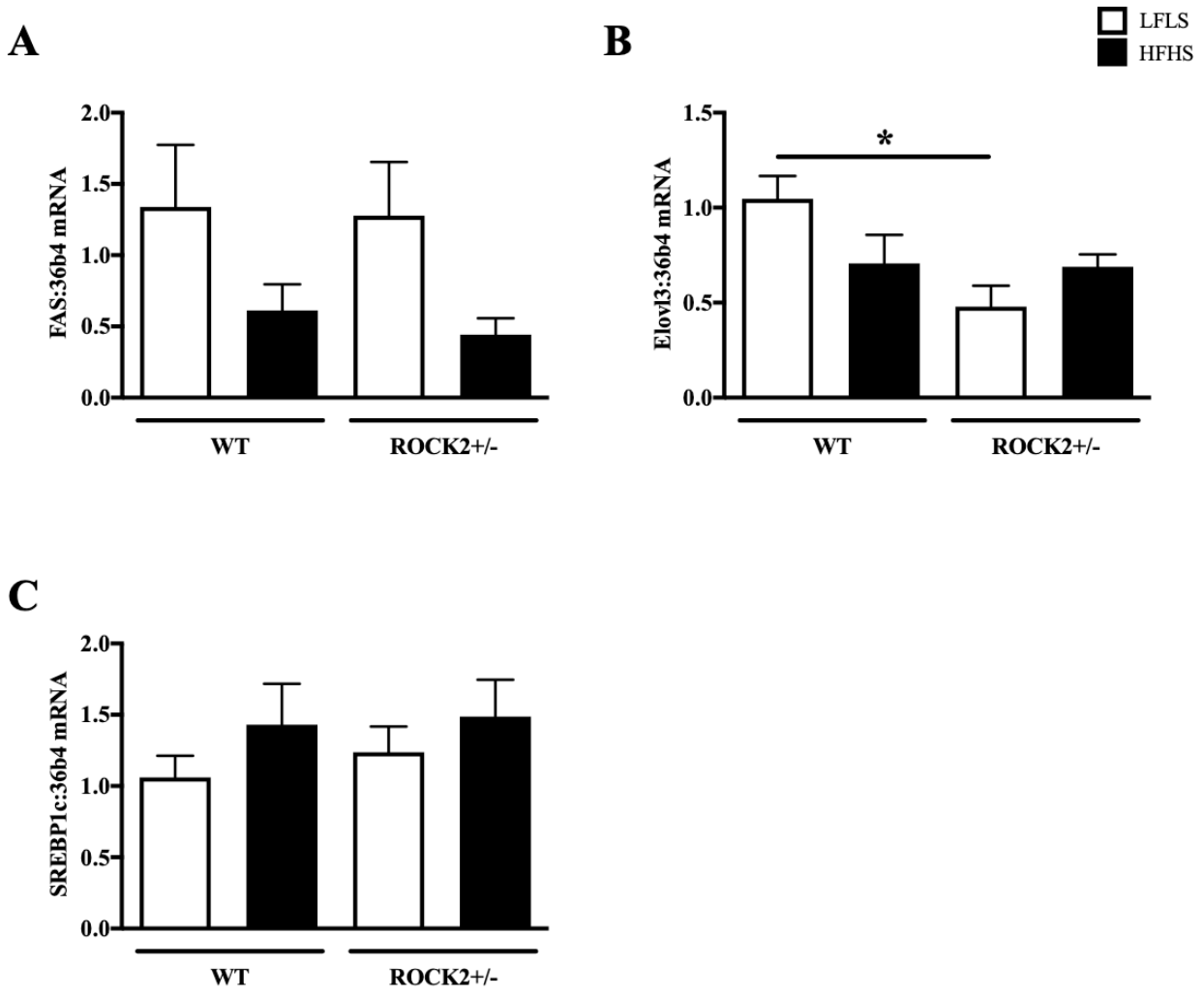

Figure 3.5 Effect of HFHS diet on the hepatic mRNA expression of lipogenic enzymes in WT and ROCK2+/- mice

mRNA expression levels of (A) FAS, (B) Elovl3, and (C) SREBP1c normalized to the endogenous control 36b4 were assessed. *$p < 0.05$. Data shown as mean ± S.E.M., n= 8 in each group.

3.3.2 Adipose tissue

3.3.2.1 Effect of HFHS feeding on adipose tissue RhoA-ROCK signaling

In accordance with what I observed in the heart (Chapter 2), the expression levels of RhoA and ROCK1 were very comparable among the different animal groups, and no significant differences were detected (Fig. 3.6A-B). LFLS and HFHS diet-fed ROCK2+/- mice demonstrated reduced ROCK2 expression by about 50% compared to their WT littermates ($p < 0.05$). No over-expression of ROCK2 was found in the adipose tissue of WT + HFHS animals, in comparison to their WT LFLS diet-fed littermates (Fig. 3.6C). In order to investigate the activity of ROCK isoforms, the phosphorylation of MYPT1 at Thr853 was measured. However, the levels of ^{Thr853}pMYPT1 were very similar among different animal groups, indicating that there was no over-activation of ROCK isoforms in HFHS diet-fed animals (Fig. 3.6D).

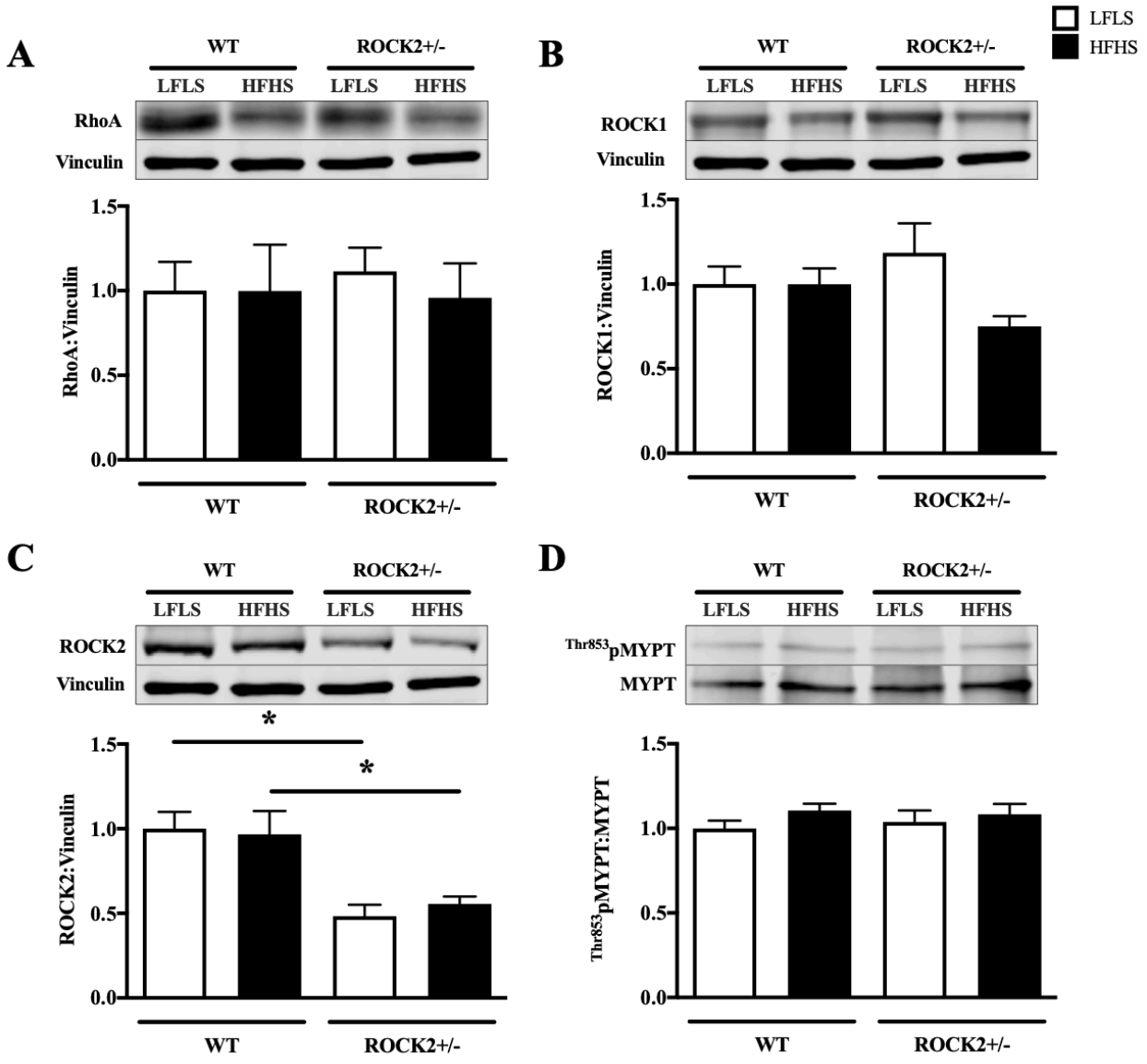

Figure 3.6 Effect of HFHS diet on adipose tissue RhoA-ROCK signaling in WT and ROCK2+/- mice

Representative Western blot images (top) and relative protein expression levels (bottom) of (A) RhoA, (B) ROCK1, (C) ROCK2, and (D) phosphorylation of MYPT1 at Thr853. *$p < 0.05$. Data shown as mean ± S.E.M., n= 8 in each group.

3.3.2.2 Effect of HFHS feeding on adipose tissue properties

Histological examination of the adipose tissue showed that WT + HFHS mice had larger adipocyte size than ROCK2+/- + HFHS mice (Fig. 3.7A-B). The morphometric analysis also revealed that ROCK2+/- + HFHS mice had a greater frequency of adipocytes that are smaller than 5000 μm^2 in comparison to WT + HFHS mice, which was also evident in the corresponding AUC (Fig. 3.7C-D). In addition, the average adipocyte area in WT + HFHS mice was around 6400 μm^2, which was significantly larger compared to that in ROCK2+/- + HFHS mice (4800 μm^2) (Fig. 3.7E). Consistent with average adipocyte area, ROCK2+/- + HFHS mice also had a higher number of adipocytes per mm^2 epididymal fat tissue compared to WT + HFHS mice (Fig. 3.7F).

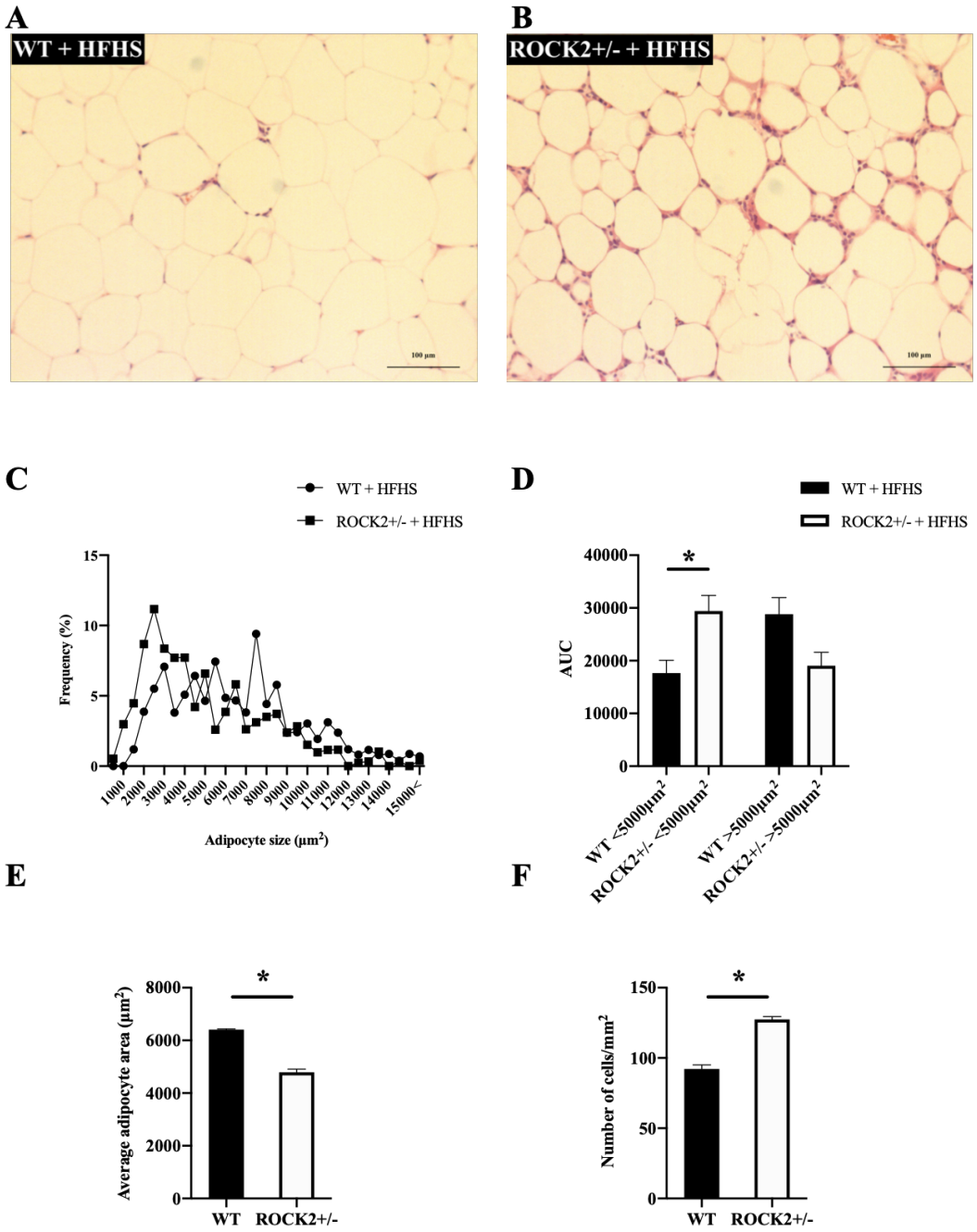

Figure 3.7 Effect of HFHS diet on adipose tissue properties in WT and ROCK2+/- mice

(A-B) Representative photomicrographs of epididymal adipose tissue stained with hematoxylin and eosin, (C) adipocyte area frequency distribution, (D) area under the adipocyte area frequency distribution curve for cells less than or more than 5000 μm^2, (E) average adipocyte area, (F) number of adipocytes per mm^2 epididymal fat tissue in each group. *$p < 0.05$. Data shown as mean ± S.E.M., n= 3 in each group.

3.3.2.3 Effect of HFHS feeding on adipose tissue insulin signaling

I observed impaired insulin signaling in livers of HFHS diet-fed mice. In addition, the previous study from our lab showed disrupted insulin signaling mediated via IRS-1 in the adipose tissue of WT + HF mice, while insulin signaling was much improved in ROCK2+/- + HF mice (Soliman *et al.*, 2016). Therefore, I also investigated insulin signaling pathway in the adipose tissue. The expression of IRS-1, and the phosphorylation of IRS-1 at Ser307 and Tyr612 were reduced dramatically in WT + HFHS diet-fed animals ($p < 0.05$) (Fig. 3.8A-C). Moreover, ROCK2+/- + HFHS mice also demonstrated disrupted insulin signaling, and heterozygous deletion of ROCK2 was not able to protect mice from HFHS diet-induced insulin resistance in the adipose tissue. In addition, significantly decreased phosphorylation of Akt at Ser473, which is a downstream target of IRS-1, was also found in both HFHS diet-fed WT and ROCK2+/- animals ($p < 0.05$) (Fig. 3.8D-E).

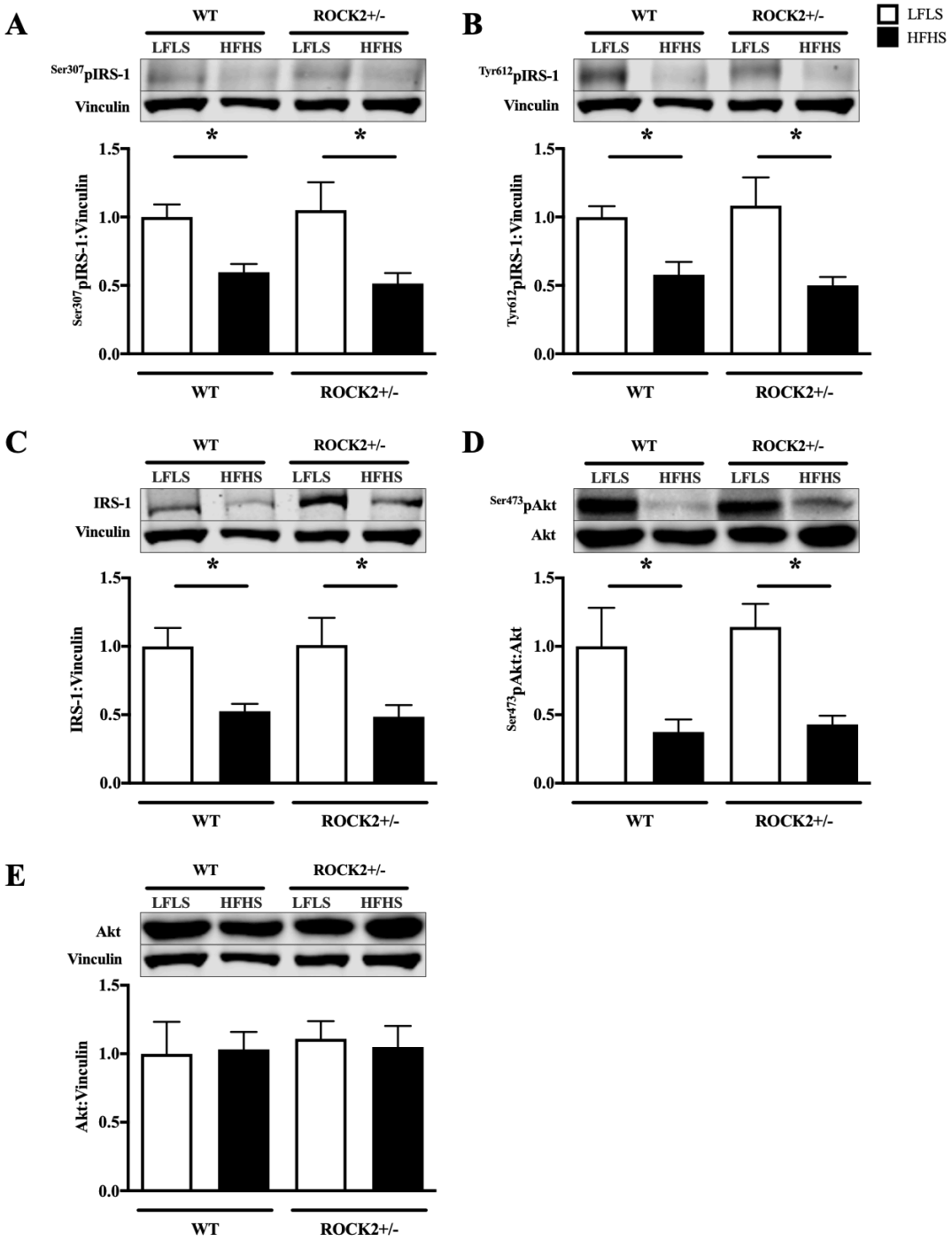

Figure 3.8 Effect of HFHS diet on the hepatic insulin signaling in WT and ROCK2+/- mice

Representative Western blot images (top) and relative protein expression levels (bottom) of (A) IRS-1, (B-C) phosphorylation of IRS-1 at Ser307, (D-E) phosphorylation of IRS-1 at Tyr612, and (F) phosphorylation of Akt at Ser473. *$p < 0.05$. Data shown as mean ± S.E.M., n= 8 in each group.

3.3.2.4 Effect of HFHS feeding on adipose tissue expression of PPARγ and inflammatory makers

Increased expression of PPARγ isoforms (PPARγ1 and PPARγ2) accompanied by reduced production of inflammatory factors including TNFα, MCP-1, and F4/80 was found in ROCK2+/- + HF animals (Soliman *et al.*, 2016). However, the expression of both PPARγ isoforms was approximately the same among various animal groups in the present study (Fig. 3.9A-B). Moreover, both WT + HFHS and ROCK2+/- + HFHS mice showed significantly increased mRNA expression of mRNA of inflammatory factors ($p < 0.05$), and heterozygous deletion of ROCK2 did not demonstrate a protective effect in HFHS diet-fed mice (Fig. 3.9C-E).

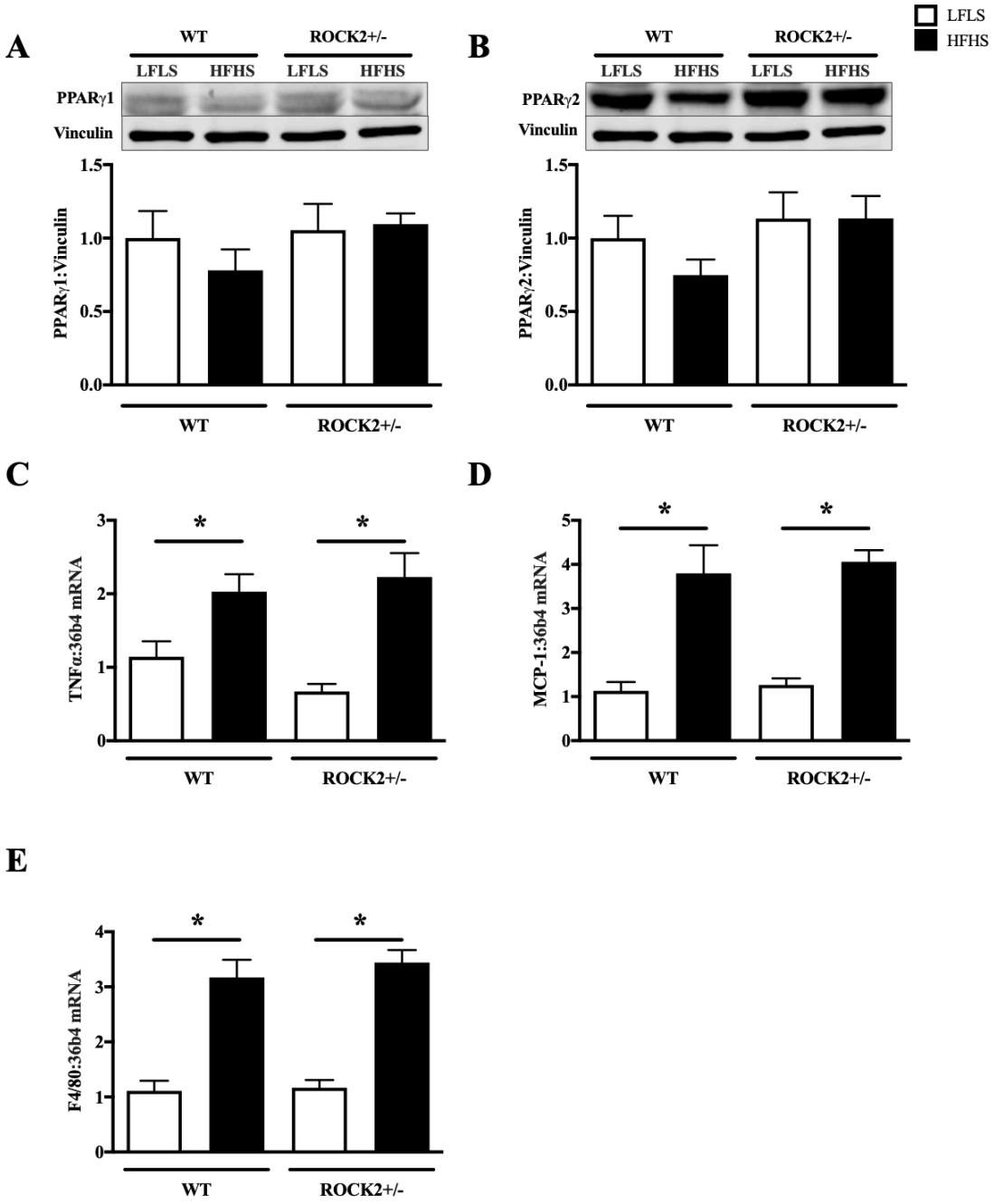

Figure 3.9 Effect of HFHS diet on adipose tissue expression of PPARγ and inflammatory makers in WT and ROCK2+/- mice

Representative Western blot images (top) and relative protein expression levels (bottom) of (A) PPARγ1 and (B) PPARγ1 were assessed. mRNA expression levels of (C) TNFα, (D)MCP-1, and (E) F4/80. *$p < 0.05$. Data shown as mean ± S.E.M., n= 8 in each group.

3.4 Discussion

In the present study, no over-expression of the RhoA-ROCK pathway was found in either liver or adipose tissue, which was consistent with what I observed in the heart in Chapter 2. However, distinct from the hearts of HFHS diet-fed mice, the liver and adipose tissue of both WT and ROCK2+/- HFHS diet-fed mice developed severe insulin resistance at the level of insulin signaling. Moreover, significantly elevated levels of hepatic triglycerides were observed in HFHS diet-fed mice in comparison to their LFLS diet-fed counterparts. Although ROCK2+/- + HFHS mice had smaller adipocyte size compared to WT + HFHS mice, both WT + HFHS and ROCK2+/- + HFHS mice developed similar extents of insulin resistance and inflammation in adipose tissue. My findings in adipose tissue of WT + HFHS mice were consistent with what we observed in our previous study in HF diet-fed WT CD-1 mice, in that the HFHS diet feeding induced adipocyte hypertrophy, reduced insulin signaling and increased inflammation levels in adipose tissue (Soliman *et al.*, 2016). However, heterozygous deletion of ROCK2 failed to protect CD-1 mice from these HFHS diet-induced complications through the activation of PPARγ isoforms as it did when mice were fed a HF diet.

Obesity is associated with excessive accumulation of triglyceride-rich lipid droplets in the liver. High levels of liver triglycerides and cholesterol indicate the rapid build-up of fatty acids in the liver (Kraegen *et al.*, 1991; Samuel and Shulman, 2012). There are three main sources of free fatty acids used for hepatic triglyceride formation: diet (15%), *de novo* lipogenesis (DNL) (25%), and adipose tissue lipolysis (60%) (Donnelly *et al.*, 2005). Impaired regulation of DNL and adipose tissue lipolysis are believed to play crucial roles in promoting hepatic steatosis (Utzschneider and Kahn, 2006). Unlike adipose tissue that can store excess fat safely to some extent, the liver cannot (Tolman *et al.*, 2007). As the adipose tissue becomes insulin resistant, there is an increased

production of free fatty acids from the adipose tissue, which is the primary source of fatty acids. These free fatty acids circulate in the bloodstream and are taken up by other organs, such as liver, to be stored in the form of triglycerides and cholesterol. In the present study, I observed greater liver weight in the ROCK2+/- + HFHS mice than the WT + HFHS mice, which is opposite to the effects on liver weight found in HF diet-fed mice in our previous study (Soliman *et al.*, 2016). In addition, significantly elevated levels of liver triglycerides were found in both WT + HFHS and ROCK2+/- + HFHS mice. It's possible that there may be differences in the underlying mechanisms contributing to obesity and insulin resistance resulting from a HF and a HFHS diet in the liver. Therefore, I investigated the effect of a HFHS diet on the liver and adipose tissue and the role of heterozygous deletion of ROCK2 in improving insulin signaling and adipocyte inflammation in this chapter.

A recent study of male C57BL/6J mice fed a diet containing 58% kcal from fat and 13% kcal from sucrose showed increased hepatic activity of ROCK1, which was associated with obesity, systemic insulin resistance, and hepatic lipid accumulation. On the other hand, mice with hepatic ROCK1 deletion had reduced weight gain and improved systemic glucose and insulin sensitivity, as well as decreased hepatic steatosis and inflammation. This suggests that upregulated expression and activation of ROCK1 in the liver is involved in the development of obesity, insulin resistance, and fatty liver disease (Huang *et al.*, 2018).

AMPK plays a crucial role in *de novo* lipogenesis through maintaining a balance between energy supply and demand. Lipogenesis, a complex but highly regulated metabolic pathway of fatty acid synthesis, contributes to an increased fat mass in the liver and adipose tissue. Therefore, a reduction in lipogenesis may be able to protect against the development of obesity. AMPK activation inhibits fatty acid synthesis and promotes fatty acid oxidation by phosphorylating ACC,

and decreasing malonyl-CoA levels (Wu *et al.*, 2018). Phosphorylation of AMPK at Threonine 172 stimulates AMPK activity, which then leads to a suppression in ATP-consuming anabolic pathways and an elevation in ATP-producing catabolic pathways (Woods *et al.*, 2017; Huang *et al.*, 2018). Studies have shown that obesity is associated with reduced AMPK activation, along with alterations in glycolysis, insulin sensitivity, hepatic lipid metabolism, and inflammation (Jeon, 2016). For example, in obese human patients with whole-body insulin resistance, the ratio of pAMPK to AMPK was reduced in visceral adipose tissue (Gauthier *et al.*, 2011). Moreover, decreased steatosis and obesity, reduced inflammation and fibrosis, and improved glucose homeostasis were observed in mice with inducible liver-specific AMPK activation (Garcia *et al.*, 2019). Huang et al demonstrated over-activation of hepatic ROCK1 activates *de novo* lipogenesis by suppressing the phosphorylation and activation of AMPK (Huang *et al.*, 2018). However, in the present study, no over-expression of ROCK1 or significantly decreased activity of AMPK was found in HFHS diet-fed mice.

As a downstream target of AMPK, ACC is closely associated with the process of DNL in the liver and adipose tissue. Phosphorylation of ACC at Ser 79 by AMPK leads to its inactivation and a reduction in the production of malonyl CoA, and further contributes to decreased fatty acid synthesis and increased fatty acid oxidation (Galic *et al.*, 2018). Several studies have shown that the inhibition of ACC activity in the liver of mice and human subjects reduces levels of triglycerides, hepatic steatosis, and hepatic insulin resistance through suppressing lipogenesis (Mao *et al.*, 2006; Kim *et al.*, 2017; Goedeke *et al.*, 2018). In the present study, I found that both the expression of total ACC isoforms and the phosphorylation of ^{Ser79}ACC1 and ^{Ser79}ACC2 were reduced significantly in HFHS diet-fed mice compared to their LFLS diet-fed counterparts, which suggests that there may be a decrease in hepatic fatty acid synthesis in these animals. Although

DNL is one of the main pathways of generating triglycerides, dietary intake and adipose tissue lipolysis also contribute to the accumulation of liver triglycerides (Utzschneider and Kahn, 2006; Saponaro *et al.*, 2015). Therefore, the high levels of liver triglycerides found in HFHS diet-fed mice may be explained by the accumulation of lipids via dietary intake and adipose tissue lipolysis. It's also possible that increased levels of liver triglycerides form a negative feedback loop acting on ACC to decrease the expression of ACC and further inhibit DNL.

AMPK interacts with lipogenic enzymes such as *fas*, *elovl3*, and *srebp1c* to regulate the process of lipogenesis. According to Huang et al, suppressed AMPK activity was associated with elevation of mRNA expressions of several hepatic lipogenic enzymes, including *fas*, *elovl3*, and *srebp1c* in obese mice, and was associated with increased lipogenesis in the liver during the development of hepatic steatosis (Huang *et al.*, 2018). Several recent studies have been demonstrated that increased mRNA and protein expression of lipogenic enzymes are associated with the suppression of AMPK activity and the development of fatty liver disease (Fang *et al.*, 2019; Luo *et al.*, 2019; Zhou *et al.*, 2019). In the current study, no significant variations of hepatic lipogenic enzyme mRNA expression were found in the HFHS diet-fed mice, except that ROCK2+/- + LFLS mice exhibited a reduced *elovl3* mRNA expression compared to WT + LFLS mice. Despite the significantly elevated levels of liver triglycerides and severe insulin resistance in the livers of HFHS diet-fed mice, the lack of changes of AMPK activation and AMPK-mediated mRNA expression of lipogenic enzymes may be due in part to the variations between mice strains and a relatively lower level of fat in the diet in the present study.

I also investigated the insulin signaling pathway in the liver as I did in hearts of these animals. A significant decreased hepatic expression of IRS-1, which regulates glucose metabolism in cells upon stimulation with insulin, found in HFHS diet-fed mice indicates that the normal

cellular response to glucose might be disrupted in livers of those animals (Shaw, 2011). Phosphorylation of IRS-1 at Ser307 inhibits insulin action by impairing insulin receptor-mediated phosphorylation of tyrosine residues such as Tyr612 (Rask-Madsen and Kahn, 2012). Decreased phosphorylation of IRS-1 at Ser307 in HFHS diet-fed mice was consistent with significantly reduced expression of total IRS-1 (Aguirre *et al.*, 2002). Furthermore, both WT + HFHS and ROCK2+/- + HFHS animals also exhibited decreased levels of ^{Ser473}pAkt, which is an indicator of the development of impaired insulin signaling, in contrast to their corresponding littermates (Abel *et al.*, 2012).

In summary, expression levels of ROCK1 and ROCK2 and the total ROCK activity were very comparable among different groups of animals, and there was only a tendency to a decrease in the phosphorylation of AMPK at Thr172 in HFHS diet-fed animals compared to LFLS diet-fed animals. Therefore, a diet containing 45% kcal from fat and 17% kcal from sucrose might be insufficient to elevate ROCK1 activity, suppress of AMPK activity and reduce AMPK-mediated inhibition of lipogenesis. In the face of significantly reduced expression of total and Ser 79 phosphorylated ACC levels, the elevated levels of liver triglycerides in livers of HFHS diet-fed mice may be explained by high levels of lipid accumulation from dietary intake and adipose tissue lipolysis. Moreover, severely impaired hepatic insulin signaling mediated through IRS-1 and its downstream target Akt may contribute to the insulin resistance found in the liver of these HFHS diet-fed animals, and further to the systemic glucose and insulin insensitivity. Furthermore, no reduction of levels of liver triglycerides or improvement of hepatic insulin signaling was found in HFHS mice with heterozygous deletion of ROCK2, possibly explaining in part why ROCK2+/- + HFHS mice were not protected from systemic glucose and insulin intolerance.

Previous studies from our lab showed that over-activation of ROCK2 in adipose tissue of CD-1 mice fed a HF diet suppressed the activation of PPARγ, and was associated with significantly enlarged adipocytes and increased production of inflammatory factors. On the other hand, heterozygous deletion of ROCK2 appeared to protect ROCK2+/- + HF mice from adipocyte hypertrophy and insulin resistance by activating PPARγ (Soliman *et al.*, 2016). In the present study, I characterized the effect of a HFHS diet on adipose tissue of CD-1 mice and investigated the effect of heterozygous deletion of ROCK2 in these animals. In accordance with our previous study in adipose tissue of HF diet-fed CD-1 mice, the expression levels of RhoA and ROCK1 were very comparable among all animal groups (Soliman *et al.*, 2016). In our previous study, WT + HF mice had significantly elevated adipose tissue ROCK2 activity compared to chow diet-fed mice, and heterozygous deletion of ROCK2 prevented HF diet-induced over-activation of ROCK2 (Soliman *et al.*, 2016). However, in the present study, although I did not measure ROCK2 activity directly, no over-expression of ROCK2 or increase in total ROCK activity were found in adipose tissue of WT + HFHS mice, suggesting that there was no over-activation of ROCK2 in the adipose tissue of WT + HFHS mice. Overall, there was no detection of over-expression or over-activation of the RhoA-ROCK pathway in adipose tissue of HFHS diet-fed mice, which is consistent with what I observed in hearts and livers of these animals.

As the enlargement of adipose tissue to store excess energy intake is also an important mechanism during the development of obesity, I investigated the adipose tissue properties in WT + HFHS and ROCK2+/- + HFHS mice. There are two main mechanisms of adipocyte expansion: hyperplasia and hypertrophy (Verboven *et al.*, 2018). Hyperplasia represents an increase in adipocyte numbers, and hypertrophy is defined as an increase in adipocyte size. In overnutrition and obesity, in order to adapt to the fat mass expansion and additional fat storage capacity in the

progression of obesity, mature adipocytes accumulate more fat and undergo cellular hypertrophy (Chan and Hsieh, 2017). Hypertrophy of adipocytes in visceral adipose tissue in obesity contributes to the development of insulin resistance, increased levels of inflammation and production of inflammatory cytokines, including TNFα and MCP-1 (Xu *et al.*, 2003; Bastard *et al.*, 2006). Adipocyte size in visceral adipose tissue was found to be positively related to the severity of whole-body insulin resistance in obese diabetic human patients, possibly through the presence of inflammatory macrophages and increased production of inflammatory cytokines (Jung and Choi, 2014). In addition, elevated production of inflammatory cytokines and chemokines, such as TNFα, MCP-1, and IL-6 was found in the enlarged adipose tissue of diet-induced obese C57BL/6J mice (Chan and Hsieh, 2017).

Activation of PPARγ isoforms in adipocytes of HF diet-induced obese mice has been demonstrated to lead to increased numbers of smaller adipocytes, decreased production of inflammatory factors, and improved adipose tissue insulin signaling and systemic insulin sensitivity (Sugii *et al.*, 2009). In the present study, WT + HFHS mice developed hypertrophy of adipocytes compared to ROCK2+/- + HFHS mice, which is consistent with our previous study in HF diet-fed animals (Soliman *et al.*, 2016). In addition, the size of adipocytes in ROCK2+/- + HFHS mice was reduced compared to WT + HFHS mice. Although the lack of LFLS diet-fed comparators makes it hard to conclude that there was no adipocyte hypertrophy in ROCK2+/- + HFHS mice, it is clear that ROCK2+/- + HFHS mice did not develop the same degree of hypertrophy as WT + HFHS mice. The reason for this is not known, since it was not associated with increased expression of PPARγ isoforms in adipose tissue from ROCK2+/- + HFHS mice. However, the lack of increase in PPARγ may explain why ROCK2+/- + HFHS mice were as insulin resistant as WT + HFHS mice, and the mRNA expression levels of inflammatory factors

such as TNFα, MCP-1, and F4/80 were comparable in both WT+ HFHS and ROCK2+/- + HFHS mice.

To conclude, dietary intake and adipose tissue lipolysis are the possible main sources of significantly increased levels of triglycerides in the liver of HFHS diet-fed mice. No over-activation of the RhoA-ROCK pathway, no suppression of AMPK, and no elevation of AMPK-mediated lipogenic enzyme expression in these mice may due at least in part to a diet containing a relatively lower content of fat and/or sucrose used in the present study compared to previous ones (Sato *et al.*, 2010; Huang *et al.*, 2018). The different mouse strain used in my study in comparison to Huang et al (CD-1 vs. C57BL/6) may be another reason contributing to the variations of the expression of AMPK and lipogenic enzymes found in HFHS diet-fed mice. The heterozygous deletion of ROCK2 appeared to protect CD-1 mice from HF diet-induced obesity-associated complications, such as insulin resistance and inflammation, by preventing increased activity of ROCK2 and allowing increased expression of PPARγ isoforms in adipose tissue. However, the HFHS diet used in the present study did not appear to increase ROCK2 activity in adipose tissue in WT mice, and there was no increase in expression of PPARγ isoforms in ROCK2+/- + HFHS mice. This might explain the disrupted insulin signaling and increased level of inflammation found in the adipose tissue of ROCK2+/- + HFHS animals, even though ROCK2+/- + HFHS mice did not develop the same degree of adipocyte hypertrophy as WT + HFHS mice. Ishimoto et al found that, although both HFHS diet-fed and HF diet-fed developed similar degree of obesity, more severe hepatic steatosis indicated by an increased degree of inflammation and fibrosis was found in mice fed a HFHS diet than mice fed a HF diet, while fructokinase knockout was able to protect HFHS diet-fed mice from the above symptoms (Ishimoto *et al.*, 2013). Therefore, it is possible that the mechanisms contributing to insulin resistance and increased inflammation in HFHS diet-

fed mice are distinct from those fed a HF diet. In addition, insulin resistance found in the liver and adipose tissue of HFHS diet-fed mice might explain the severe systemic glucose and insulin intolerance in these animals. Moreover, the fact that heterozygous deletion of ROCK2 had no effect on improving insulin signaling in either the liver or adipose tissue, and reducing the production of inflammatory factors in adipose tissue, possibly explains why ROCK2+/- + HFHS mice were not protected from systemic glucose and insulin intolerance.

Chapter 4: Conclusions

4.1 Summary and conclusions

As a worldwide phenomenon, obesity contributes to an impaired quality of life, shortened life expectancy, and increased mortality rate in the human population (Abdelaal *et al.*, 2017). In particular, cardiovascular disease accounts for the greatest mortality risk associated with obesity. One of the complications, obesity cardiomyopathy, is associated with changes in the structure and function of the myocardium, which contribute to LV dysfunction independent of other risk factors, including hypertension and coronary artery disease (Regan *et al.*, 1977; Rodrigues *et al.*, 1998).

Increased activation of the RhoA-ROCK pathway has been shown to be involved in diabetic and obesity cardiomyopathy (Soliman *et al.*, 2012, 2015). Previous studies from our lab demonstrated that HF diet-induced obesity leads to over-activation of ROCK2 in the heart and adipose tissue of CD-1 mice, as well as mild cardiac contractile dysfunction, systemic insulin resistance, and adipose tissue inflammation. On the other hand, heterozygous deletion of ROCK2 protected mice from these HF diet-induced complications through suppressing the activity of ROCK2 (Soliman *et al.*, 2015, 2016). In addition, in our preliminary study, we found that a HFHS diet, containing 45% kcal from fat and 17% kcal from sucrose, which more closely resembles the human "Western diet" leads to a more detrimental effect on cardiac structure and function than a HF diet, containing 60% kcal from fat and 7% kcal from sucrose, in WT C57BL/6J mice. However, it was not clear whether a HFHS diet would also lead to cardiac dysfunction and obesity-associated comorbidities, including insulin resistance and inflammation, in CD-1 mice, and if heterozygous deletion of ROCK2 would be able to protect these mice from obesity-related complications as it did in HF diet-fed animals.

In order to address these concerns, in Chapter 2, I investigated the effect of a HFHS diet on cardiac function, systemic glucose and insulin tolerance, and insulin signaling in hearts of WT and ROCK2+/- CD-1 mice. Consistent with our previous findings in HF diet-fed animals, WT + HFHS mice developed severe obesity and whole-body glucose and insulin intolerance. Importantly, no over-expression of ROCK2 was observed in hearts of mice fed a HFHS diet, and hearts of these HFHS diet-fed animals were resistant to the development of cardiac contractile dysfunction and disrupted cardiac insulin signaling even after a period of 24 weeks of feeding. The lack of cardiac contractile dysfunction detected in WT + HFHS mice may be explained in part by the lack of ROCK2 over-expression, cardiac mitochondrial dysfunction and impaired cardiac insulin signaling in these animals. The exact underlying mechanisms are still not clear, but it's possible that the (1) relatively low sucrose content used in my study, compared to other studies that observed cardiac dysfunction in a CD-1 mice fed a HFHS diet (42% kcal from fat and 30% kcal from sucrose) (Carbone *et al.*, 2015, 2017; Chen *et al.*, 2017; Zhang *et al.*, 2017), (2) the slightly lower energy density of the HFHS diet in comparison to the HF diet, and (3) genetic variations between C57BL/6J mouse strain and CD-1 mouse strain, might help to explain the lack of development of cardiac dysfunction in HFHS diet-fed WT CD-1 mice. However, the loss of protection of heterozygous deletion of ROCK2 on the systemic glucose and insulin intolerance still needed further evaluation.

The liver is one of major sites of glucose metabolism and storage, and impaired glucose metabolism contributes to insulin resistance in obesity and diabetes (Adeva-Andany *et al.*, 2016). The significantly greater liver weight found in ROCK2+/- + HFHS mice than WT + HFHS mice and the elevated sucrose content in the HFHS diet in comparison to the HF diet suggested that the adverse effects of fructose may contribute to the underlying mechanisms that lead to obesity and

insulin resistance in livers from mice fed a HFHS diet. Therefore, I characterized liver properties, lipogenic enzyme expression, and insulin signaling in the liver in Chapter 3. The comparable levels of the expression of AMPK, which is a main regulator of lipogenesis, and the mRNA expression of AMPK-mediated lipogenic enzymes observed among the different diet groups may due in part to the relatively lower fat and sucrose content in the HFHS diet compared to other studies (Sato *et al.*, 2010; Huang *et al.*, 2018), and to variations between mouse strains. Although levels of liver triglycerides increased dramatically in HFHS diet-fed mice, the expression of ACC dropped significantly in HFHS diet-fed mice. Hence, elevated levels of liver triglycerides may be explained by increased dietary intake of fatty acids and adipose tissue lipolysis, instead of through DNL mediated through ACC. Severely impaired insulin resistance at the level of insulin signaling in the liver may contribute to the systemic glucose and insulin insensitivity in HFHS diet-fed mice.

According to our previous study, heterozygous deletion of ROCK2 protected HF diet-fed CD-1 mice from obesity-induced adipocyte hypertrophy, disrupted insulin signaling, and inflammation in the adipose tissue via inhibiting the activity of ROCK2 and promoting the activation of PPARγ. In the present study, no over-expression of ROCK2 and no increased activity of total ROCK isoforms were found in HFHS diet-fed animals. Even though ROCK2+/- + HFHS mice did not develop the same degree of adipocyte hypertrophy as WT + HFHS mice, there was no elevation in expression of PPARγ. This may explain the similar extent of impaired insulin signaling and inflammation observed in both WT + HFHS and ROCK2+/- + HFHS mice. Whole-body glucose and insulin intolerance in ROCK2+/- + HFHS diet-fed mice may due at least in part to the loss of effect of heterozygous deletion of ROCK2 on improving insulin signaling and reducing levels of inflammatory factor production in adipose tissue.

Taken together, the results of Chapter 2 characterized the effect of a HFHS diet containing 45% kcal from fat and 17% kcal from sucrose on cardiac function, and systemic glucose and insulin tolerance in CD-1 mice. Chapter 3 further evaluated the underlying mechanisms of the whole-body glucose and insulin intolerance at the level of the liver and adipose tissue, and whether heterozygous deletion of ROCK2 was able to promote normal insulin signaling and decreasing levels of inflammatory factor production. The major findings of these studies were that:

- The lack of the development of cardiac contractile dysfunction in WT CD-1 mice after a 24-week of a HFHS (45% kcal from fat and 17% kcal from sucrose) diet feeding may be explained by (1) relatively low sucrose content used (2) the slightly lower energy density of the HFHS diet in comparison to the HF diet, and (3) genetic variations between C57BL/6J mouse strain and CD-1 mouse strain.
- Although ROCK2+/- + HFHS mice were as insulin intolerant as WT + HFHS mice per GTT and ITT measurements, no insulin resistance was identified at the level of insulin signaling in hearts of HFHS diet-fed mice.
- The development of cardiac dysfunction found in WT + HF mice and the effect of heterozygous deletion of ROCK2 to improve cardiac function in ROCK2+/- + HF mice confirmed the protective effects of heterozygous deletion of ROCK2 on HF diet-induced cardiac contractile dysfunction in CD-1 mice.
- Systemic glucose and insulin intolerance found in HFHS diet-fed mice may due in part to the impaired insulin signaling in the liver and adipose tissue, and elevated levels of inflammatory factor production in these animals.
- Heterozygous deletion of ROCK2 failed to improve insulin signaling in the liver and adipose tissue and to reduce inflammation in the adipose tissue of HFHS diet-fed mice.

The greatest strength of the work presented in this thesis is the characterization of the effects of a HFHS diet containing 45% kcal from fat and 17% kcal from sucrose in CD-1 mice, and the role of heterozygous deletion of ROCK2 in HFHS diet-induced obesity and associated comorbidities. Although the work and findings in this thesis are novel, there are several limitations to the studies conducted here. First of all, due to the limitation of study period, cardiac contractile function in CD-1 mice was only assessed at week 16-18 (set 1 mice) and at week 24 (set 2 mice). Thus, it was not clear whether a HFHS diet containing 45% kcal from fat and 17% kcal from sucrose would be able to induce cardiac dysfunction and impair cardiac insulin signaling with a longer period of diet feeding. Secondly, the lack of direct comparison of changes in the liver of HF diet-fed mice to HFHS diet-fed mice means that I do not know whether the differences between HF and HFHS diet-fed mice in the effects of ROCK2+/- heterozygous deletion on insulin and glucose tolerance arise from differences in the response of the liver to these 2 diets. Lastly, although I measured the expression levels of the RhoA-ROCK pathway and total ROCK activity, I cannot conclude whether over-activation of ROCK2 was present because no isoform specific activity was investigated in the current study.

In conclusion, this study characterized the effect of a HFHS diet containing 45% kcal from fat and 17% kcal from sucrose on cardiac function and systemic insulin sensitivity of WT CD-1 mice, and investigated the differences in the effect of heterozygous deletion of ROCK2 on HFHS diet-induced obesity in comparison to HF diet-induced obesity. Although over-activation of ROCK2 does not appear to contribute to the complications of obesity arising from a HFHS diet in CD-1 mice, my results suggest the goal of improving HFHS diet-induced impaired insulin signaling and inflammation may be achieved at the level of the liver and adipose tissue.

4.2 Future directions

4.2.1 Determining the effect of a HFHS diet with increased sucrose content on cardiac contractile function and insulin signaling in hearts of WT CD-1 mice

Despite the development of severe obesity and systemic insulin resistance, HFHS diet-fed WT CD-1 animals were resistant to the development of cardiac contractile dysfunction when fed a HFHS diet containing 45% kcal from fat and 17% kcal from sucrose. Several studies have shown that CD-1 mice fed a HFHS with a similar amount of fat but 30% kcal from sucrose diet develop cardiac systolic and diastolic dysfunction after 8 weeks of feeding (Carbone *et al.*, 2015, 2017; Chen *et al.*, 2017; Zhang *et al.*, 2017). Hence, it would be of interest to determine whether a HFHS diet with increased sucrose content is able to induce cardiac contractile dysfunction and impair cardiac insulin signaling in WT CD-1 mice, and whether this is associated with increased activation of ROCK2.

4.2.2 Evaluating whether disrupted mitochondrial morphology contributes to the development of mitochondrial dysfunction and cardiac dysfunction

Since mitochondrial homeostasis plays a crucial role in maintaining normal cardiac function, if a HFHS diet with increased sucrose content is able to induce cardiac contractile dysfunction and impair cardiac insulin signaling in WT CD-1 mice, it will be important to determine whether disrupted mitochondrial morphology contributes to the development of mitochondrial dysfunction and cardiac dysfunction.

4.2.3 Determining whether heterozygous deletion of ROCK2 protects HFHS diet-induced obesity-associated complications

If a HFHS diet with increased sucrose content is able to induce cardiac contractile dysfunction and impair cardiac insulin signaling in WT CD-1 mice, it will be crucial to determine

whether heterozygous deletion of ROCK2 improves HFHS diet-induced obesity-associated complications.

4.2.4 Assessing insulin sensitivity at the level of insulin signaling in skeletal muscle in HFHS diet-fed WT and ROCK2+/- animals

As the skeletal muscle is one of the key sites of glucose uptake and utilization, assessing insulin signaling in skeletal muscle may help to further understand the basis of insulin resistance in HFHS diet-fed animals. The expression and activity of ROCK isoforms will be evaluated to determine the effect of heterozygous deletion of ROCK2 on skeletal muscle of these animals.

Bibliography

Abarca-Gómez L, Abdeen ZA, Hamid ZA, Abu-Rmeileh NM, Acosta-Cazares B, Acuin C, Adams RJ, Aekplakorn W, Afsana K, Aguilar-Salinas CA, Agyemang C, Ahmadvand A, Ahrens W, Ajlouni K, Akhtaeva N, Al-Hazzaa HM, Al-Othman AR, Al-Raddadi R, Al Buhairan F, Al Dhukair S, Ali MM, Ali O, Alkerwi A, Alvarez-Pedrerol M, Aly E, Amarapurkar DN, Amouyel P, Amuzu A, Andersen LB, Anderssen SA, Andrade DS, Ängquist LH, Anjana RM, Aounallah-Skhiri H, Araújo J, Ariansen I, Aris T, Arlappa N, Arveiler D, Aryal KK, Aspelund T, Assah FK, Assunção MCF, Aung MS, Avdicová M, Azevedo A, Azizi F, Babu B V, Bahijri S, Baker JL, Balakrishna N, Bamoshmoosh M, Banach M, Bandosz P, Banegas JR, Barbagallo CM, Barceló A, Barkat A, Barros AJ, Barros MV, Bata I, Batieha AM, Batista RL, Batyrbek A, Baur LA, Beaglehole R, Romdhane H Ben, Benedics J, Benet M, Bennett JE, Bernabe-Ortiz A, Bernotiene G, Bettiol H, Bhagyalaxmi A, Bharadwaj S, Bhargava SK, Bhatti Z, Bhutta ZA, Bi H, Bi Y, Biehl A, Bikbov M, Bista B, Bjelica DJ, Bjerregaard P, Bjertness E, Bjertness MB, Björkelund C, Blokstra A, Bo S, Bobak M, Boddy LM, Boehm BO, Boeing H, Boggia JG, Boissonnet CP, Bonaccio M, Bongard V, et al. (2017) Worldwide trends in body-mass index, underweight, overweight, and obesity from 1975 to 2016: a pooled analysis of 2416 population-based measurement studies in 128·9 million children, adolescents, and adults. *Lancet* **390**:2627–2642.

Abdelaal M, le Roux CW, and Docherty NG (2017) Morbidity and mortality associated with obesity. *Ann Transl Med* **5**:161.

Abe K, Shimokawa H, Morikawa K, Uwatoku T, Oi K, Matsumoto Y, Hattori T, Nakashima Y, Kaibuchi K, Sueishi K, and Takeshit A (2004) Long-Term Treatment With a Rho-Kinase Inhibitor Improves Monocrotaline-Induced Fatal Pulmonary Hypertension in Rats. *Circ Res*

94:385–393.

Abel ED (2004) Glucose transport in the heart. *Front Biosci* **9**:201.

Abel ED (2004) Insulin signaling in heart muscle: Lessons from genetically engineered mouse models. *Curr Hypertens Rep* **6**:416–423.

Abel ED, O'Shea KM, and Ramasamy R (2012) Insulin Resistance: Metabolic Mechanisms and Consequences in the Heart. *Arterioscler Thromb Vasc Biol* **32**:2068–2076.

Adeva-Andany MM, Pérez-Felpete N, Fernández-Fernández C, Donapetry-García C, and Pazos-García C (2016) Liver glucose metabolism in humans. *Biosci Rep* **36**:e00416.

Aguirre V, Werner ED, Giraud J, Lee YH, Shoelson SE, and White MF (2002) Phosphorylation of Ser ^{307} in Insulin Receptor Substrate-1 Blocks Interactions with the Insulin Receptor and Inhibits Insulin Action. *J Biol Chem* **277**:1531–1537.

Al-Goblan AS, Al-Alfi MA, and Khan MZ (2014) Mechanism linking diabetes mellitus and obesity. *Diabetes Metab Syndr Obes* **7**:587–91.

Amano M, Nakayama M, and Kaibuchi K (2010) Rho-kinase/ROCK: A key regulator of the cytoskeleton and cell polarity. *Cytoskeleton* **67**:545–554.

Aroor AR, Mandavia CH, and Sowers JR (2012) Insulin Resistance and Heart Failure: Molecular Mechanisms. *Heart Fail Clin* **8**:609-617.

Bain J, Plater L, Elliott M, Shpiro N, Hastie CJ, McLauchlan H, Klevernic I, Arthur JSC, Alessi DR, and Cohen P (2007) The selectivity of protein kinase inhibitors: a further update. *Biochem J* **408**:297–315.

Ballinger SW (2005) Mitochondrial dysfunction in cardiovascular disease. *Free Radic Biol Med* **38**:1278–1295.

Barouch LA, Gao D, Chen L, Miller KL, Xu W, Phan AC, Kittleson MM, Minhas KM, Berkowitz

DE, Wei C, and Hare JM (2006) Cardiac Myocyte Apoptosis Is Associated With Increased DNA Damage and Decreased Survival in Murine Models of Obesity. *Circ Res* **98**:119–124.

Bastard J-P, Maachi M, Lagathu C, Kim MJ, Caron M, Vidal H, Capeau J, and Feve B (2006) Recent advances in the relationship between obesity, inflammation, and insulin resistance. *Eur Cytokine Netw* **17**:4–12.

Belke DD, Betuing S, Tuttle MJ, Graveleau C, Young ME, Pham M, Zhang D, Cooksey RC, McClain DA, Litwin SE, Taegtmeyer H, Severson D, Kahn CR, and Abel ED (2002) Insulin signaling coordinately regulates cardiac size, metabolism, and contractile protein isoform expression. *J Clin Invest* **109**:629–639.

Bertrand L, Horman S, Beauloye C, and Vanoverschelde J-L (2008) Insulin signalling in the heart. *Cardiovasc Res* **79**:238–248.

Bhadoria A, Sahoo K, Sahoo B, Choudhury A, Sufi N, and Kumar R (2015) Childhood obesity: Causes and consequences. *J Fam Med Prim Care* **4**:187–192.

Bhatheja S, Panchal HB, Ventura H, and Paul TK (2016) Obesity Cardiomyopathy: Pathophysiologic Factors and Nosologic Reevaluation. *Am J Med Sci* **352**:219–222.

Böhm C, Benz V, Clemenz M, Sprang C, Höft B, Kintscher U, and Foryst-Ludwig A (2013) Sexual dimorphism in obesity-mediated left ventricular hypertrophy. *Am J Physiol - Hear Circ Physiol* **305**:H211-8.

Borch KH, Nyegaard C, Hansen J-B, Mathiesen EB, Njølstad I, Wilsgaard T, and Brækkan SK (2011) Joint Effects of Obesity and Body Height on the Risk of Venous Thromboembolism. *Arterioscler Thromb Vasc Biol* **31**:1439–1444.

Boudina S, and Abel ED (2010) Diabetic cardiomyopathy, causes and effects. *Rev Endocr Metab Disord* **11**:31–39.

Brainard RE, Watson LJ, DeMartino AM, Brittian KR, Readnower RD, Boakye AA, Zhang D, Hoetker JD, Bhatnagar A, Baba SP, and Jones SP (2013) High fat feeding in mice is insufficient to induce cardiac dysfunction and does not exacerbate heart failure. *PLoS One* **8**:e83174.

Brownsey R, Boone AN, and Allard MF (1997) Actions of insulin on the mammalian heart: metabolism, pathology and biochemical mechanisms. *Cardiovasc Res* **34**:3–24.

Burcelin R, Crivelli V, Dacosta A, Roy-Tirelli A, and Thorens B (2002) Heterogeneous metabolic adaptation of C57BL/6J mice to high-fat diet. *Am J Physiol Metab* **282**:E834–E842.

Burchfield James G., Kebede MA, Meoli CC, Stöckli J, Whitworth PT, Wright AL, Hoffman NJ, Minard AY, Ma X, Krycer JR, Nelson ME, Tan S-X, Yau B, Thomas KC, Wee NKY, Khor E-C, Enriquez RF, Vissel B, Biden TJ, Baldock PA, Hoehn KL, Cantley J, Cooney GJ, James DE, and Fazakerley DJ (2018) High dietary fat and sucrose result in an extensive and time-dependent deterioration in health of multiple physiological systems in mice. *J Biol Chem* **293**:5731–5745.

Burchfield James G, Kebede MA, Meoli CC, Stöckli J, Whitworth PT, Wright AL, Hoffman NJ, Minard AY, Ma X, Krycer JR, Nelson ME, Tan S-X, Yau B, Thomas KC, Wee NKY, Khor E-C, Enriquez RF, Vissel B, Biden TJ, Baldock PA, Hoehn KL, Cantley J, Cooney GJ, James DE, and Fazakerley DJ (2018) High dietary fat and sucrose results in an extensive and time-dependent deterioration in health of multiple physiological systems in mice. *J Biol Chem* **293**:5731–5745.

Calligaris SD, Lecanda M, Solis F, Ezquer M, Gutiérrez J, Brandan E, Leiva A, Sobrevia L, and Conget P (2013) Mice Long-Term High-Fat Diet Feeding Recapitulates Human Cardiovascular Alterations: An Animal Model to Study the Early Phases of Diabetic

Cardiomyopathy. *PLoS One* **8**:e60931.

Camacho P, Fan H, Liu Z, and He J-Q (2016) Small mammalian animal models of heart disease. *Am J Cardiovasc Dis* **6**:70–80.

Camacho S, and Ruppel A (2017) Is the calorie concept a real solution to the obesity epidemic? *Glob Health Action* **10**:1289650.

Cao L, Qin X, Peterson MR, Haller SE, Wilson KA, Hu N, Lin X, Nair S, Ren J, and He G (2016) CARD9 knockout ameliorates myocardial dysfunction associated with high fat diet-induced obesity. *J Mol Cell Cardiol* **92**:185–195.

Carbone S, Lee PJH, Mauro AG, Mezzaroma E, Buzzetti R, Van Tassell B, Abbate A, and Toldo S (2017) Interleukin-18 mediates cardiac dysfunction induced by western diet independent of obesity and hyperglycemia in the mouse. *Nutr Diabetes* **7**:e258.

Carbone S, Mauro AG, Mezzaroma E, Kraskauskas D, Marchetti C, Buzzetti R, Van Tassell BW, Abbate A, and Toldo S (2015) A high-sugar and high-fat diet impairs cardiac systolic and diastolic function in mice. *Int J Cardiol* **198**:66–69.

Chalasani N, Younossi Z, Lavine JE, Charlton M, Cusi K, Rinella M, Harrison SA, Brunt EM, and Sanyal AJ (2018) The diagnosis and management of nonalcoholic fatty liver disease: Practice guidance from the American Association for the Study of Liver Diseases. *Hepatology* **67**:328–357.

Chan P-C, and Hsieh P-S (2017) The Role of Adipocyte Hypertrophy and Hypoxia in the Development of Obesity-Associated Adipose Tissue Inflammation and Insulin Resistance. *Adiposity - Omics and Molecular Understanding* **7**:127-141.

Chen K, Zheng X, Feng M, Li D, and Zhang H (2017) Gut Microbiota-Dependent Metabolite Trimethylamine N-Oxide Contributes to Cardiac Dysfunction in Western Diet-Induced

Obese Mice. *Front Physiol* **8**:139.

Chistiakov DA, Shkurat TP, Melnichenko AA, Grechko A V., and Orekhov AN (2018) The role of mitochondrial dysfunction in cardiovascular disease: a brief review. *Ann Med* **50**:121–127.

Christoffersen C, Bollano E, Lindegaard MLS, Bartels ED, Goetze JP, Andersen CB, and Nielsen LB (2003) Cardiac Lipid Accumulation Associated with Diastolic Dysfunction in Obese Mice. *Endocrinology* **144**:3483–3490.

Ciaraldi TP, Mudaliar S, Barzin A, Macievic JA, Edelman S V, Park KS, and Henry RR (2005) Skeletal muscle GLUT1 transporter protein expression and basal leg glucose uptake are reduced in type 2 diabetes. *J Clin Endocrinol Metab* **90**:352–8.

Clinical guidelines on the identification, evaluation, and treatment of overweight and obesity in adults: executive summary. Expert Panel on the Identification, Evaluation, and Treatment of Overweight in Adults (1998) . *Am J Clin Nutr* **68**:899–917.

Coleman ML, Sahai EA, Yeo M, Bosch M, Dewar A, and Olson MF (2001) Membrane blebbing during apoptosis results from caspase-mediated activation of ROCK I. *Nat Cell Biol* **3**:339–345.

Cox CL, Stanhope KL, Schwarz JM, Graham JL, Hatcher B, Griffen SC, Bremer AA, Berglund L, McGahan JP, Havel PJ, and Keim NL (2012) Consumption of fructose-sweetened beverages for 10 weeks reduces net fat oxidation and energy expenditure in overweight/obese men and women. *Eur J Clin Nutr* **66**:201–208.

Csige I, Ujvárosy D, Szabó Z, Lőrincz I, Paragh G, Harangi M, and Somodi S (2018) The Impact of Obesity on the Cardiovascular System. *J Diabetes Res* **2018**:1–12.

Dağ ZÖ, and Dilbaz B (2015) Impact of obesity on infertility in women. *J Turkish Ger Gynecol Assoc* **16**:111–7.

Dedkova EN, and Blatter LA (2012) Measuring mitochondrial function in intact cardiac myocytes. *J Mol Cell Cardiol* **52**:48–61.

DeFronzo RA, and Tripathy D (2009) Skeletal Muscle Insulin Resistance Is the Primary Defect in Type 2 Diabetes. *Diabetes Care* **32**:S157–S163.

Dela Cruz CS, and Matthay RA (2009) Role of Obesity in Cardiomyopathy and Pulmonary Hypertension. *Clin Chest Med* **30**:509–523.

Donnelly KL, Smith CI, Schwarzenberg SJ, Jessurun J, Boldt MD, and Parks EJ (2005) Sources of fatty acids stored in liver and secreted via lipoproteins in patients with nonalcoholic fatty liver disease. *J Clin Invest* **115**:1343–1351.

Ebong IA, Goff DC, Rodriguez CJ, Chen H, and Bertoni AG (2014) Mechanisms of heart failure in obesity. *Obes Res Clin Pract* **8**: e540-8.

Fabbrini E, Sullivan S, and Klein S (2010) Obesity and nonalcoholic fatty liver disease: biochemical, metabolic, and clinical implications. *Hepatology* **51**:679–89.

Fang CX, Dong F, Thomas DP, Ma H, He L, and Ren J (2008) Hypertrophic cardiomyopathy in high-fat diet-induced obesity: role of suppression of forkhead transcription factor and atrophy gene transcription. *Am J Physiol Circ Physiol* **295**:H1206–H1215.

Fang K, Wu F, Chen G, Dong H, Li J, Zhao Y, Xu L, Zou X, and Lu F (2019) Diosgenin ameliorates palmitic acid-induced lipid accumulation via AMPK/ACC/CPT-1A and SREBP-1c/FAS signaling pathways in LO2 cells. *BMC Complement Altern Med* **19**:255.

Fengler VHI, Macheiner T, Kessler SM, Czepukojc B, Gemperlein K, Müller R, Kiemer AK, Magnes C, Haybaeck J, Lackner C, and Sargsyan K (2016) Susceptibility of Different Mouse Wild Type Strains to Develop Diet-Induced NAFLD/AFLD-Associated Liver Disease. *PLoS One* **11**:e0155163.

Feuvray D, Idell-Wenger JA, and Neely JR (1979) Effects of ischemia on rat myocardial function and metabolism in diabetes. *Circ Res* **44**:322–9.

Fillmore N, Mori J, and Lopaschuk GD (2014) Mitochondrial fatty acid oxidation alterations in heart failure, ischaemic heart disease and diabetic cardiomyopathy. *Br J Pharmacol* **171**:2080–2090.

Franco M, Bilal U, Ordunez P, Benet M, Morejon A, Caballero B, Kennelly JF, and Cooper RS (2013) Population-wide weight loss and regain in relation to diabetes burden and cardiovascular mortality in Cuba 1980-2010: repeated cross sectional surveys and ecological comparison of secular trends. *BMJ* **346**:f1515.

Fricovsky ES, Suarez J, Ihm S-H, Scott BT, Suarez-Ramirez JA, Banerjee I, Torres-Gonzalez M, Wang H, Ellrott I, Maya-Ramos L, Villarreal F, and Dillmann WH (2012) Excess protein O-GlcNAcylation and the progression of diabetic cardiomyopathy. *Am J Physiol Integr Comp Physiol* **303**:R689–R699.

Froesch ER (1976) Disorders of fructose metabolism. *Clin Endocrinol Metab* **5**:599–611.

Galgani JE, Moro C, and Ravussin E (2008) Metabolic flexibility and insulin resistance. *Am J Physiol Endocrinol Metab* **295**: E1009-17.

Galic S, Loh K, Murray-Segal L, Steinberg GR, Andrews ZB, and Kemp BE (2018) AMPK signaling to acetyl-CoA carboxylase is required for fasting- and cold-induced appetite but not thermogenesis. *Elife* **7**:e32656.

Galloway CA, and Yoon Y (2015) Mitochondrial dynamics in diabetic cardiomyopathy. *Antioxid Redox Signal* **22**:1545–62.

Gao M, Ma Y, and Liu D (2015) High-fat diet-induced adiposity, adipose inflammation, hepatic steatosis and hyperinsulinemia in outbred CD-1 mice. *PLoS One* **10**:e0119784.

Garcia D, Hellberg K, Chaix A, Wallace M, Herzig S, Badur MG, Lin T, Shokhirev MN, Pinto AFM, Ross DS, Saghatelian A, Panda S, Dow LE, Metallo CM, and Shaw RJ (2019) Genetic Liver-Specific AMPK Activation Protects against Diet-Induced Obesity and NAFLD. *Cell Rep* **26**:192–208.

Gauthier M-S, O'Brien EL, Bigornia S, Mott M, Cacicedo JM, Xu XJ, Gokce N, Apovian C, and Ruderman N (2011) Decreased AMP-activated protein kinase activity is associated with increased inflammation in visceral adipose tissue and with whole-body insulin resistance in morbidly obese humans. *Biochem Biophys Res Commun* **404**:382–387.

Goedeke L, Bates J, Vatner DF, Perry RJ, Wang T, Ramirez R, Li L, Ellis MW, Zhang D, Wong KE, Beysen C, Cline GW, Ray AS, and Shulman GI (2018) Acetyl-CoA Carboxylase Inhibition Reverses NAFLD and Hepatic Insulin Resistance but Promotes Hypertriglyceridemia in Rodents. *Hepatology* **68**:2197–2211.

Goldberg IJ, Trent CM, and Schulze PC (2012) Lipid Metabolism and Toxicity in the Heart. *Cell Metab* **15**:805–812.

González-Sánchez JL, and Serrano-Ríos M (2007) Molecular basis of insulin action. *Drug News Perspect* **20**:527.

Haggerty CM, Mattingly AC, Kramer SP, Binkley CM, Jing L, Suever JD, Powell DK, Charnigo RJ, Epstein FH, and Fornwalt BK (2015) Left ventricular mechanical dysfunction in diet-induced obese mice is exacerbated during inotropic stress: A cine DENSE cardiovascular magnetic resonance study. *J Cardiovasc Magn Reson* **17**:75.

Han TS, and Lean ME (2016) A clinical perspective of obesity, metabolic syndrome and cardiovascular disease. *JRSM Cardiovasc Dis* **5**:204800401663337.

Hartmann S, Ridley AJ, and Lutz S (2015) The Function of Rho-Associated Kinases ROCK1 and

ROCK2 in the Pathogenesis of Cardiovascular Disease. *Front Pharmacol* **6**:276.

Hotamisligil G, Shargill N, and Spiegelman B (1993) Adipose expression of tumor necrosis factor-alpha: direct role in obesity-linked insulin resistance. *Science (80-)* **259**:87–91.

Hotamisligil GS (2003) Inflammatory pathways and insulin action. *Int J Obes* **27**:S53–S55.

Hotamisligil GS, Arner P, Caro JF, Atkinson RL, and Spiegelman BM (1995) Increased adipose tissue expression of tumor necrosis factor-alpha in human obesity and insulin resistance. *J Clin Invest* **95**:2409–2415.

Huang H, Lee S-H, Sousa-Lima I, Kim SS, Hwang WM, Dagon Y, Yang W-M, Cho S, Kang M-C, Seo JA, Shibata M, Cho H, Belew GD, Bhin J, Desai BN, Ryu MJ, Shong M, Li P, Meng H, Chung B-H, Hwang D, Kim MS, Park KS, Macedo MP, White M, Jones J, and Kim Y-B (2018) Rho-kinase/AMPK axis regulates hepatic lipogenesis during overnutrition. *J Clin Invest* **128**:5335–5350.

Hubert HB, Feinleib M, McNamara PM, and Castelli WP (1983) Obesity as an independent risk factor for cardiovascular disease: a 26-year follow-up of participants in the Framingham Heart Study. *Circulation* **67**:968–77.

Ijuin T, Hatano N, Hosooka T, and Takenawa T (2015) Regulation of insulin signaling in skeletal muscle by PIP3 phosphatase, SKIP, and endoplasmic reticulum molecular chaperone glucose-regulated protein 78. *Biochim Biophys Acta - Mol Cell Res* **1853**:3192–3201.

Ishikura K, Yamada N, Ito M, Ota S, Nakamura M, Isaka N, and Nakano T (2006) Beneficial Acute Effects of Rho-Kinase Inhibitor in Patients With Pulmonary Arterial Hypertension. *Circ J* **70**:174–178.

Ishimoto T, Lanaspa MA, Rivard CJ, Roncal-Jimenez CA, Orlicky DJ, Cicerchi C, McMahan RH, Abdelmalek MF, Rosen HR, Jackman MR, MacLean PS, Diggle CP, Asipu A, Inaba S,

Kosugi T, Sato W, Maruyama S, Sánchez-Lozada LG, Sautin YY, Hill JO, Bonthron DT, and Johnson RJ (2013) High-fat and high-sucrose (western) diet induces steatohepatitis that is dependent on fructokinase. *Hepatology* **58**:1632–1643.

Janevski M, Ratnayake S, Siljanovski S, McGlynn MA, Cameron-Smith D, and Lewandowski P (2012) Fructose containing sugars modulate mRNA of lipogenic genes ACC and FAS and protein levels of transcription factors ChREBP and SREBP1c with no effect on body weight or liver fat. *Food Funct* **3**:141–149.

Jaswal JS, Keung W, Wang W, Ussher JR, and Lopaschuk GD (2011) Targeting fatty acid and carbohydrate oxidation — A novel therapeutic intervention in the ischemic and failing heart. *Biochim Biophys Acta - Mol Cell Res* **1813**:1333–1350.

Jensen T, Abdelmalek MF, Sullivan S, Nadeau KJ, Green M, Roncal C, Nakagawa T, Kuwabara M, Sato Y, Kang D-H, Tolan DR, Sanchez-Lozada LG, Rosen HR, Lanaspa MA, Diehl AM, and Johnson RJ (2018) Fructose and sugar: A major mediator of non-alcoholic fatty liver disease. *J Hepatol* **68**:1063–1075.

Jeon SM (2016) Regulation and function of AMPK in physiology and diseases. *Exp Mol Med* **48**:e245.

Jernås M, Palming J, Sjöholm K, Jennische E, Svensson P-A, Gabrielsson BG, Levin M, Sjögren A, Rudemo M, Lystig TC, Carlsson B, Carlsson LMS, and Lönn M (2006) Separation of human adipocytes by size: hypertrophic fat cells display distinct gene expression. *FASEB J* **20**:1540–1542.

Julian L, and Olson MF (2014) Rho-associated coiled-coil containing kinases (ROCK). *Small GTPases* **5**:e29846.

Jung UJ, and Choi MS (2014) Obesity and its metabolic complications: The role of adipokines and

the relationship between obesity, inflammation, insulin resistance, dyslipidemia and nonalcoholic fatty liver disease. *Int J Mol Sci* **15**:6184-6223.

Juraschek SP, Miller ER, Gelber AC, and Gelber AC (2013) Body mass index, obesity, and prevalent gout in the United States in 1988-1994 and 2007-2010. *Arthritis Care Res (Hoboken)* **65**:127–32.

Kaibuchi K, Kuroda S, and Amano M (1999) Regulation of the Cytoskeleton and Cell Adhesion by the Rho Family GTPases in Mammalian Cells. *Annu Rev Biochem* **68**:459–486.

Kamei N, Tobe K, Suzuki R, Ohsugi M, Watanabe T, Kubota N, Ohtsuka-Kowatari N, Kumagai K, Sakamoto K, Kobayashi M, Yamauchi T, Ueki K, Oishi Y, Nishimura S, Manabe I, Hashimoto H, Ohnishi Y, Ogata H, Tokuyama K, Tsunoda M, Ide T, Murakami K, Nagai R, and Kadowaki T (2006) Overexpression of Monocyte Chemoattractant Protein-1 in Adipose Tissues Causes Macrophage Recruitment and Insulin Resistance. *J Biol Chem* **281**:26602–26614.

Kanda H, Tateya S, Tamori Y, Kotani K, Hiasa K, Kitazawa R, Kitazawa S, Miyachi H, Maeda S, Egashira K, and Kasuga M (2006) MCP-1 contributes to macrophage infiltration into adipose tissue, insulin resistance, and hepatic steatosis in obesity. *J Clin Invest* **116**:1494–1505.

Kasper EK, Hruban RH, and Baughman KL (1992) Cardiomyopathy of obesity: a clinicopathologic evaluation of 43 obese patients with heart failure. *Am J Cardiol* **70**:921–4.

Kenchaiah S, Evans JC, Levy D, Wilson PWF, Benjamin EJ, Larson MG, Kannel WB, and Vasan RS (2002) Obesity and the Risk of Heart Failure. *N Engl J Med* **347**:305–313.

Kim CW, Addy C, Kusunoki J, Anderson NN, Deja S, Fu X, Burgess SC, Li C, Chakravarthy M, Previs S, Milstein S, Fitzgerald K, Kelley DE, and Horton JD (2017) Acetyl CoA Carboxylase Inhibition Reduces Hepatic Steatosis but Elevates Plasma Triglycerides in Mice and Humans:

A Bedside to Bench Investigation. *Cell Metab* **26**:394–406.

Kim MS, Krawczyk SA, Doridot L, Fowler AJ, Wang JX, Trauger SA, Noh HL, Kang HJ, Meissen JK, Blatnik M, Kim JK, Lai M, and Herman MA (2016) ChREBP regulates fructose-induced glucose production independently of insulin signaling. *J Clin Invest* **126**:4372–4386.

King A, and Austin A (2017) Animal Models of Type 1 and Type 2 Diabetes Mellitus. *Animal Models for the Study of Human Disease* **2**:245–265.

Kinlen D, Cody D, and O'Shea D (2018) Complications of obesity. *QJM An Int J Med* **111**:437–443.

Kishi T, Hirooka Y, Masumoto A, Ito K, Kimura Y, Inokuchi K, Tagawa T, Shimokawa H, Takeshita A, and Sunagawa K (2005) Rho-Kinase Inhibitor Improves Increased Vascular Resistance and Impaired Vasodilation of the Forearm in Patients With Heart Failure. *Circulation* **111**:2741–2747.

Kohut A, Patel N, and Singh H (2016) Comprehensive Echocardiographic Assessment of the Right Ventricle in Murine Models. *J Cardiovasc Ultrasound* **24**:229–238.

Kraegen EW, Clark PW, Jenkins AB, Daley EA, Chisholm DJ, and Storlien LH (1991) Development of Muscle Insulin Resistance After Liver Insulin Resistance in High-Fat-Fed Rats. *Diabetes* **40**:1397–1403.

Kraigher-Krainer E, Shah AM, Gupta DK, Santos A, Claggett B, Pieske B, Zile MR, Voors AA, Lefkowitz MP, Packer M, McMurray JJ, Solomon SD, and Investigators P (2014) Impaired systolic function by strain imaging in heart failure with preserved ejection fraction. *J Am Coll Cardiol* **63**:447–456.

Krishnan A, Samtani R, Dhanantwari P, Lee E, Yamada S, Shiota K, Donofrio MT, Leatherbury L, and Lo CW (2014) A detailed comparison of mouse and human cardiac development.

Pediatr Res **76**:500–507.

Lakerveld J, and Mackenbach J (2017) The Upstream Determinants of Adult Obesity. *Obes Facts* **10**:216-222.

Last AR, and Wilson SA (2006) Low-Carbohydrate Diets. *Am Fam Physician* **73**:1942–8.

Lazar MA (2005) PPARγ, 10 years later. *Biochimie* **87**:9–13.

Lewis GF, and Steiner G (1996) Acute Effects of Insulin in the Control of VLDL Production in Humans: Implications for the insulin-resistant state. *Diabetes Care* **19**:390–393.

Lin G, Brownsey RW, and MacLeod KM (2014) Complex Regulation of PKCβ2 and PDK-1/AKT by ROCK2 in Diabetic Heart. *PLoS One* **9**:e86520.

Lin G, Craig GP, Zhang L, Yuen VG, Allard M, McNeill JH, and MacLeod KM (2007) Acute inhibition of Rho-kinase improves cardiac contractile function in streptozotocin-diabetic rats. *Cardiovasc Res* **75**:51–8.

Loirand G, Guérin P, and Pacaud P (2006) Rho Kinases in Cardiovascular Physiology and Pathophysiology. *Circ Res* **98**:322–334.

Lopaschuk GD (2016) Fatty Acid Oxidation and Its Relation with Insulin Resistance and Associated Disorders. *Ann Nutr Metab* **68**:15–20.

Lopaschuk GD, Ussher JR, Folmes CDL, Jaswal JS, and Stanley WC (2010) Myocardial Fatty Acid Metabolism in Health and Disease. *Physiol Rev* **90**:207–258.

Luo L (2000) RHO GTPASES in neuronal morphogenesis. *Nat Rev Neurosci* **1**:173–180.

Luo L, Fang K, Dan X, and Gu M (2019) Crocin ameliorates hepatic steatosis through activation of AMPK signaling in db/db mice. *Lipids Health Dis* **18**:11.

Lutz TA, and Woods SC (2012) Overview of Animal Models of Obesity. *Curr Protoc Pharmacol* **58**:5.61.1-5.61.18.

Magliano M (2008) Obesity and arthritis. *Menopause Int* **14**:149–154.

Mao J, DeMayo FJ, Li H, Abu-Elheiga L, Gu Z, Shaikenov TE, Kordari P, Chirala SS, Heird WC, and Wakil SJ (2006) Liver-specific deletion of acetyl-CoA carboxylase 1 reduces hepatic triglyceride accumulation without affecting glucose homeostasis. *Proc Natl Acad Sci U S A* **103**:8552–8557.

Masumoto A, Hirooka Y, Shimokawa H, Hironaga K, Setoguchi S, and Takeshita A (2001) Possible Involvement of Rho-Kinase in the Pathogenesis of Hypertension in Humans. *Hypertension* **38**:1307–1310.

Masumoto A, Mohri M, Shimokawa H, Urakami L, Usui M, and Takeshita A (2002) Suppression of Coronary Artery Spasm by the Rho-Kinase Inhibitor Fasudil in Patients With Vasospastic Angina. *Circulation* **105**:1545–1547.

Montgomery MK, and Turner N (2015) Mitochondrial dysfunction and insulin resistance: an update. *Endocr Connect* **4**:R1–R15.

Morino K, Petersen KF, Dufour S, Befroy D, Frattini J, Shatzkes N, Neschen S, White MF, Bilz S, Sono S, Pypaert M, and Shulman GI (2005) Reduced mitochondrial density and increased IRS-1 serine phosphorylation in muscle of insulin-resistant offspring of type 2 diabetic parents. *J Clin Invest* **115**:3587–3593.

Movahed MR, and Saito Y (2009) Lack of Association between Obesity and Left Ventricular Systolic Dysfunction. *Echocardiography* **26**:128–132.

Muir LA, Neeley CK, Meyer KA, Baker NA, Brosius AM, Washabaugh AR, Varban OA, Finks JF, Zamarron BF, Flesher CG, Chang JS, DelProposto JB, Geletka L, Martinez-Santibanez G, Kaciroti N, Lumeng CN, and O'Rourke RW (2016) Adipose tissue fibrosis, hypertrophy, and hyperplasia: Correlations with diabetes in human obesity. *Obesity* **24**:597–605.

Muniyappa R, Montagnani M, Koh KK, and Quon MJ (2007) Cardiovascular Actions of Insulin. *Endocr Rev* **28**:463–491.

Nakae J, Kido Y, and Accili D (2001) Distinct and Overlapping Functions of Insulin and IGF-I Receptors. *Endocr Rev* **22**:818–835.

Okamoto R, Li Y, Noma K, Hiroi Y, Liu P-Y, Taniguchi M, Ito M, and Liao JK (2013) FHL2 prevents cardiac hypertrophy in mice with cardiac-specific deletion of ROCK2. *FASEB J* **27**:1439–49.

Ormazabal V, Nair S, Elfeky O, Aguayo C, Salomon C, and Zuñiga FA (2018) Association between insulin resistance and the development of cardiovascular disease. *Cardiovasc Diabetol* **17**:122.

Ortiz VE, and Kwo J (2015) Obesity: physiologic changes and implications for preoperative management. *BMC Anesthesiol* **15**:97.

Ottensmeyer FP, Beniac DR, Luo RZ-T, and Yip CC (2000) Mechanism of Transmembrane Signaling: Insulin Binding and the Insulin Receptor †. *Biochemistry* **39**:12103–12112.

Palmer AJ, Chung M-Y, List EO, Walker J, Okada S, Kopchick JJ, and Berryman DE (2009) Age-Related Changes in Body Composition of Bovine Growth Hormone Transgenic Mice. *Endocrinology* **150**:1353–1360.

Parker R (2018) The role of adipose tissue in fatty liver diseases. *Liver Res* **2**:35–42.

Parlee SD, Lentz SI, Mori H, and MacDougald OA (2014) Quantifying Size and Number of Adipocytes in Adipose Tissue. *Methods in enzymology* **537**:93–122.

Pascual M, Pascual DA, Soria F, Vicente T, Hernández AM, Tébar FJ, and Valdés M (2003) Effects of isolated obesity on systolic and diastolic left ventricular function. *Heart* **89**:1152–1156.

Pulinilkunnil T, Kienesberger PC, Nagendran J, Sharma N, Young ME, and Dyck JRB (2014) Cardiac-specific adipose triglyceride lipase overexpression protects from cardiac steatosis and dilated cardiomyopathy following diet-induced obesity. *Int J Obes* **38**:205–215.

Qureshi K, and Abrams GA (2007) Metabolic liver disease of obesity and role of adipose tissue in the pathogenesis of nonalcoholic fatty liver disease. *World J Gastroenterol* **13**:3540–53.

Rask-Madsen C, and Kahn CR (2012) Tissue-specific insulin signaling, metabolic syndrome, and cardiovascular disease. *Arterioscler Thromb Vasc Biol* **32**:2052–9.

Regan TJ, Lyons MM, Ahmed SS, Levinson GE, Oldewurtel HA, Ahmad MR, and Haider B (1977) Evidence for cardiomyopathy in familial diabetes mellitus. *J Clin Invest* **60**:884–99.

Reuvekamp EJ, Bulten BF, Nieuwenhuis AA, Meekes MRA, de Haan AFJ, Tol J, Maas AHEM, Elias-Smale SE, and de Geus-Oei LF (2016) Does diastolic dysfunction precede systolic dysfunction in trastuzumab-induced cardiotoxicity? Assessment with multigated radionuclide angiography (MUGA). *J Nucl Cardiol* **23**:824–32.

Riento K, and Ridley AJ (2003) ROCKs: multifunctional kinases in cell behaviour. *Nat Rev Mol Cell Biol* **4**:446–456.

Rinella ME, and Sanyal AJ (2016) Management of NAFLD: a stage-based approach. *Nat Rev Gastroenterol Hepatol* **13**:196–205.

Rodrigues B, Cam MC, and McNeill JH (1998) Metabolic disturbances in diabetic cardiomyopathy. *Mol Cell Biochem* **180**:53–7.

Romero-Corral A, Caples SM, Lopez-Jimenez F, and Somers VK (2010) Interactions between obesity and obstructive sleep apnea: implications for treatment. *Chest* **137**:711–9.

Rudge MF, and Duncan CJ (1988) Ultrastructural changes in the cardiomyopathy of dystrophic hamsters and mice. *Tissue Cell* **20**:249-53.

Samuel VT (2011) Fructose induced lipogenesis: From sugar to fat to insulin resistance. *Trends Endocrinol Metab* **22**:60-5.

Samuel VT, and Shulman GI (2012) Mechanisms for Insulin Resistance: Common Threads and Missing Links. *Cell* **148**:852–871.

Saponaro C, Gaggini M, Carli F, and Gastaldelli A (2015) The subtle balance between lipolysis and lipogenesis: A critical point in metabolic homeostasis. *Nutrients* **7**:9453-74.

Sato A, Kawano H, Notsu T, Ohta M, Nakakuki M, Mizuguchi K, Itoh M, Suganami T, and Ogawa Y (2010) Antiobesity Effect of Eicosapentaenoic Acid in. *Diabetes* **59**:2495–504.

Schäfer K, Fujisawa K, Konstantinides S, and Loskutoff DJ (2001) Disruption of the plasminogen activator inhibitor 1 gene reduces the adiposity and improves the metabolic profile of genetically obese and diabetic ob/ob mice. *FASEB J* **15**:1840–1842.

Schipke JD (1994) Cardiac efficiency. *Basic Res Cardiol* **89**:207–40.

Sebbagh M, Hamelin J, Bertoglio J, Solary E, and Bréard J (2005) Direct cleavage of ROCK II by granzyme B induces target cell membrane blebbing in a caspase-independent manner. *J Exp Med* **201**:465–471.

Sebbagh M, Renvoizé C, Hamelin J, Riché N, Bertoglio J, and Bréard J (2001) Caspase-3-mediated cleavage of ROCK I induces MLC phosphorylation and apoptotic membrane blebbing. *Nat Cell Biol* **3**:346–352.

Shaw LM (2011) The insulin receptor substrate (IRS) proteins. *Cell Cycle* **10**:1750–1756.

Shi J, Zhang Y-W, Yang Y, Zhang L, and Wei L (2010) ROCK1 plays an essential role in the transition from cardiac hypertrophy to failure in mice. *J Mol Cell Cardiol* **49**:819–28.

Shibuya M, Hirai S, Seto M, Satoh S, Ohtomo E, and Fasudil Ischemic Stroke Study Group (2005) Effects of fasudil in acute ischemic stroke: Results of a prospective placebo-controlled

double-blind trial. *J Neurol Sci* **238**:31–39.

Shimizu T, Narang N, Chen P, Yu B, Knapp M, Janardanan J, Blair J, and Liao JK (2017) Fibroblast deletion of ROCK2 attenuates cardiac hypertrophy, fibrosis, and diastolic dysfunction. *JCI insight* **2**:e93187.

Shimokawa H, Hiramori K, Iinuma H, Hosoda S, Kishida H, Osada H, Katagiri T, Yamauchi K, Yui Y, Minamino T, Nakashima M, and Kato K (2002) Anti-anginal Effect of Fasudil, a Rho-Kinase Inhibitor, in Patients With Stable Effort Angina: A Multicenter Study. *J Cardiovasc Pharmacol* **40**:751–761.

Shoelson SE, Herrero L, and Naaz A (2007) Obesity, Inflammation, and Insulin Resistance. *Gastroenterology* **132**:2169–2180.

Shulman GI (2000) Cellular mechanisms of insulin resistance. *J Clin Invest* **106**:171-6.

Siasos G, Tsigkou V, Kosmopoulos M, Theodosiadis D, Simantiris S, Tagkou NM, Tsimpiktsioglou A, Stampouloglou PK, Oikonomou E, Mourouzis K, Philippou A, Vavuranakis M, Stefanadis C, Tousoulis D, and Papavassiliou AG (2018) Mitochondria and cardiovascular diseases-from pathophysiology to treatment. *Ann Transl Med* **6**:256.

Smith U (2002) Impaired ('diabetic') insulin signaling and action occur in fat cells long before glucose intolerance—is insulin resistance initiated in the adipose tissue? *Int J Obes* **26**:897–904.

Softic S, Gupta MK, Wang GX, Fujisaka S, O'Neill BT, Rao TN, Willoughby J, Harbison C, Fitzgerald K, Ilkayeva O, Newgard CB, Cohen DE, and Kahn CR (2017) Divergent effects of glucose and fructose on hepatic lipogenesis and insulin signaling. *J Clin Invest* **127**:4059–4074.

Soliman H, Gador A, Lu Y-H, Lin G, Bankar G, and MacLeod KM (2012) Diabetes-induced

increased oxidative stress in cardiomyocytes is sustained by a positive feedback loop involving Rho kinase and PKCβ $_2$. *Am J Physiol Circ Physiol* **303**:H989–H1000.

Soliman H, Nyamandi V, Garcia-Patino M, Varela JN, Bankar G, Lin G, Jia Z, and MacLeod KM (2015) Partial deletion of ROCK2 protects mice from high-fat diet-induced cardiac insulin resistance and contractile dysfunction. *Am J Physiol Circ Physiol* **309**:H70–H81.

Soliman H, Varela JN, Nyamandi V, Garcia-Patino M, Lin G, Bankar GR, Jia Z, and MacLeod KM (2016) Attenuation of obesity-induced insulin resistance in mice with heterozygous deletion of ROCK2. *Int J Obes* **40**:1435–1443.

Speakman JR (2019) Use of high-fat diets to study rodent obesity as a model of human obesity. *Int J Obes* **43**:1491–1492.

Spiering D, and Hodgson L (2011) Dynamics of the Rho-family small GTPases in actin regulation and motility. *Cell Adh Migr* **5**:170–180.

Stanton T, Leano R, and Marwick TH (2009) Prediction of all-cause mortality from global longitudinal speckle strain: Comparison with ejection fraction and wall motion scoring. *Circ Cardiovasc Imaging* **2**:356–364.

Statovci D, Aguilera M, MacSharry J, and Melgar S (2017) The impact of western diet and nutrients on the microbiota and immune response at mucosal interfaces. *Front Immunol* **8**:838.

Stienstra R, Duval C, Müller M, and Kersten S (2007) PPARs, Obesity, and Inflammation. *PPAR Res* **2007**:95974.

Stryjecki C, Alyass A, and Meyre D (2018) Ethnic and population differences in the genetic predisposition to human obesity. *Obes Rev* **19**:62-80.

Sugii S, Olson P, Sears DD, Saberi M, Atkins AR, Barish GD, Hong S-H, Castro GL, Yin Y-Q,

Nelson MC, Hsiao G, Greaves DR, Downes M, Yu RT, Olefsky JM, and Evans RM (2009) PPARgamma activation in adipocytes is sufficient for systemic insulin sensitization. *Proc Natl Acad Sci U S A* **106**:22504–9.

Sunamura S, Satoh K, Kurosawa R, Ohtsuki T, Kikuchi N, Elias-Al-Mamun M, Shimizu T, Ikeda S, Suzuki K, Satoh T, Omura J, Nogi M, Numano K, Siddique MAH, Miyata S, Miura M, and Shimokawa H (2018) Different roles of myocardial ROCK1 and ROCK2 in cardiac dysfunction and postcapillary pulmonary hypertension in mice. *Proc Natl Acad Sci U S A* **115**:E7129–E7138.

Sung MMY, Koonen DPY, Soltys CLM, Jacobs RL, Febbraio M, and Dyck JRB (2011) Increased CD36 expression in middle-aged mice contributes to obesity-related cardiac hypertrophy in the absence of cardiac dysfunction. *J Mol Med* **89**:459–469.

Szczepaniak LS, Dobbins RL, Metzger GJ, Sartoni-D'Ambrosia G, Arbique D, Vongpatanasin W, Unger R, and Victor RG (2003) Myocardial triglycerides and systolic function in humans: In vivo evaluation by localized proton spectroscopy and cardiac imaging. *Magn Reson Med* **49**:417–423.

Taegtmeyer H, McNulty P, and Young ME (2002) Adaptation and Maladaptation of the Heart in Diabetes: Part I. *Circulation* **105**:1727–1733.

Tappy L, and Lê K-A (2010) Metabolic Effects of Fructose and the Worldwide Increase in Obesity. *Physiol Rev* **90**:23–46.

Ternacle J, Wan F, Sawaki D, Surenaud M, Pini M, Mercedes R, Ernande L, Audureau E, Dubois-Rande J-L, Adnot S, Hue S, Czibik G, and Derumeaux G (2017) Short-term high-fat diet compromises myocardial function: a radial strain rate imaging study. *Eur Hear J - Cardiovasc Imaging* **18**:1283–1291.

Thiebaud D, Jacot E, Defronzo RA, Maeder E, Jequier E, and Felber J-P (1982) The Effect of Graded Doses of Insulin on Total Glucose Uptake, Glucose Oxidation, and Glucose Storage in Man. *Diabetes* **31**:957–963.

Thirone ACP, Huang C, and Klip A (2006) Tissue-specific roles of IRS proteins in insulin signaling and glucose transport. *Trends Endocrinol Metab* **17**:72–78.

Thorens B (2015) GLUT2, glucose sensing and glucose homeostasis. *Diabetologia* **58**:221–32.

Thorn SL, Gollob MH, Harper ME, Beanlands RS, Dekemp RA, and Dasilva JN (2013) Chronic AMPK activity dysregulation produces myocardial insulin resistance in the human Arg302Gln-PRKAG2 glycogen storage disease mouse model. *EJNMMI Res* **3**:1–9.

Thumkeo D, Keel J, Ishizaki T, Hirose M, Nonomura K, Oshima H, Oshima M, Taketo MM, and Narumiya S (2003) Targeted disruption of the mouse rho-associated kinase 2 gene results in intrauterine growth retardation and fetal death. *Mol Cell Biol* **23**:5043–55.

Tolman KG, Fonseca V, Dalpiaz A, and Tan MH (2007) Spectrum of Liver Disease in Type 2 Diabetes and Management of Patients With Diabetes and Liver Disease. *Diabetes Care* **30**:734–743.

Tseng Y-H, Cypess AM, and Kahn CR (2010) Cellular bioenergetics as a target for obesity therapy. *Nat Rev Drug Discov* **9**:465–482.

Unger RH, and Orci L (2002) Lipoapoptosis: its mechanism and its diseases. *Biochim Biophys Acta* **1585**:202–12.

Utzschneider KM, and Kahn SE (2006) Review: The role of insulin resistance in nonalcoholic fatty liver disease. *J Clin Endocrinol Metab* **91**:4753-61.

Verboven K, Wouters K, Gaens K, Hansen D, Bijnen M, Wetzels S, Stehouwer CD, Goossens GH, Schalkwijk CG, Blaak EE, and Jocken JW (2018) Abdominal subcutaneous and visceral

adipocyte size, lipolysis and inflammation relate to insulin resistance in male obese humans. *Sci Rep* **8**:4677.

Vicari RM, Chaitman B, Keefe D, Smith WB, Chrysant SG, Tonkon MJ, Bittar N, Weiss RJ, Morales-Ballejo H, Thadani U, and Fasudil Study Group (2005) Efficacy and Safety of Fasudil in Patients With Stable Angina. *J Am Coll Cardiol* **46**:1803–1811.

Walter F, and Addis T (1939) ORGAN WORK AND ORGAN WEIGHT. *J Exp Med* **69**:467–483.

Wang C-Y, and Liao JK (2012) A Mouse Model of Diet-Induced Obesity and Insulin Resistance. *Methods in molecular biology* **821**:421–433.

Wang Y, Zheng XR, Riddick N, Bryden M, Baur W, Zhang X, and Surks HK (2009) ROCK Isoform Regulation of Myosin Phosphatase and Contractility in Vascular Smooth Muscle Cells. *Circ Res* **104**:531–540.

Weisberg Stuart P., McCann D, Desai M, Rosenbaum M, Leibel RL, and Ferrante AW (2003) Obesity is associated with macrophage accumulation in adipose tissue. *J Clin Invest* **112**:1796–1808.

Weisberg Stuart P, McCann D, Desai M, Rosenbaum M, Leibel RL, Ferrante AW, and Jr. (2003) Obesity is associated with macrophage accumulation in adipose tissue. *J Clin Invest* **112**:1796–808.

Wilcox G (2005) Insulin and insulin resistance. *Clin Biochem Rev* **26**:19–39.

Willows R, Sanders MJ, Xiao B, Patel BR, Martin SR, Read J, Wilson JR, Hubbard J, Gamblin SJ, and Carling D (2017) Phosphorylation of AMPK by upstream kinases is required for activity in mammalian cells. *Biochem J* **474**:3059–3073.

Wong C, and Marwick TH (2007) Obesity cardiomyopathy: pathogenesis and pathophysiology. *Nat Clin Pract Cardiovasc Med* **4**:436–443.

Woods A, Williams JR, Muckett PJ, Mayer F V., Liljevald M, Bohlooly-Y M, and Carling D (2017) Liver-Specific Activation of AMPK Prevents Steatosis on a High-Fructose Diet. *Cell Rep* **18**:3043–3051.

Wu H, and Ballantyne CM (2017) Skeletal muscle inflammation and insulin resistance in obesity. *J Clin Invest* **127**:43–54.

Wu L, Zhang L, Li B, Jiang H, Duan Y, Xie Z, Shuai L, Li Jia, and Li Jingya (2018) AMP-Activated Protein Kinase (AMPK) Regulates Energy Metabolism through Modulating Thermogenesis in Adipose Tissue. *Front Physiol* **9**:122.

Xu H, Barnes GT, Yang Q, Tan G, Yang D, Chou CJ, Sole J, Nichols A, Ross JS, Tartaglia LA, and Chen H (2003) Chronic inflammation in fat plays a crucial role in the development of obesity-related insulin resistance. *J Clin Invest* **112**:1821–1830.

Yan J, Young ME, Cui L, Lopaschuk GD, Liao R, and Tian R (2009) Increased glucose uptake and oxidation in mouse hearts prevent high fatty acid oxidation but cause cardiac dysfunction in diet-induced obesity. *Circulation* **119**:2818–2828.

Yang Z-H, Miyahara H, Takeo J, and Katayama M (2012) Diet high in fat and sucrose induces rapid onset of obesity-related metabolic syndrome partly through rapid response of genes involved in lipogenesis, insulin signalling and inflammation in mice. *Diabetol Metab Syndr* **4**:32.

Yoneda A, Multhaupt HAB, and Couchman JR (2005) The Rho kinases I and II regulate different aspects of myosin II activity. *J Cell Biol* **170**:443–453.

Zakim D (1972) THE EFFECT OF FRUCTOSE ON HEPATIC SYNTHESIS OF FATTY ACIDS. *Acta Med Scand* **192**:205–214.

Zaugg M, Schaub MC, Pasch T, and Spahn DR (2002) Modulation of beta-adrenergic receptor

subtype activities in perioperative medicine: mechanisms and sites of action. *Br J Anaesth* **88**:101–23.

Zhang H, Meng J, and Yu H (2017) Trimethylamine N-oxide Supplementation Abolishes the Cardioprotective Effects of Voluntary Exercise in Mice Fed a Western Diet. *Front Physiol* **8**:944.

Zhang Y-M, Bo J, Taffet GE, Chang J, Shi J, Reddy AK, Michael LH, Schneider MD, Entman ML, Schwartz RJ, and Wei L (2006) Targeted deletion of ROCK1 protects the heart against pressure overload by inhibiting reactive fibrosis. *FASEB J* **20**:916–925.

Zhou W, Yang J, Zhu J, Wang Y, Wu Y, Xu L, and Yang Y (2019) Fetuin B aggravates liver X receptor-mediated hepatic steatosis through AMPK in HepG2 cells and mice. *Am J Transl Res* **11**:1498–1509.

Zhou Z, Meng Y, Asrar S, Todorovski Z, and Jia Z (2009) A critical role of Rho-kinase ROCK2 in the regulation of spine and synaptic function. *Neuropharmacology* **56**:81–9.

Appendix

Compositions of diets used in this study

Diets		CH	LFLS		HFHS		HF	
Class description	Ingredient	Calories (% total)	Grams (g)	Calories (% total)	Grams (g)	Calories (% total)	Grams (g)	Calories (% total)
Protein	Casein, Lactic, 30 Mesh	25	200.00	20	200.00	20	200.00	20
	Cystine, L		3.00		3.00		3.00	
Carbohydrates	Starch, Corn	59	506.20	63	72.80	18	-	13
	Lodex 10		125.00		100.00		125.00	
	Sucrose	3	72.80	7	176.80	17	72.80	7
Fat	Soybean oil	13	25.00	10	25.00	45	25.00	60
	Lard		20.00		177.5		245.00	